

Copyright © 1985, by the author(s).
All rights reserved.

Permission to make digital or hard copies of all or part of this work for personal or classroom use is granted without fee provided that copies are not made or distributed for profit or commercial advantage and that copies bear this notice and the full citation on the first page. To copy otherwise, to republish, to post on servers or to redistribute to lists, requires prior specific permission.

CHARACTERIZATION OF INORGANIC RESIST
FOR VLSI FABRICATION

by
Wing Yu Leung

Memorandum No. UCB/ERL M85/76

26 September 1985

cc 10/1/85

Characterization of Inorganic Resist for VLSI fabrication

Copyright © 1985

by

Wing Yu Leung

CHARACTERIZATION OF INORGANIC RESIST
FOR VLSI FABRICATION

by
Wing Yu Leung

Memorandum No. UCB/ERL M85/76

26 September 1985

ELECTRONICS RESEARCH LABORATORY
College of Engineering
University of California, Berkeley
94720

Characterization of Inorganic Resist for VLSI fabrication

Copyright © 1985

by

Wing Yu Leung

CHARACTERIZATION OF INORGANIC RESIST FOR VLSI FABRICATION

Wingyu Leung

*Department of Electrical Engineering and Computer Sciences
University of California, Berkeley, California 94720, U.S.A.*


Research Advisor

ABSTRACT

This dissertation concentrates on the study of the image formation mechanisms of the $Ge_{0.1}Se_{0.9}$ resist and the assessment of the resist for VLSI fabrication. A laboratory $Ge_{0.1}Se_{0.9}$ resist process has been established based on the one developed by Tai and coworkers at Bell Labs. and the resolution results similar to theirs have been obtained. A simulation program for the exposure model of the resist has been written and incorporated to the SAMPLE program. The model describes the Ag transport mechanisms in the resist system which are the lateral diffusion and photobleaching of Ag in the Ag_2Se layer and the vertical photodoping of Ag from the Ag_2Se to the $Ge_{0.1}Se_{0.9}$ layer. The simulation model has been verified by comparing the simulation and experimental results.

Laboratory experiment and computer simulation has been used to study the four exposure phenomena: edge sharpening, contrast enhancement, feature-dependent amplification and feature-dependent photodoping suppression. The phenomena result from the photobleaching and lateral diffusion mechanisms which occur in the sensitized layer of the resist system during the exposure process. The conditions under which these phenomena occur has been identified. Their practical impact on the resolution capability of the resist has been evaluated. For normal exposures ($<150mJ/cm^2$), these

phenomena do not occur.

The mechanism of Ag photodoping in $Ge_{0.1}Se_{0.9}$ glass has been studied. The photodoping process has been found to obey Fick's diffusion law. From RBS results, the vertical diffusivity of Ag in $Ge_{0.1}Se_{0.9}$ glass at $21^{\circ}C$, $2mW/cm^2$ intensity and $436nm$ wavelength is calculated to be $2.7nm^2/sec$. Lateral diffusivity of Ag in $Ge_{0.1}Se_{0.9}$ glass has been estimated. The temperature dependence of the diffusivity follows an Arrhenius-type behavior. The diffusivity is directly proportional to the radiation intensity.

Dry development of the $Ge_{0.1}Se_{0.9}$ resist using a SF_6 plasma has been implemented successfully. Features with critical dimensions down to $0.8\mu m$ have been resolved. Using the dry development, a 40% increase in the resist sensitivity has been obtained with no loss in developed image quality. Submicron patterns with critical dimension down to $0.35\lambda/NA$ have been resolved. The possibility of using feature dependent phenomena to compensate aerial image proximity effects and suppress the printability of open defects has been demonstrated by adjusting the AgSe layer thickness and exposure time.

The potential contamination effects of $Ge_{0.1}Se_{0.9}$ resist on integrated circuit devices have been studied. Junction diodes, MOS capacitors and transistor have been fabricated with and without the $Ge_{0.1}Se_{0.9}$ resist. No difference was observed in the IV, CV and CT characteristics between the devices fabricated using $Ge_{0.1}Se_{0.9}$ resist and the devices fabricated with conventional positive resist. Thus devices fabricated with $Ge_{0.1}Se_{0.9}$ resist have density of defects, oxide trapped charge, surface states and heavy metal ions comparable with those of the devices fabricated without the $Ge_{0.1}Se_{0.9}$ resist. Temperature stress of the MOS capacitors fabricated with $Ge_{0.1}Se_{0.9}$ resist show a mobile ion density of less than $10^{10}/cm^2$.

Acknowledgements

I am in debt to many people who contribute directly or indirectly to this work. First, I would like to express my sincere thanks to my research advisor Professor Andrew R. Neureuther for his guidance, encouragement, and support.

I also wish to thank Professor W. G. Oldham for his guidance, Professor Nathan W. Cheung for his advice in the material aspect of this research, Ping W. Li for his advice in IC processing, Professor Ping K. Ko for his suggestions and help in device characterization, and Professors Charles Stone and Arthur M. Hopkin for serving on my dissertation committee.

This research project began with my summer employment at Bell Labs. under the supervision of King L. Tai. I am very grateful to his generous advice in the Ge-Se resist process and the resist model during and after the employment. I am also grateful to Edith Ong and R. G. Vadimsky for their suggestions.

Contributions from fellow students John Hui, Dave Lopez, Kin Yu, Sharad Nandgaonkar, Michael Rosenfield, Gino Addiego, Keunmyung Lee, Mark Prouty, Alber Chen and the late John Reynolds are greatly acknowledged. I would also like to thank Sharad Nandgaonkar and Gino Addiego for their critical review of this manuscript.

Thanks also go to staff members of the microelectronics lab. Bob Hamilton, Kim Chan, James Parish, Dorothy McDaniel, Don Rogers and Katalin Voros for their help in the lab.

I would also like to thank my parents, brothers, sisters and particularly my wife Louise for their love, encouragement and financial support.

This research was sponsored by the National Science Foundation and Joint Services Electronic Program under grant ECS-8106234 and F49620-84-C-0057 respectively.

Acknowledgements

Table of Contents

CHAPTER 1 INTRODUCTION

1.1 Limits of optical lithography

1.2 Historical background

1.3 Dissertation Outline

CHAPTER 2 The $Ge_{0.1}Se_{0.9}$ resist process

2.1 The processing sequence

2.2 Processing equipment

2.3 Process characterization

2.4 Chemical handling

CHAPTER 3 The exposure mechanisms

3.1 Overview

3.2 Photodoping

3.3 Lateral diffusion

CHAPTER 4 The resist model and its parameters

4.1 The resist model

4.2 Resist parameter extraction

CHAPTER 5 The exposure phenomena

5.1 Introduction

5.2 The exposure model

5.3 Contrast enhancement

5.4 Edge sharpening

5.5 Feature-dependent amplification

5.6 Feature-dependent photodoping suppression

5.7 Summary of exposure phenomena

CHAPTER 6 Lithographic applications

6.1 Introduction

6.2 Resolution

6.3 Dry development

6.4 Shaping of the resist profile

6.5 Image effect compensation

6.6 Conclusions

CHAPTER 7 Contamination effects of Ge-Se resist

7.1 Introduction

7.2 Experimental

7.3 Results

7.4 Conclusions

CHAPTER 8 Conclusions and suggestions for future work

8.1 Summary

8.2 Suggestions for future work

Appendix I Ge-Se resist simulation program

Appendix II MOS capacitor process

Appendix III Modified NMOS process

Chapter 1: INTRODUCTION

§ 1.1 Limits of optical projection lithography

Optical projection lithography has become the dominant technology for pattern delineation in integrated circuit (IC) fabrication. The shrinking of feature dimensions for higher packing density and better device performance pushes the limits of optical lithography.

For an optical system with a numerical aperture NA and an exposure wavelength λ , the minimum linewidth L that can be resolved is given by the equation:

$$L = k \frac{\lambda}{NA} \quad (1)$$

where k is a 'figure of merit' whose value depends on the resist system, surface topography, substrate reflectivity, etc. The resolution limit of optical lithography can therefore be lowered by the development of optical systems with better image quality or resist systems with higher resolution. The former is pursued through the development of lenses with larger numerical aperture [1] and shorter wavelengths [2]. The latter is pursued through the development of resist material with surface induction effects [3], and resist systems which minimize the effects of surface topography and substrate reflectivity, for examples systems with multi-layer resist [4,5], anti-reflection layer [6], and contrast enhancement layer [7]. The work on the development of the bilevel Ge_xSe_{1-x} resist belongs to the latter category. The resist system combines the advantages of multi-layer resists with unique material characteristics [8] offers the highest resolution reported for any optical resist system.

§ 1.2 Historical background

The development of inorganic resists has its origin in the discovery of enhanced photosensitivity of chalcogenide films deposited on metal substrates by Kostyshin et al [9]. The term "photodoping" was subsequently introduced by Kokado et al to describe the photo-enhanced reaction between metals and chalcogenide glasses [10]. Through the

work of Kokado et al [11] and Goldschmidt et al [12], the mechanisms of photodoping of Ag in As_2S_3 have become better known. Successful application of Ag photodoping in chalcogenide glass for microlithography was first reported by Yoshikawa et al [13]. Negative relief images were produced on a $GeSe_2$ film coated with a thin layer of Ag. The resultant system has significantly higher contrast and resolution compared to polymer resists. Using a system consisting of a thin film of Ag_2Se and Ge_xSe_{1-x} on top of a planarizing layer of polymer, Tai and coworkers developed a bilevel resist system which offers the highest resolution reported for any optical resist system [14,15]. Also, Tai et al showed that $Ag_2Se / Ge_{0.1}Se_{0.9}$ system offers a photosensitivity ten times the value of $Ag_2Se / GeSe_2$ system [16]. Despite this result, $Ge_{0.1}Se_{0.9}$ resist still suffers from the disadvantage of low photosensitivity compared to positive polymer resists. The disadvantage was somewhat moderated when Huggett et al showed that $Ge_{0.1}Se_{0.9}$ resist has a photosensitivity comparable to that of positive polymer resists when developed in SF_6 plasma [17].

§ 1.3 Dissertation Outline

The modeling of the image formation in Ge_xSe_{1-x} resists was pioneered by Tai et al [18]. Among the results are two equations which describe the transport of Ag in the resist system under actinic irradiation. The development of this resist model for computer simulation, verification of this model and application of this model to optical projection lithography form the basis of this dissertation. The work reported in this dissertation can be divided into five parts: (1) Development of a simulation program for the resist model and a laboratory resist process for experiments, (2) Verification of the resist model by comparing simulation and experimental results, (3) Investigation of the exposure phenomena which affect the photodoped Ag image (latent image), (4) Application of the resist system to meet challenging lithographic requirements, and (5) Study of the contamination effects of $Ge_{0.1}Se_{0.9}$ resist on integrated circuit devices.

The $Ge_{0.1}Se_{0.9}$ resist process and its characterization are elaborated in chapter 2. The design of some of the processing equipment is also described. Chapter 3 discusses the Ag transport mechanisms which occur when the resist is under actinic irradiation. Results on the studies of these mechanisms are also presented. The resist model and the simulation program are described in chapter 4. Methods for the extraction of the resist parameters from experimental data are also elaborated. Chapter 5 discusses the exposure phenomena which affect the latent image. The conditions under which these phenomena occur are identified. Their role in optical projection lithography is characterized in terms of Ag diffusion length, exposure time and Ag_2Se layer thickness. Chapter 6 describes the applications of the resist system to resolve lithographic patterns which cannot be resolved by existing polymer resists. The advantages for using the bilevel $Ge_{0.1}Se_{0.9}$ resist system for IC fabrication are also discussed. The contamination effects of $Ge_{0.1}Se_{0.9}$ resist on IC devices are studied in chapter 7. Characteristics of MOS (Metal-Oxide-Semiconductor) capacitors and transistors fabricated using $Ge_{0.1}Se_{0.9}$ resist are compared with those fabricated using positive polymer resist (Kodak 820). Junction leakage current, surface states density and oxide charge density of the devices are quantified. Chapter 8 summarizes the principal results of this dissertation. Suggestions for future work are also given.

References

- [1] W. G. Oldham and A. R. Neureuther, "Projection lithography with high numerical aperture optics," *Solid State Technology*, vol. 24, no. 5, p.106, 1981.
- [2] V. Miller and H. L. Stover, "Submicron optical lithography: I-line wafer stepper and photoresist technology," *Solid State Technology*, vol. 28, no. 1, p.127, 1985.
- [3] D. J. Kim, W. G. Oldham and A. R. Neureuther, "Development of Positive Photoresist," *IEEE Trans. Electron Dev.*, vol. ED-31, no. 12, p. 1730, 1984.
- [4] B. J. Lin, E. Bassous, V. W. Chao and K. E. Petrillo, "Practicing the Novolac deep-UV portable conformable masking technique," *J. of Vac. Sci. Technol.*, vol. 19, no. 4, p.1313, 1981.
- [5] K. Bartlett, G. Hillis, M. Chen, R. Trutna and M. Watts, "A two-layer photoresist process in a production environment," *Proc. of SPIE*, vol. 394, p.49, 1983.
- [6] C. H. Ting and K. L. Liauw, "Improved DUV multilayer resist process," *Semiconductor International*, p. 102, Nov. 1984.
- [7] B. F. Griffing and P. R. West, "Contrast enhanced photolithography," *IEEE Electron Dev. Lett.*, vol. EDL-4, no. 1 p. 14, 1983.
- [8] K. L. Tai, E. Ong and R. G. Vadimsky, "Inorganic resist systems for VLSI microlithography," *Proc. of ECS*, vol. 82-9, p. 9, 1982.
- [9] M. T. Kostyshin, E. V. Mikhailovskaya and P. F. Romanenko, "Photographic sensitivity effect in thin semiconducting films on metal substrates," *Soviet Physics - Solid State*, vol. 8, no. 2, p.451, 1966.
- [10] H. Kokado, I. Shmizu and E. Inoue, "Discussion of the mechanism of photodoping," *J. of Non-crystalline Solids*, vol. 20, p.131, 1976.
- [11] H. Kokado, I. Shimizu, T. Tatsuno and E. Inoue, "A photo-electric study on the interface between metallic silver and vitreous As_2S_3 ," *J. of Non-crystalline Solids*, vol. 21, no. 2 p.225, 1976.

- [12] D. Goldschmidt and P. S. Rudman, "The kinetics of photodissolution of Ag in amorphous As_2S_3 films," J. of Non-crystalline Solids, vol. 22, no. 2, p.229, 1976.
- [13] A. Yoshikawa, O. Ochi, H. Nagai and Y. Mizushima, "A novel inorganic photoresist utilizing Ag photodoping in Ge-Se glass film," Appl. Phys. Lett., vol. 29, no. 10, p.677, 1976.
- [14] K. L. Tai, W. R. Sinclair, R. G. Vadimsky and J. M. Moran, "Bi-level high resolution photolithographic technique for us with wafers with stepped and/or reflecting surfaces," J. of Vacc. Sci. Technol., vol. 16, no. 6, p.1977, 1979.
- [15] K. L. Tai, R. G. Vadimsky, C. T. Kemmerer, J. S. Wagner, V. E. Lamberti, and A. G. Timko, "Submicron optical lithography using an inorganic resist/polymer bilevel scheme," J. of Vacc. Sci. Technol., vol. 17, no. 5, p.1169, 1980.
- [16] C. H. Chen and K. L. Tai, "Electron diffraction studies of Ag photodoping in Ge_xSe_{1-x} glass films," Appl. Phys. Lett., vol. 37, no. 7, p.605, 1980.
- [17] P. G. Huggett, K. Frick and H. W. Lehmann, "Development of silver sensitized Germanium Selenide photoresist by reactive sputter etching in SF_6 ." Appl. Phys. Lett., vol. 42, no. 7, p.592, 1983.
- [18] K. L. Tai, E. Ong, R. G. Vadimsky, C. T. Kemmerer and P. M. Bridenbaugh, "Modeling of image formation in $Ag_2Se/Ge-Se$ resist systems: Implications for microlithography," Proc. of ECS, vol. 82-9, p.49, 1982.

Chapter 2: THE $Ge_{0.1}Se_{0.9}$ RESIST PROCESS

§ 2.1 The processing sequence

The resist system studied in this dissertation is a bilevel resist system. It consists of a polymer layer with a $Ag_2Se / Ge_{0.1}Se_{0.9}$ system on top. The process was developed based on the work by Tai et al at Bell Labs. [1]. The processing sequence is shown in Fig. 2.1. A layer of polymer resist (AZ1350J or KTI820) is spun on the substrate for surface planarization. Hardening of the film is carried out using high temperature baking. The polymer layer has a final thickness of $1.5\mu m$. Next, a $200nm$ $Ge_{0.1}Se_{0.9}$ film is deposited using e-beam evaporation. A $9nm$ Ag_2Se layer is subsequently coated by immersing in an aqueous solution of $AgNO_3$ and KCN . When the $Ag_2Se / Ge_{0.1}Se_{0.9}$ system is exposed, Ag in the Ag_2Se layer migrates to the $Ge_{0.1}Se_{0.9}$ layer; the process is called photodoping. After exposure, Ag in the top layer is stripped in an aqueous solution of KI and iodine. The final relieved image can be obtained using wet or dry etching. Wet etching is carried out by immersing in an aqueous solution of $(CH_3)_4NOH$ and Na_2S . Dry etching is carried out in SF_6 plasma. The pattern may be transferred to the polymer layer using the portable-conformal-mask (PCM) or reactive-ion-etching (RIE) scheme. In the PCM scheme, the $Ge_{0.1}Se_{0.9}$ layer serves as a contact mask and the polymer resist is delineated by first flood exposing under UV light and then etching in positive resist developer. In the RIE scheme, the $Ge_{0.1}Se_{0.9}$ layer serves as an RIE etch mask and the polymer layer is delineated by reactive ion-etching in oxygen plasma.

§ 2.2 Processing equipments

All the equipment used in this process is readily available in the Berkeley microfabrication laboratory except the containers holding the chemical solutions. The containers are designed to maintain the cleanliness and control the temperature of the chemical baths, which are necessary for obtaining consistent experimental results. Fig. 2.2 shows the design of the containers. The core of the design is a cascaded structure in which the

chemical solution circulates. The circulation is maintained by a micro-pump. The micro-filter removes particulates in the solution. The cascade structure sits in a plastic box containing water which controls the temperature of the chemical solution. The water is circulated from a temperature-controlled circulation bath.

The lithography equipment used for the experiments in this dissertation includes: A GCA DSW6200 stepper, a 10X mask reduction camera, and a Canon 4X stepper. The GCA stepper has a numerical aperture (NA) of 0.28, an open field intensity (I_0) of $500mW/cm^2$, a partial coherence factor (σ) of 0.7 and an exposure wavelength (λ) of $436nm$. The 10X camera has a NA of 0.35, an I_0 of $2mW/cm^2$, a σ which can be varied between 0.1 and 1 and a λ of $436nm$. The Canon stepper has a NA of 0.28, an I_0 of about $50mW/cm^2$, a σ of 0.3 and exposure wavelengths of 404 and $436nm$.

§ 2.3 Process characterization

§ 2.3.1 Surface planarization

Surface planarization provides a relatively flat surface which allows a thin ($200nm$) $Ge_{0.1}Se_{0.9}$ layer with uniform thickness to be deposited. Surface planarization is accomplished by spin-coating a thick polymer layer on the substrate. Polymer resists such as AZ1350J and KTI820 are used in this process because they are readily available and easy to apply. The absorptivity of these materials also helps to minimize the amount of light reflected from the substrate which can degrade the quality of the image formed at the surface of the $Ge_{0.1}Se_{0.9}$ layer (latent image) [2].

The upper limit on the thickness of the polymer layer is governed by the feasibility of transferring the pattern from the $Ge_{0.1}Se_{0.9}$ layer to the polymer layer without a large linewidth variation. The lower limit is determined by the height of the surface topographical features. Results of study reported by White et al [3] show that a $0.5\mu m$ step height can be planarized to $0.1\mu m$ with a polymer coating of less than $1.5\mu m$. In this process, the polymer has a nominal thickness of $1.3\mu m$. The film is hardened in an con-

vection oven. The baking temperature and time is determined by the technologies used for the pattern transfer process. The PCM scheme requires the polymer resist layer to be sensitive to UV radiation. The requirement is satisfied when the resist is baked at 90°C for 20–30 seconds. The RIE scheme requires the polymer resist to be baked at a temperature higher than 180°C for 1 hour in order to minimize the amount of under-cutting during the etch.

§ 2.3.2 Ge_xSe_{1-x} deposition

To maintain uniform Ge_xSe_{1-x} film composition, e-beam evaporation is used for depositing the film. The resultant film has a composition of $x=0.1$. The composition was verified by the result of Rutherford Backscattering Spectrometry (RBS). Fig. 2.3 (a) shows the RBS spectra of a computer simulated Ge_xSe_{1-x} sample with $x=0.1$. The sample contains a layer of polymer in the bottom, a 20nm $Ge_{0.1}Se_{0.9}$ film in the middle and a 9nm Ag_2Se film in the top. The polymer layer, consisting of carbon and oxygen, has its spectral yield concentrated in the low energy region between channel 0 to 200. The spectral yield of the Ge and Se lies between channel 400 and 450 and the spectral yield of Ag lies between channel 450 and 500. The RBS spectra of typical Ge_xSe_{1-x} resist sample prepared in Berkeley Microfabrication Lab. (BML) is shown in Fig. 2.3 (b). The spectral yield of the Ge and Se elements in this sample is approximately equal to that of the Ge and Se in the simulated sample. The result confirms that the deposited Ge_xSe_{1-x} film has a composition of $x=0.1$.

The e-beam evaporated $Ge_{0.1}Se_{0.9}$ film has a phase-separated columnar structure. Results of studies reported by Phillips [4] and Tai et al [5] show that the film is composed of two kinds of columns: the Se-rich and the Ge-rich. The columns have diameters in the 20–30nm range. The columnar structure accounts for the anisotropic etching of the $Ge_{0.1}Se_{0.9}$ film in the wet development process.

The lower limit on the film thickness is imposed by the pin-hole density and the upper limit is restricted by the amount of under-cutting that occurs during the

development process. A thicker film has smaller pin-hole density but takes longer to develop through and hence has more severe undercutting than a thinner film. The $Ge_{0.1}Se_{0.9}$ films deposited in BML have thickness between 200–300nm. The range is chosen based on the results reported by Tai et al [1] which show that a $Ge_{0.1}Se_{0.9}$ film thicker than 0.2 μm has zero pin-hole density. The thickness of the deposited film can be measured by the etch time calibrated against RBS measurement.

§ 2.3.3 Ag sensitization

Ag sensitization is the process of coating a thin Ag_2Se film on the $Ge_{0.1}Se_{0.9}$ film to make the resist system sensitive to radiation. The process is carried out by immersing in an aqueous solution of KCN and $AgNO_3$. The chemical aspects of this process are documented by Tzinis et al and Lamberti et al [6] and [7]. The growth rate of Ag_2Se on $Ge_{0.1}Se_{0.9}$ is a function of time and temperature.

The functional dependence of Ag_2Se layer thickness on immersion time has been studied at Berkeley. Wafers coated with $Ge_{0.1}Se_{0.9}$ film were immersed in an aqueous solution of KCN and $AgNO_3$ at room temperature (27°C) for different lengths of time. The thicknesses of the Ag_2Se films were measured using RBS technique. The results are shown in Fig. 2.4 where the Ag_2Se layer thickness is plotted as a function of immersion time. The growth rate is approximately constant with a value of 0.15nm/s showing that the sensitization reaction is not diffusion limited for the range of sensitization time taken in this experiment. Similar results were also obtained by Lamberti et al [7].

The thickness of the Ag_2Se layer has significant effects on the sensitivity of the resist. Results reported by Lamberti et al [7] show that an optimum thickness exists at which the exposure energy required for the printing of a pattern is minimum. The sensitivity of $Ge_{0.1}Se_{0.9}$ resist as a function of the Ag_2Se resist thickness originally published by Lamberti et al [7] is shown in Fig. 2.5. The optimum Ag_2Se layer thickness lies between 8–10nm. Using a thickness value outside this range results in significant loss in photo-sensitivity. Fig. 2.4 shows that a Ag_2Se layer of thickness in this range can be

obtained with a sensitization time of 60 seconds. The effects of Ag_2Se layer thickness on the photodoping rate and therefore the sensitivity of $Ge_{0.1}Se_{0.9}$ resist will be discussed in detail in chapter 5.

§ 2.3.4 Exposure

When an $Ag_2Se/Ge_{0.1}Se_{0.9}$ system is under exposure, Ag in the Ag_2Se layer migrates downward into the $Ge_{0.1}Se_{0.9}$ layer and the process is called photodoping. Unlike polymer resist, $Ge_{0.1}Se_{0.9}$ resist is not reciprocal. That is, keeping the exposure energy constant, different exposure time and intensities produce different photodoped Ag distributions (latent images). In addition, the exposure energy required for the printing of a pattern depends on the development technique. In general, because of the material characteristics of the resist (see chapter 3), large exposure and development windows are obtained at high exposure dosages. In normal practice, a 10% development latitude can be obtained using exposure doses of 90 and $140mJ/cm^2$ for dry and wet development respectively.

§ 2.3.5 Ag stripping

Ag stripping is the first of the two-stage development process. Ag stripping is carried out by immersion in an aqueous solution of KI and KI_3 solution for 30–45 seconds. The chemistry of this process is published in [8]. During the stripping process, Ag atoms in the Ag_2Se layer react with the solution to form soluble complex $KAgI_2$. The process has a large process latitude because the attack by the stripping solution on the photodoped Ag in the $Ge_{0.1}Se_{0.9}$ layer is much slower than that on the Ag in the Ag_2Se layer. For a normal exposure of 0.45 second with the GCA stepper, the stripping time can be varied from 30 to 45 seconds without producing noticeable difference in the resultant developed pattern.

§ 2.3.6 Ge-Se etching

The second stage of the development is the etching of the unexposed $Ge_{0.1}Se_{0.9}$ areas. The development is carried out by immersing in a 2-component developer or in SF_6 plasma. The 2-component developer is an aqueous solution of Na_2S and a strong alkali such as $NaOH$ or $(CH_3)_4NOH$. The Na_2S attacks the Se-rich columns in the $Ge_{0.1}Se_{0.9}$ film and the $NaOH$ attacks the Ge-rich columns. The concentrations of the Na_2S and the alkali are adjusted so that the etch rate of the Se-rich columns is slower than the etch rate of the Ge-rich columns. During the development process, etching of the Ge-rich columns is rapid in the unexposed area. As the etching proceeds, the uncovered Se-rich columns are attacked not only from the top but also from the side. The complete etching of the film in the unexposed region therefore requires roughly etching to the radius of the Se-rich columns ($\approx 10nm$). In the exposed area, however, the surface of the $Ge_{0.1}Se_{0.9}$ film is protected by the photodoped Ag and on the side by the relatively insoluble Se-rich columns. Consequently, very little undercutting occurs during the development process. This anisotropic wet-development mechanism was discovered and verified experimentally by Tai et al [5].

The anisotropic etch results in high development contrast of 5-6 [1] and large development latitude of + and - 10% [9]. Fig. 2.6 shows the SEM micrographs of L/S features with linewidths of 0.8 to $10\mu m$ after the pattern-transfer step. The $Ge_{0.1}Se_{0.9}$ pattern was developed using the 2-stage wet development and the polymer layer was defined using RIE in oxygen plasma. The high development contrast enables the simultaneous printing of these features with less than 10% linewidth variation.

Dry development of the $Ge_{0.1}Se_{0.9}$ film using CF_4 or SF_6 plasma was reported by Vadimsky et al [8] and Huggett et al [10] respectively. Using reactive ion etching in SF_6 plasma, Huggett et al obtained a development contrast of 7 and a sensitivity of $50mJ/cm^2$ in the $Ge_{0.1}Se_{0.9}$ resist. In the Berkeley micro-fabrication labs., dry development is carried out in a Plasma Therm parallel-plate reactor with SF_6 gas at $40\mu m$

pressure, 30Watt power, 15sccm flow rate for 40 seconds. Using such conditions, a sensitivity of $90mJ/cm^2$ was obtained. The advantages and results of using dry development for micro-lithography will be discussed in chapter 6.

§ 2.3.7 Pattern transfer

Patterns in the $Ge_{0.1}Se_{0.9}$ layer can be transfer to the planarizing polymer layer using two different technological schemes: portable conformal mask (PCM) and reactive ion etching (RIE). Both schemes have been successfully implemented at Berkeley.

§ 2.3.7.1 PCM scheme

In the PCM scheme, the polymer layer is photosensitive and the $Ge_{0.1}Se_{0.9}$ layer serves as a portable conformable mask for the delineation of the polymer layer. The delineation of the polymer layer is carried out using flood exposure under radiation to which the polymer layer is photosensitive; followed by development in specific developer suitable for the polymer layer. The success of the PCM scheme relies on the high absorptivity of the $Ge_{0.1}Se_{0.9}$ layer in stopping the actinic radiation from reaching the underlying photosensitive polymer layer. Fig. 2.7 shows the transmission spectrum of Ge_xSe_{1-x} films published by Tai et al [1]. The high absorptivity of the $Ge_{0.1}Se_{0.9}$ film at radiation wavelengths less than $0.45\mu m$ enables the polymer layer to be delineated with the same radiation wavelength as that used for delineating the $Ge_{0.1}Se_{0.9}$ resist. Printing of sub-micron features using the PCM schemes with $Ge_{0.1}Se_{0.9}$ resist as the top layer and polymer resists which are sensitive to deep UV (PMMA) and UV (AZ2400) radiation as the underlying layer were demonstrated by Tai et al [11].

The inorganic PCM scheme developed at Berkeley uses UV resists such as AZ1350J and KTI820 for the planarizing layer and the $Ge_{0.1}Se_{0.9}$ resist on the top. Both the $Ge_{0.1}Se_{0.9}$ and polymer resist are delineated using UV light. Fig. 2.8 shows the SEM micrographs of L/S features defined using the PCM scheme. The $Ge_{0.1}Se_{0.9}$ resist was delineated using the Canon stepper which has exposure wavelengths of 404 and 436nm.

The AZ1350J resist was delineated by flood exposure in the Kasper contact printer which has a broad-band spectrum of a mercury arc lamp. Features with linewidths down to $0.9\mu\text{m}$ were well resolved.

§ 2.3.7.2 RIE Scheme

$\text{Ge}_{0.1}\text{Se}_{0.9}$ glass has a high dry-etch resistance to an oxygen plasma [10,11]. Therefore the patterned $\text{Ge}_{0.1}\text{Se}_{0.9}$ resist can be used as a mask for the reactive-ion-etching of the underlying polymer layer. The RIE scheme has many advantages over the PCM scheme: (1) The polymer resist layer need not be photosensitive, therefore material for the planarizing layer can be chosen to optimize for other processing requirements. For instance high temperature polymer like polyimide which can withstand higher current density without deformation during ion implantation can be used. (2) The etch profile can be controlled easily to meet process requirements such as those required for the lift-off process.

In BML, the reactive ion etching of the polymer layer is carried out in a Plasma Therm parallel-plate reactor with oxygen plasma at $8\mu\text{m}$ pressure, 150W power and 10sccm flow rate. a etch rate of $0.25\mu\text{m}/\text{min}$ is obtained for the etching of KTI820 polymer resist. The result of etching using these conditions is illustrated in Fig. 2.9 where the cross section of $0.5\mu\text{m}$ lines in a $1.5\mu\text{m}$ pitch defined on $1.3\mu\text{m}$ KTI820 is shown. The $\text{Ge}_{0.1}\text{Se}_{0.9}$ layer serving as the RIE mask is also shown. The high quality of the etching is illustrated by the steep side-wall slope of the resist profile.

§ 2.4 Chemical handling

The $\text{Ge}_{0.1}\text{Se}_{0.9}$ resist process uses chemicals which are poisonous and carcinogenic, for example, KCN and Se. To avoid any accident which can endanger the life of the user or other people working in the laboratory, these chemicals must be handled with extreme care. The procedure of handling these chemicals in Berkeley Micro-Fabrication Laboratory is outlined below.

KCN when mixed with acids produces HCN, a very toxic gas, therefore the sensitization bath must be kept away from any acid. In the laboratory, the sensitization, stripping and development bath are kept in the same sink since the solutions are base in nature and they do not react with each other. The sink however is prohibited for any processing which involves acid. When changing the sensitization solution, the chemical waste (old solution) is kept in plastic or glass bottles for disposal through a regulated disposal agency. Pouring cyanide solution down the sink is prohibited by environmental law.

The glass chamber of the e-beam evaporator can be cleaned using RT2 solution which contains sulfuric and chromic acid. To avoid selenium contamination, the resultant chemical waste should be discarded using the same procedure for the disposal of the KCN waste.

References

- [1] K. L. Tai, W. R. Sinclair, R. G. Vadimsky and J. M. Moran, "Bi-level high resolution photolithographic technique for use with wafers with stepped and/or reflecting surfaces," J. of Vacc. Sci. Technol., vol. 16, no. 6, p.1977, 1979.
- [2] A. R. Neureuther, P. K. Jain and W. G. Oldham, "Factors affecting linewidth control including multiple wavelength exposure and chromatic aberration," Proc. of SPIE, vol. 275, p.110, 1981.
- [3] L. K. White, "Planarization properties of resist and polyimide coatings," J. of ECS, vol. 130, no. 7, p.1543, 1983.
- [4] J. C. Phillips, "Phase separation and submicrostructure in semiconductive glasses," Proc. of ECS, vol. 82-9, p.147, 1982.
- [5] K. L. Tai, E. Ong, R. G. Vadimsky, C. T. Kemmerer, and P. M. Bridenbaugh, "Model of image formation in $Ag_2Se/Ge-Se$ resist systems: Implication for microlithography," Proc. of ECS, vol. 82-9, p.147, 1982.
- [6] C. H. Tzini, C. H. Chen and C. T. Kemmerer, "The reaction products of silver ions and Ge-Se glasses," Proc. of ECS, vol. 82-9, p.157, 1982.
- [7] V. E. Lamberti, S. M. Vincent, C. T. Kemmerer and R. G. Vadimsky, "Growth of c- Ag_2Se on g- $Ge_{0.1}Se_{0.9}$ inorganic photoresist: The effect of its thickness on lithographic performance," Proc. of ECS, vol. 82-9, p.191, 1982.
- [8] R. G. Vadimsky, K. L. Tai, E. Ong, " $Ag_2Se/Ge-Se$ resist systems," Proc. of ECS, vol. 82-9, p.37, 1982.
- [9] K. L. Tai, R. G. Vadimsky, C. T. Kemmerer, J. S. Wagner, V. E. Lamberti, and A. G. Timko, "Submicron optical lithography using an inorganic resist/polymer bilevel scheme", J. of Vacc. Sci. Technol., vol. 17, no. 5, p.1169, 1980.
- [10] P. G. Huggett, K. Frick and H. W. Lehmann, "Development of silver sensitized Germanium-Selenide photoresist by reactive sputter etching in SF_6 ," Appl. Phys.

Lett., vol. 42, no. 7, p.592, 1983.

- [11] K. L. Tai, E. Ong and R. G. Vadimsky, "Inorganic resist systems for VLSI microlithography." Proc. of ECS, vol. 82-9, p.9, 1982.

Figure captions

Fig. 2.1 Process sequence of the bilevel $Ge_{0.1}Se_{0.9}$ resist system.

Fig. 2.2 Schematic of the chemical bath container.

Fig. 2.3 RBS Spectra of (a) simulated $Ag_2Se / Ge_{0.1}Se_{0.9}$ sample and (b) actual.

Fig. 2.4 Ag_2Se layer thickness as a function of sensitization time.

Fig. 2.5 Sensitivity of $Ge_{0.1}Se_{0.9}$ resist as a function of Ag_2Se layer thickness. (Courtesy of Lamberti et al [7]).

Fig. 2.6 SEM micrographs of (a) L/S features with linewidths of 0.8 to $10\mu m$ defined using the GCA stepper with $225mJ/cm^2$, (b) magnified L/S features in (a) with linewidths of 0.8, 1.0 and $1.25\mu m$.

Fig. 2.7 Transmission characteristics of $Ag_2Se / Ge-Se$ system. (Courtesy of Tai et al [1])

Fig. 2.8 SEM micrographs of (a) L/S features with linewidths of 2.5, 1.25, and $0.93\mu m$ defined using the Cannon stepper and flood exposure under mercury arc lamp. (b) cross-section of the $1.25\mu m$ L/S feature. and (c) cross-section of the $0.93\mu m$ L/S feature.

Fig. 2.9 SEM micrograph of $0.5\mu m$ resist lines in $1.5\mu m$ pitch defined using the RIE scheme.

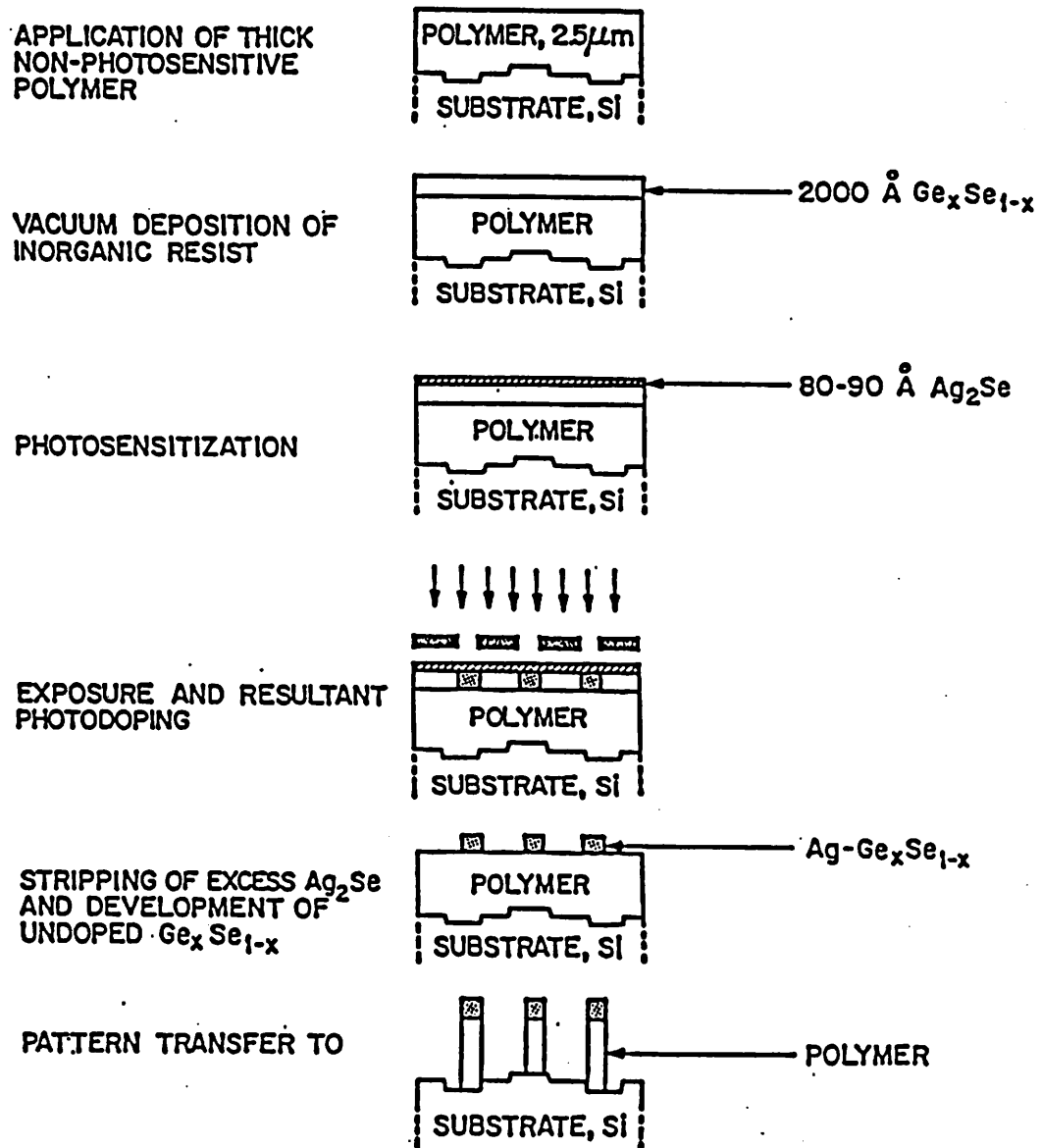


Fig. 2.1

THE DESIGN OF THE CIRCULATION TANK

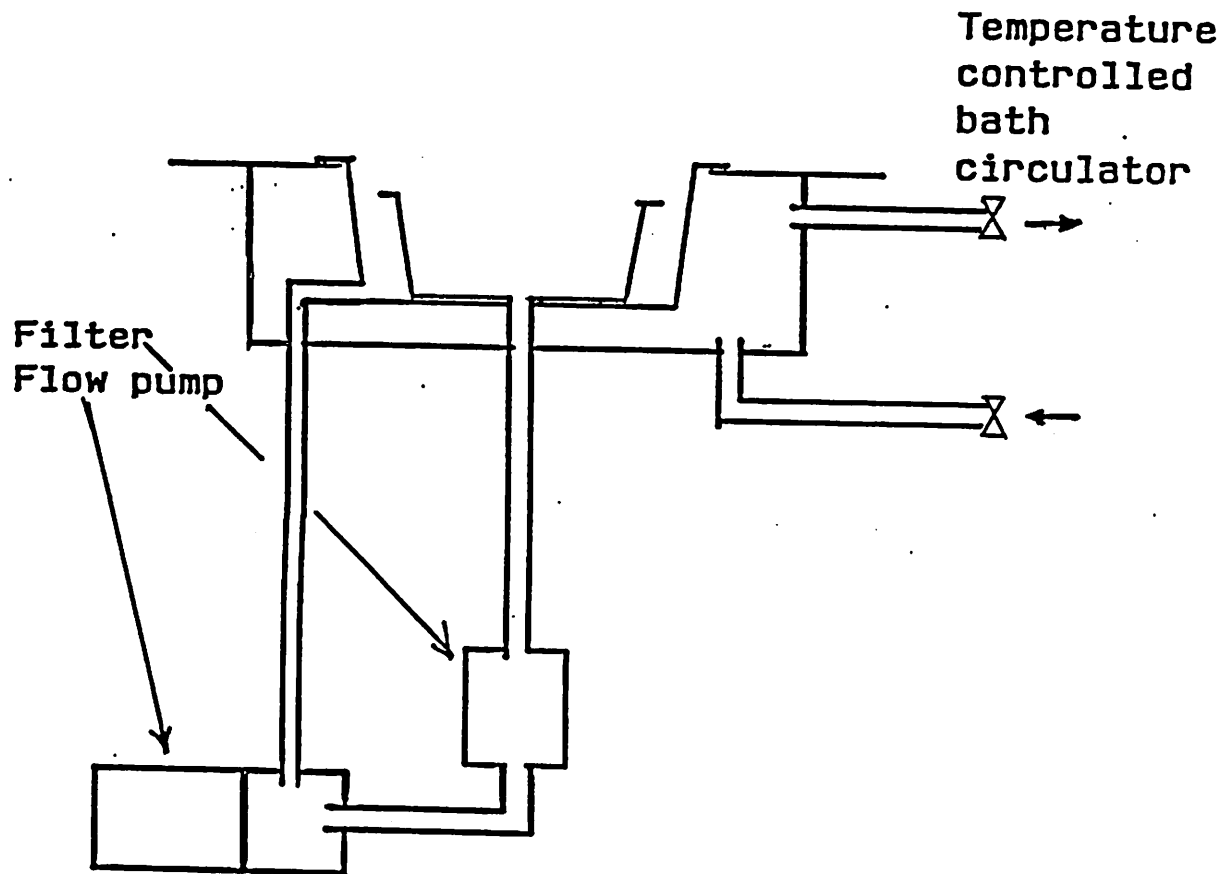


Fig. 2.2

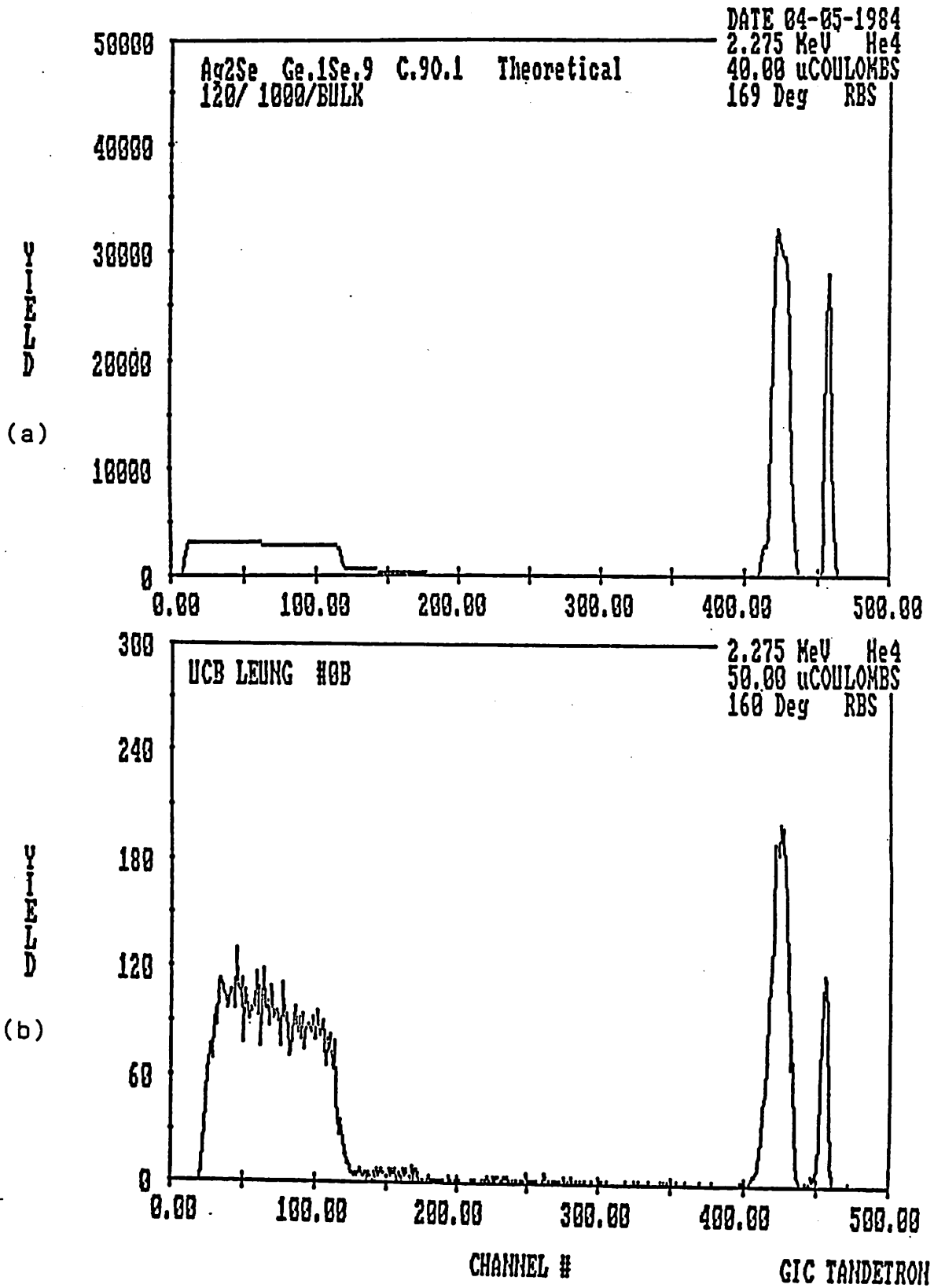


Fig. 2.3

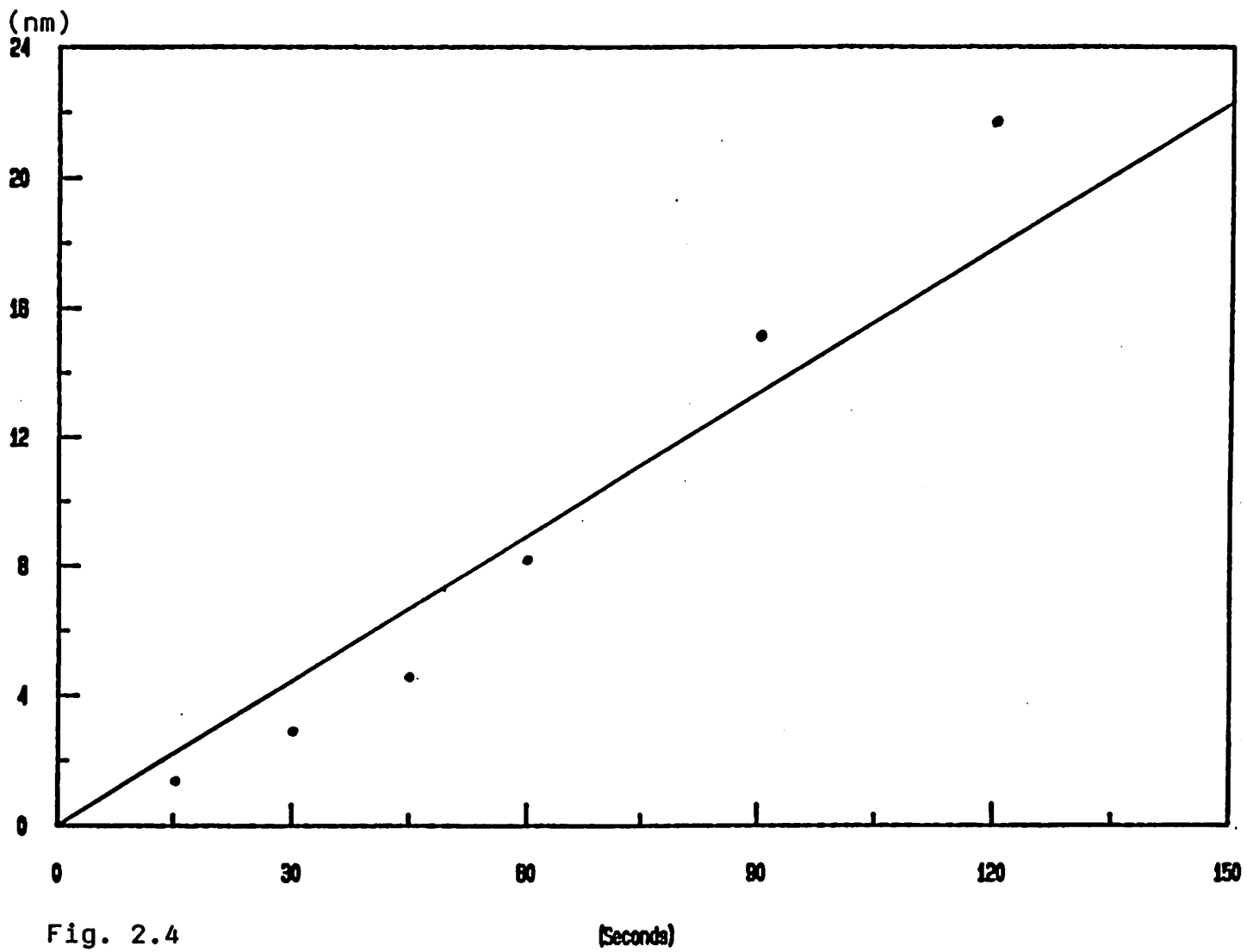
Ag₂Se thickness vs. sensitization time

Fig. 2.4

(Seconds)

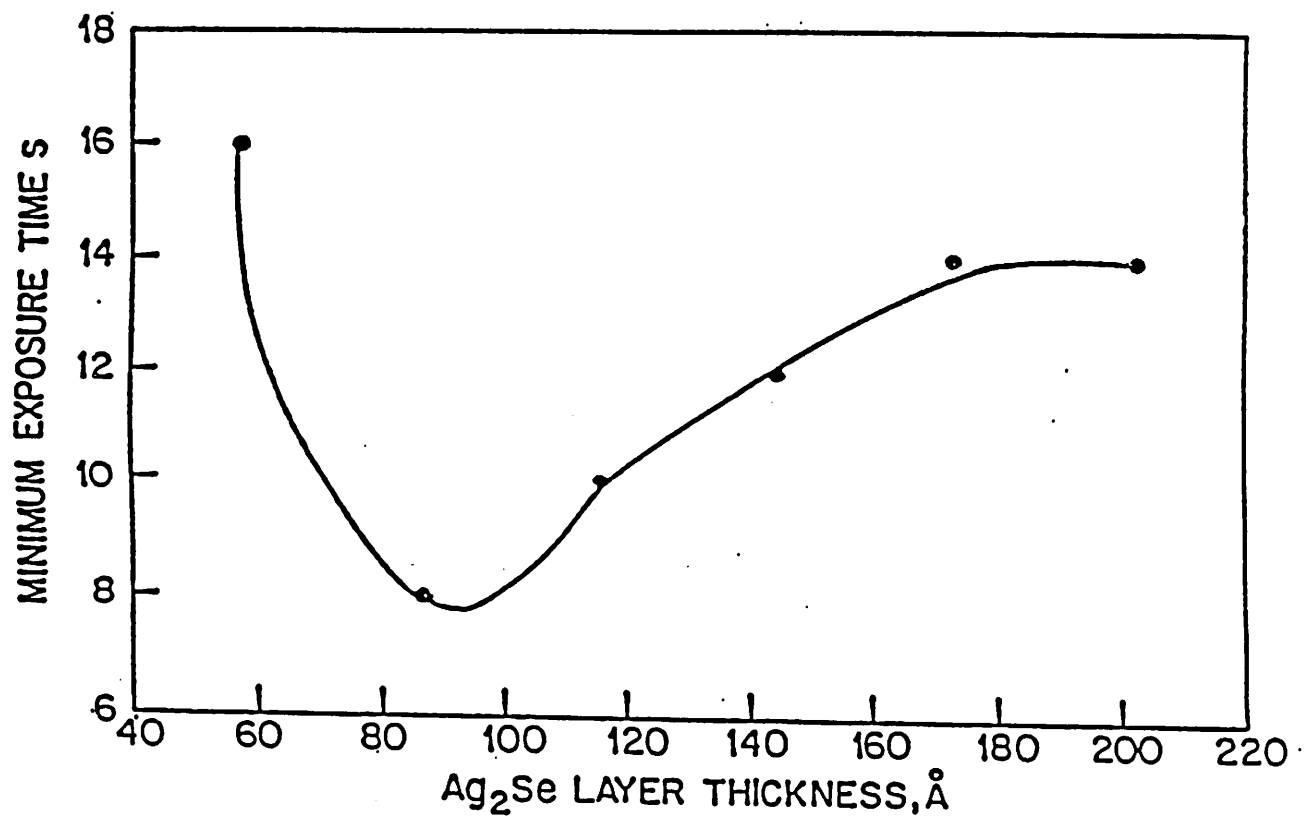


Fig. 2.5

(a)

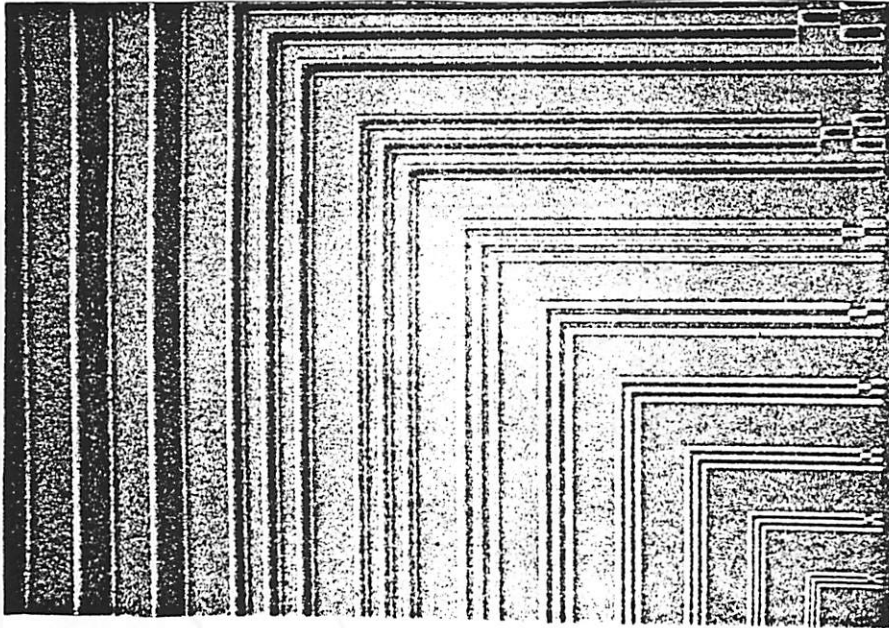
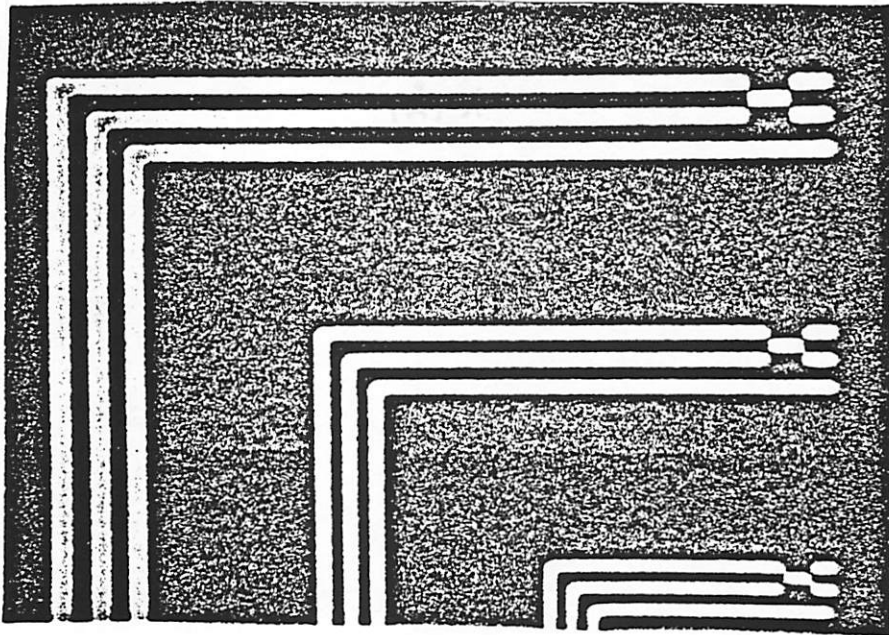


Fig. 2.6

(b)



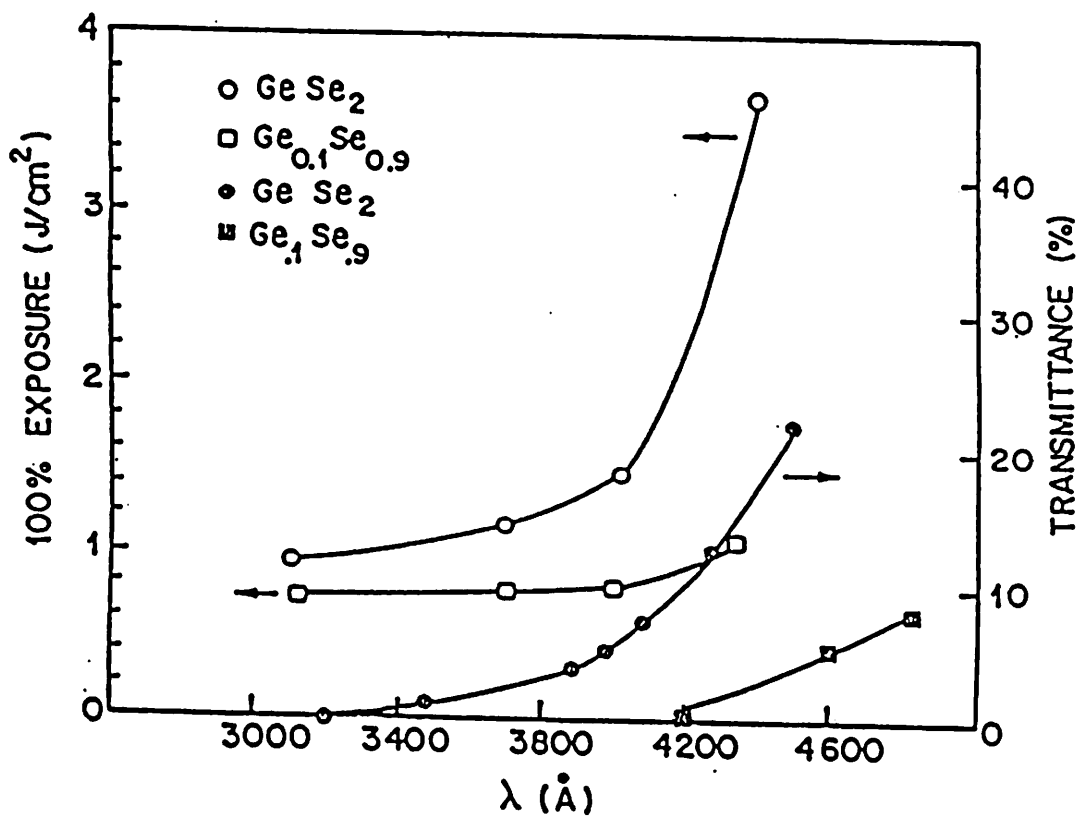
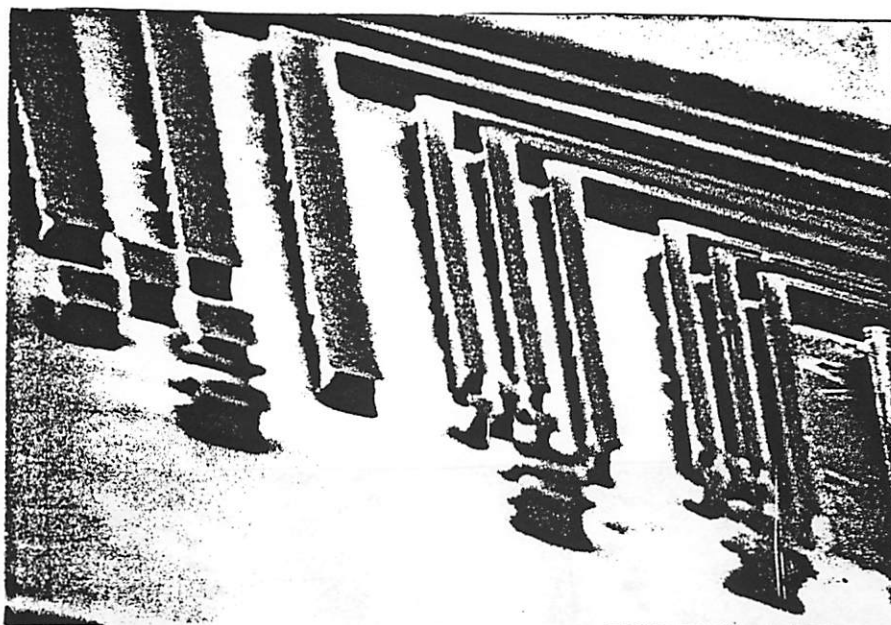
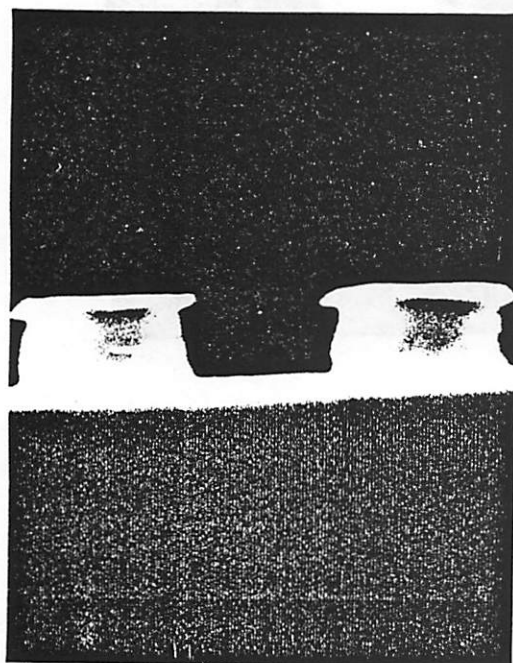


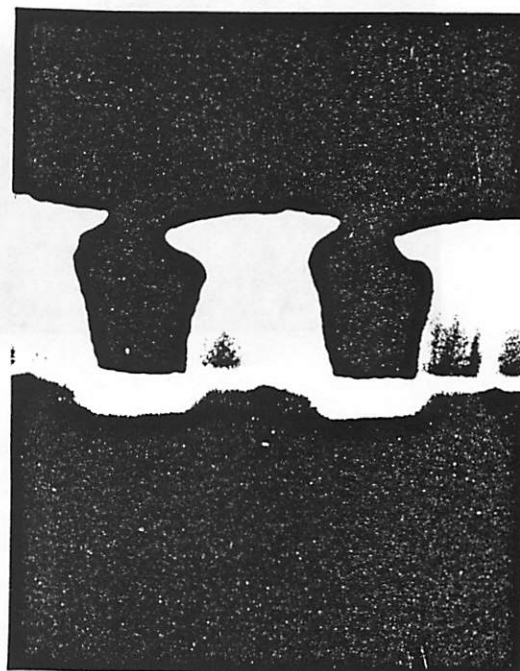
Fig. 2.7



(a)



(b)



(c)

Fig. 2.8

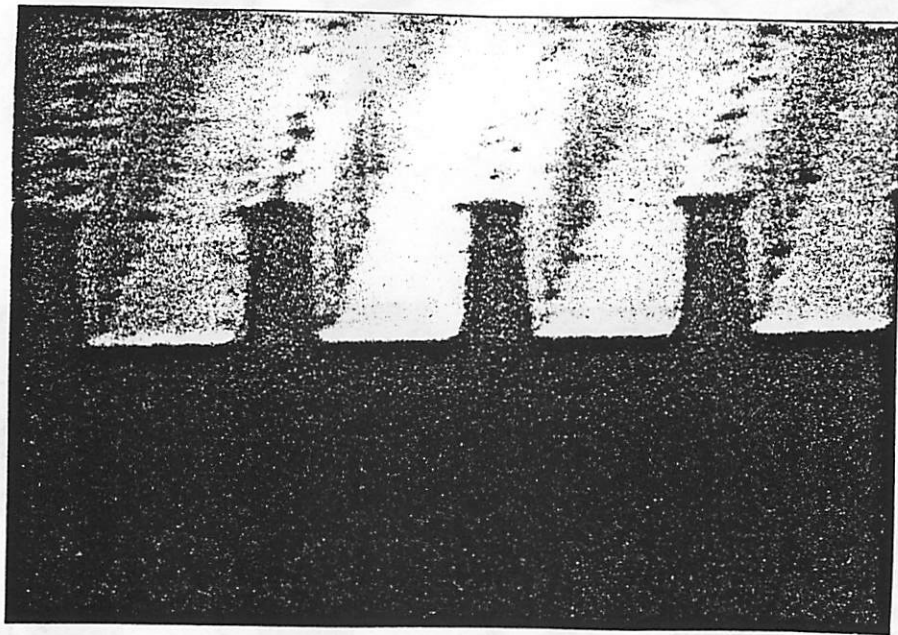


Fig. 2.9

(c)

(d)

Fig. 2.9

Chapter 3: THE EXPOSURE MECHANISMS

§ 3.1 Overview

The active components of the Ge_xSe_{1-x} resist system consists of a thin layer of Ag_2Se ($\approx 9nm$) on top of a film of Ge_xSe_{1-x} ($\approx 200nm$) glass. A thick organic planarizing layer ($\geq 1.3\mu m$) beneath the Ge_xSe_{1-x} film completes the "bi-level" resist system [1]. As illustrated in Fig. 3.1, during the exposure process, Ag in the bright region migrates from the Ag_2Se layer downward into the Ge_xSe_{1-x} film. The process is called photodoping. Photodoping creates Ag concentration gradients in the Ag_2Se layer and causes Ag to diffuse laterally from dark to bright areas [2]. The mechanisms of photodoping and lateral diffusion are responsible for forming the latent image, that is, the concentration distribution of the photodoped Ag. For a typical exposure with UV radiation, the photodoped Ag stays in a 10–20nm region in the upper-most part of the Ge_xSe_{1-x} film. Since the development rate in an area depends on the local photodoped Ag concentration, the latent image plays an important role in determining the quality of the developed image. The photodoping and lateral diffusion mechanisms are the subjects of study in this chapter.

§ 3.2 Photodoping

§ 3.2.1 Overview

The term "photodoping" was first introduced by Shimizu et al [3-5] to describe the migration of a metal into chalcogenide glasses upon exposure to radiation. Recent success in the application of Ag photodoping in Ge_xSe_{1-x} glass resulted in a resist system which has the highest resolution reported for any optical resist system [6]. Despite the dramatic progress in the application of Ag photodoping, the mechanism of Ag photodoping in chalcogenide glasses is still not well understood. The mechanism has been the subject of investigation in many research groups [7-17]. However, most of the investigations has been focused on As_2S_3 systems and the kinetics of photodoping in Ge_xSe_{1-x} and

As_2S_3 systems appear to be different [7,18]. Even within the Ge_xSe_{1-x} family, the microstructure of $Ge_{0.1}Se_{0.9}$ film is different from that of $GeSe_2$ film [19] and the Ag photodoping mechanisms in these two systems may not be the same. The following sub-sections discuss the experiments on the study of Ag photodoping in $Ge_{0.1}Se_{0.9}$ glass carried out at Berkeley. Using the techniques of microlithography and Rutherford Back-scattering Spectrometry (RBS), the experiments were designed to "shed light" on: (1) The rate limiting process of Ag photodoping in the $Ag_2Se / Ge_{0.1}Se_{0.9}$ system, (2) The temperature dependence of the photodoping process, (3) The dependence of the process on irradiation intensity and time, and (4) The region of actinic radiation absorption which triggers the photodoping process.

Potentially, the transport of Ag in an Ag_2Se / Ge_xSe_{1-x} system takes place in three different ways: (1) the diffusion of Ag in Ag_2Se , (2) the vertical diffusion of Ag in Ge_xSe_{1-x} in the direction of grain structure, and (3) the horizontal diffusion of Ag in Ge_xSe_{1-x} against grain structure. The directions of the transport are illustrated in Fig. 3.1.

§ 3.2.2 Lateral photodoping distance versus time

In experiment 1, the horizontal transport of Ag in $Ge_{0.1}Se_{0.9}$ glass is studied. In particular, the functional dependence of Ag photodoping distance on exposure time is investigated. The experimental procedure is summarized in Fig. 3.2. Silicon wafers of 2-inch diameter were first planarized with a coating of a $1.3\mu m$ layer of AZ1350J polymer resist (PR). A layer of Ge_xSe_{1-x} was then deposited on top by E-beam evaporation. The resultant film had a composition of x equal to 0.1 and thickness of $200nm$. Next, a polymer-resist sensitization mask was formed on top of the $Ge_{0.1}Se_{0.9}$ film using the following processing steps: a layer of $1\mu m$ thick AZ1350J resist (AZ) was spin-coated on the $Ge_{0.1}Se_{0.9}$ film, delineated by contact exposure, and then etched in 1:1 water-diluted MFP314 developer. The contact exposure mask contains arrays of square openings. Next, selective Ag sensitization was carried out by immersing the wafer in an aqueous

solution of $AgNO_3$ and KCN for 15 minutes. The sensitization converts uncovered $Ge_{0.1}Se_{0.9}$ region to Ag_2Se and the thickness of the Ag_2Se is approximately $150nm$. The high absorptivity of Ag_2Se prohibits any vertical photodoping in subsequent processing steps [20]. Next, the sensitization mask was removed by first flood exposing under UV light for 3 seconds and then etching in undiluted MFP developer. The UV light source has two major spectral components of wavelengths 404 and 436 nm . The light intensity at the wafer was $14mW/cm^2$.

Flood exposure was next carried out under the same light source for different lengths of time: 0, 3, 6, 9, 15 and 20 minutes on different samples to induce photodoping. The samples were then immersed in Ge-Se developer, a 5 to 1 water-diluted AZ351 developer with added Na_2S , to remove the non-Ag-doped $Ge_{0.1}Se_{0.9}$ region. Finally, the lateral dimension of the resultant profiles was measured by a Vicker's 1000X optical microscope.

Detail features of a square for 6 and 9 minute exposures are illustrated in Figs. 3.3 (a) and (b) respectively by SEM micrographs. They are taken with the same magnification. The central part of the square is the Ag sensitized area which has a side length of $18.25\mu m$. The peripheral region is where the photodoped Ag migrated. Fig. 3.3 (c) plots the square of the width of the peripheral region (w^2) as a function of exposure time (t) for two exposure intensities. In both cases w^2 varies linearly with t . The same functional dependence is also obtained for exposure intensities of 5.8, 8.8 and 11.7 mW/cm^2 . The results agree with what predicted by Fick's diffusion equation for the transport of Ag from Ag_2Se to the $Ge_{0.1}Se_{0.9}$ region, i.e.

$$\frac{\partial C}{\partial t} = D \frac{\partial^2 C}{\partial x^2} \quad (1)$$

where C is the Ag concentration, D is the lateral diffusivity of Ag in $Ge_{0.1}Se_{0.9}$ glass and x is the lateral distance from the Ag sensitized area. Since Ag diffuses much faster in Ag_2Se , [21] the Ag photodoping process in $Ge_{0.1}Se_{0.9}$ glass is limited by the diffusion of Ag from the Ag doped to the undoped $Ge_{0.1}Se_{0.9}$ region. Equation (1) has also been used

to describe the photo-induced vertical Ag diffusion in $GeSe_2$ glass [10]. The result suggests that the rate-limiting mechanisms for Ag photodoping in $Ge_{0.1}Se_{0.9}$ and $GeSe_2$ systems may be similar. Equation (1) has a solution described by equation (2)

$$C(x) = C_0 \operatorname{erfc} \left(\frac{x}{2\sqrt{Dt}} \right) \quad (2)$$

where x is the lateral dimension perpendicular to the $Ag_2Se / Ge_{0.1}Se_{0.9}$ interface, C_0 is the Ag concentration at the edge of the sensitized region before exposure. If a threshold development model is assumed, then the regions with Ag concentration less than the threshold value is developed away and the Ag concentration at the edge of the photo-doped region $C(w)$ is equal to the threshold value. The lateral diffusivity can therefore be estimated using this value in equation (2). Table 3.1 lists the diffusivity values for different normalized threshold values ($C(w) / C_0$).

§ 3.2.3 Vertical diffusivity of Ag in $Ge_{0.1}Se_{0.9}$ glass

Experiment 2 determines the vertical diffusivity of Ag in $Ge_{0.1}Se_{0.9}$ glass under UV exposure using Rutherford Backscattering Spectrometry (RBS). This technique was used by Wagner et al in their study of Ag diffusion in $GeSe_2$ glass [10]. In our experiment, wafers were first coated with AZ1350J resist for planarization. After the deposition of $Ge_{0.1}Se_{0.9}$ film, the wafers were Ag-sensitized for 90 seconds and then flood exposed under light for different lengths of time. The light source had a spectral wavelength of 436 nm and an intensity (I) of 2 mW/cm² measured at the wafer surface. The exposures were carried out at a temperature (T) of 21°C. RBS was carried out with 2.275 MeV $4He^+$ ions. Each spectrum was taken with a dose of 2μC. By monitoring the ion-beam induced Ag movement, the ion beam was found to cause negligible Ag diffusion at this dose level.

The RBS spectra with 0 and 130 sec exposure are shown in Fig. 3.4 (a). If the samples are modeled by a structure consisting of a thin film of Ag on top of a semi-infinitely thick substrate of $Ge_{0.1}Se_{0.9}$, the solution of the diffusion equation

$$\frac{\partial C(y,t)}{\partial t} = D \frac{\partial^2 C(y,t)}{\partial y^2} \quad (3)$$

is a Gaussian distribution

$$C(y,t) = \frac{1}{\sqrt{\pi Dt}} \exp\left[-\frac{y^2}{4Dt}\right] \quad (4)$$

where C is the normalized Ag concentration distribution; y is the distance measured from the surface of the sample; D is the diffusion coefficient of Ag in $Ge_{0.1}Se_{0.9}$ and t is the exposure time. The Gaussian function G_{RBS} , which can be calculated from the RBS yield-energy profiles shown in Fig. 3.4 (a), is the result of the convolution of C and another Gaussian function G_D which models the broadening in the RBS spectra due to the energy resolution of the detector. If σ_{RBS}^2 and σ_D^2 are the variances of G_{RBS} and G_D respectively, then their relation with D is given by

$$\sigma_{RBS}^2 = 2Dt + \sigma_D^2 \quad (5)$$

Equation (5) holds for values of y less than zero which corresponds to channel numbers less than 457 in the RBS spectra. The values of σ_{RBS}^2 can be calculated from the area under the RBS spectral profile. It is plotted as a function of exposure time (t) in Fig. 3.4 (b). The functional dependence described by Equation (5) is clearly shown. The diffusion coefficient D calculated from the slope of the graph is $2.7nm^2/sec$. The intercept $\sigma_D^2 (=4 \times 10^2 nm^2)$ agrees well with the $20nm$ depth resolution of the solid state detector.

§ 3.2.4 Lateral photodoping distance versus temperature

The temperature dependence of Ag diffusivity in $Ge_{0.1}Se_{0.9}$ glass was studied in experiment 3. As shown in Fig. 3.2, the experimental procedure follows that of experiment 1. After the removal of the polymer sensitization mask, the wafer was diced into small samples of $1cm^2$ and the samples were mounted on the surface of an aluminum box for flood exposure to induce Ag diffusion. The temperature of the box was controlled by a temperature-controlled circulation bath. The spectral wavelength of the light source was $436nm$ and the intensity measured at the sample was $2mW/cm^2$. Since

Ag_2Se films aggregate at temperatures higher than $70^\circ C$, the exposures were carried out at temperatures between 10 to $70^\circ C$. The range of exposure times was between 10 to 30 minutes. Exposure time below this may result in a Ag diffusion distance less than $0.5\mu m$ which is the resolution limit of our optical microscope. The exposed samples were subsequently immersed in Ge_xSe_{1-x} developer for 30 seconds to develop away the Ge_xSe_{1-x} region lacking photodoped Ag. The lateral dimensions of the resultant patterns were measured by a Vicker's 1000X optical microscope.

The SEM picture of a resultant pattern and its cross-section profile is shown in Figs. 3.5 (a) and (b). The central square region consists of Ag_2Se and the periphery is the photodoped $Ge_{0.1}Se_{0.9}$ region. If the Ag concentration threshold of the development is the same for all the samples, then the width of the periphery region (w) is directly proportional to \sqrt{Dt} , where D is the diffusivity of Ag in $Ge_{0.1}Se_{0.9}$ glass and t is the flood-exposure time. In Fig. 3.6, $\ln \left[\frac{w^2}{t} \right]$ is plotted as a function of $1/T$, where T is the temperature during the exposure in $^\circ K$. The linearity of the plot clearly shows that the temperature dependence of the diffusion follows an Arrhenius-type equation with an activation energy Q of 5.32 Kcal/mole (0.23 eV). Fig. 3.5 (b) shows the cross section of a developed pattern. The gradual slope of the peripheral region, where photodoped Ag resides, shows that the surface diffusion is much smaller than the bulk diffusion. If this was not the case, then in the photodoped region the Ag concentration at the surface would be higher than that at the bulk, and the cross-section could show an under-cut profile. Assuming a development threshold of 0.01, the calculated lateral diffusivity of Ag at $2mW/cm^2$ intensity at 436nm wavelength is $156nm^2/s$. This value is considerably larger than the vertical diffusivity value estimated in section 3.2.3 ($2.7nm^2/s$). The result is expected because in the case of lateral diffusion, the $Ag_2Se-Ge_{0.1}Se_{0.9}$ interface is directly exposed to light. However, in the case of vertical diffusion, the interface is covered and the light which induces Ag diffusion has to penetrate the Ag_2Se layer where its intensity is attenuated. Since the diffusivity is directly proportional to the light

intensity (see results in section 3.2.5), the lateral diffusivity estimated in this section is therefore larger than the vertical diffusivity calculated in section 3.2.3.

§ 3.2.5 Reciprocity of photodoping

The dependence of lateral Ag diffusion in $Ge_{0.1}Se_{0.9}$ glass on irradiation intensity was found in the experiment 4. As shown in Fig. 3.2, the experimental procedure follows that of experiment 1 and 3. After the polymer sensitization mask was stripped, the wafer was subsequently diced into small test samples which were then flood exposed under a light source with wavelengths of 404 and 436 nm. A neutral density filter was put between the light source and the sample to control the exposure intensity (I). Filters used had transmissions of 0.5, 0.6, 0.7 and 0.8. Without the filter, the intensity measured at the sample was $14mW/cm^2$. The exposures were carried out at a room temperature of $21^\circ C$. The lengths of exposures were chosen so that the product of exposure time (t) and exposure intensity (I) is constant. Exposed samples were subsequently immersed in developer for 30 seconds to develop away the region lacking Ag.

Optical measurements show that the width of the Ag-doped region (w) in all the samples were equal to within $0.5\mu m$ which is the resolution limit of the optical microscope. The result confirms that reciprocity holds between I and t with respect to the diffusion distance. Assuming Ag concentration threshold of the development to be the same for all samples, D is directly proportional to w^2/t . In Fig. 3.7 w^2/t is plotted as a function of I and the linear relation between D and I is clearly illustrated. The reciprocity relationship studied here should not be confused with the reciprocity relationship between I and t with respect to the amount of photodoped Ag. Polasko et al showed that this relationship fails in an $Ag_2Se/GeSe_2$ system at $500kW/cm^2$ exposure at 249nm exposure wavelength [22].

§ 3.2.6 Light absorption regions and photodoping

Experiments 5 and 6 identify the region of absorption which trigger the photodop-

ing process. Experiment 5 determines whether confining the light absorption to the Ag_2Se region alone is sufficient for Ag photodoping. As shown in Fig. 3.2, the experimental procedure follows that of the first experiment except in steps (c) and (e). In step (c), Palladium (Pd) was used for the sensitization mask as it would also be used as a conformal exposure mask in the photodoping induction exposure (step (e)). The Pd layer, $0.5\mu m$ thick, was sputter-deposited on the $Ge_{0.1}Se_{0.9}$ film. To pattern the Pd layer, first a layer of spin-coated AZ1350J resist (AZ) was delineated by contact exposure and developed in 1:1 diluted MFP314 developer. Then, the AZ1350J pattern was transferred to the Pd layer by immersing in type TFB Nickel etchant. The AZ layer was subsequently removed. After selective Ag sensitization, step (e) was carried out under UV light for 10 minutes. The Pd layer completely reflects the light and thus irradiation is only in the Ag_2Se regions. Subsequently, the Pd sensitization mask is removed by TFB Nickel etchant and the non-Ag-doped region is removed by Ge-Se developer.

The lateral dimension of the resultant square patterns was measured optically. Results showed that the width of the photodoped region was essentially unchanged, that is, no obvious lateral diffusion was observed. The absence of a lateral Ag diffusion region suggests that light absorption in the Ag_2Se region alone has little effect on Ag photodoping.

Since confining light irradiation to the Ag_2Se region alone does not produce observable Ag diffusion, it is interesting to assess the effects of exposure on the $Ge_{0.1}Se_{0.9}$ region alone and this is the object of experiment 6. As shown in Fig. 3.2, the procedure for defining the Ag_2Se region with an AZ sensitization mask follows that described in experiment 1. However, in step (e), a second contact exposure mask was used to localize light irradiation to the area of interest. The mask was designed so that the light irradiation region is separated from the Ag_2Se region. The separation distance (X_c) varies from 1 to $9\mu m$. Alignment keys were installed to align the second exposure mask to the Ag sensitized area and to determine the misalignment distance (X_{ma}).

The schematic depicted in Fig. 3.8 (a) shows the cross section of a sample during the photodoping induction exposure. After the exposure, non-Ag-doped $Ge_{0.1}Se_{0.9}$ was removed by Ge-Se developer and the width of the Ag photodoping region (w) was measured optically from the pattern. Next, the misalignment distance (X_{ma}) was estimated based on the symmetry of the alignment key. The actual separation between the Ag_2Se and the irradiated region (X_a) was calculated using the following equation:

$$X_a = X_e - X_{ma} \quad (6)$$

where X_e is the intended distance between the light irradiation region and the Ag_2Se region, and X_{ma} is the misalignment distance. X_a , X_e and X_{ma} are also shown in Fig. 3.8 (a). Due to misalignment, the value of X_a can be negative, that is, the light irradiation region can overlap with the Ag_2Se region.

Fig. 3.8 (b) shows the plot of w as a function of X_a . Three regions can be distinguished: (1) For X_a values less than $0.5\mu m$, w assumes a constant value of $2.6\mu m$. In particular, the values of w are the same for the case when part of the Ag_2Se region and the $Ge_{0.1}Se_{0.9}$ region are simultaneously exposed ($X_e < 0$) and for the case when the light absorption is confined to the $Ge_{0.1}Se_{0.9}$ but in close proximity to the Ag_2Se region ($0 \leq X_a \leq 0.5\mu m$). This result can be explained by light diffraction off the edge of the second contact mask. In this case the diffracted light reaches a distance of $0.5\mu m$ into the masked area. (2) For X_a values between 0.5 to $3\mu m$, w decreases with increasing X_a and the rate is approximately linear. (3) For X_a values greater than $3\mu m$, w is essentially zero. These results together with those obtained in experiment 5 show that Ag photodoping is caused mainly by light absorption in the $Ge_{0.1}Se_{0.9}$ near the interface of the Ag containing and non-Ag-doped region. Furthermore, they show that Ag photodoping takes place even when the light irradiation is up to $3\mu m$ away from the Ag containing region. The occurrence of Ag photodoping under this condition suggests that light absorption in $Ge_{0.1}Se_{0.9}$ has a long range effect. The exact mechanism of this effect is not known. The effect may be caused by photo-contraction in the irradiated $Ge_{0.1}Se_{0.9}$ region

[23]. Since the life-time of carriers in amorphous semiconductor is short, for instance the life-time of carriers in amorphous silicon is in the range of 1 to 10ns [24], diffusion of holes and electrons in amorphous $Ge_{0.1}Se_{0.9}$ for such a long distance is not likely.

§ 3.2.7 Summary of experimental results

In summary, the photodoping of Ag in $Ge_{0.1}Se_{0.9}$ glass under UV light irradiation was studied using microlithography and RBS techniques. Lateral Ag photodoping in $Ge_{0.1}Se_{0.9}$ glass, like Ag photodoping in $GeSe_2$ glass, can be described by Fick's diffusion equation. The diffusion coefficient at $21^\circ C$ and $2mW/cm^2$ is $2.7nm^2/sec$. The temperature dependence of the diffusion follows an Arrhenius-type equation with an activation energy of 5.32 Kcal/mole and a pre-exponent factor of $2.5 \times 10^4 nm^2/sec$. The reciprocity between irradiation intensity and exposure time with respect to diffusion distance is confirmed for a narrow range of intensity ($7-14mW/cm^2$). Specifically, the diffusivity is found to be directly proportional to the irradiation intensity. The photodoping process is limited by the diffusion of Ag from Ag-doped to undoped $Ge_{0.1}Se_{0.9}$ region. Light absorption in the Ag_2Se region has little effect on Ag photodoping. Ag photodoping is caused mainly by light absorption in the $Ge_{0.1}Se_{0.9}$ near the interface between the Ag containing and non-Ag-doped region. Ag diffusion takes place even when light irradiation is away (up to $3\mu m$) from the Ag_2Se region. The occurrence of Ag photodoping under this condition suggests that light absorption in $Ge_{0.1}Se_{0.9}$ glass has a long range effect.

§ 3.3 Lateral diffusion of Ag in Ag_2Se

§ 3.3.1 Evidence in normal use

When a Ge_xSe_{1-x} resist system is under exposure, non-uniform photodoping creates a Ag concentration gradient in the top layer and causes Ag to diffuse laterally from dark (higher Ag concentration) to bright (lower Ag concentration) areas. This mechanism was first used by Tai et al to explain the edge sharpening phenomenon when

they observed that the edge of a developed resist profile is thicker than the interior of the profile [25]. This observation contradicts the prediction using the optical image alone since the light intensity at the edge is lower than that in the interior region. They explain the phenomenon by the lateral diffusion of Ag from the dark to bright area and the photodoping of most of this lateral-diffused Ag at the edge of the profile. The result is that the edge of the profile has higher photodoped Ag concentration than the central part of the profile does. The edge sharpening phenomenon will be discussed in more detail in chapter 5.

Other evidence of lateral diffusion of Ag are also published in [25]. One of the experiments was repeated at Berkeley and the result is shown in Fig. 3.9. The optical micrograph shows a test pattern which was double exposed using the Canon 4X stepper with the pattern shifted between the exposures. Of particular interest are the bright areas of the second exposure which overlap small and large dark areas of the first exposure as illustrated by region A and B respectively in the figure. The total exposure dose in region A is larger than or equal to that in region B. However, the appearance of a resist gap in region A shows that photodoped Ag concentration in region A is less than that in region B. The result can be explained by the lateral diffusion mechanism. During the first exposure, Ag in the small gap diffuses laterally to the nearby bright areas leaving only a small amount left for the second exposure.

§ 3.3.2 Estimate for lateral diffusivity of Ag in Ag_2Se

The diffusion of Ag in Ag/Se system has been studied in detail by Pines et al [26] and Johnson et al [27]. Among the results of their studies are: (1) Ag diffuses from the a region in Se to another with lower Ag concentration. (2) The diffusivity of Ag in Ag_2Se at room temperature is $1 \times 10^{-8} cm^2 / s$. (3) The temperature dependence of the diffusivity follows an Arrhenius type equation with an activation energy of $12.0 kcal / mole$. Rough estimation on the lateral Ag diffusivity of the Ge-Se resist system were also made by Tai et al based on the edge sharpening effects [25]. Their result is

in the same order of magnitude as that obtained by Johnson et al [27].

References

- [1] K. L. Tai, W. R. Sinclair, R. G. Vadimsky and J. M. Moran, "Bi-level high resolution photolithographic technique for use with wafers with stepped and/or reflecting surfaces", *J. of Vacc. Sci. Technol.*, vol. 16, no. 6, p.1977, 1979.
- [2] K. L. Tai, E. Ong, R. G. Vadimsky, C. T. Kemmerer and A. M. Bridenbaugh, "Model of image formation in $Ag_2Se / Ge - Se$ resist systems: Implications for microlithography", *Proc. of ECS*, vol. 82-9, p.49, 1982.
- [3] I. Shimizu, H. Sakuma, H. Kokado, and E. Ioue, "Metal-chalcogenides systems as imaging materials", *Photographic Sci. and Engineering*, vol. 16, no. 4, p.291, 1972.
- [4] T. Shirakawa, I. Shimizu, H. Kokado, and E. Inoue, "Relief image in Ag-Chalcogenide glass sensors", *Photographic Sci. and Engineering*, vol. 19, no. 2, p.139, 1975.
- [5] H. Kodado, I. Shimizu and E. Inoue, "Discussion on the mechanism of photodoping", *J. of Non-crystalline Solids*, vol. 20, p.131, 1976.
- [6] K. L. Tai, R. G. Vadimsky, and E. Ong, "Multi-level Ge-Se film based resist systems", *Proc. of SPIE*, vol. 333, p.32, 1982.
- [7] H. Kokado, I. Shimiza and E. Inoue, "A photoelectric study on the interface between metallic silver and vitreous As_2S_3 ", *J. of Non-cryst. Sol.*, vol. 21, p.225, 1976.
- [8] R. Ishikawa, "Photo-enhanced diffusion of Ag in amorphous Ge_2S_3 films", *Sol. Stat. Comm.*, vol. 30, p.99, 1979.
- [9] T. Suzuki, Y. Hirose and H. Hirose, "Modeling of photodoping mechanisms in Ag / As_2S_3 system through ESCA analysis", *Proc. of ECS*, vol. 82-9, p.255, 1982.
- [10] A. Wagner and D. Barr, "Silver diffusion in Germanium Selenide resist systems", *Proc. of ECS*, vol. 82-9, p.281, 1982.
- [11] J. M. Lavine, S. A. Lis, G. M. Goldberg and J. I. Masters, "Experiments on Ag-photodoping of As_2S_3 ", *Proc. of ECS*, vol. 82-9, p.265, 1982.

- [12] D. Goldschmidt and P. S. Rudman, "The kinetics of photodissolution of Ag in amorphous As_2S_3 films", J. of Non-cryst. Sol., vol. 22, p.229, 1976.
- [13] M. Janai, "Photodissolution of silver in amorphous As_2S_3 films", Phys. Rev. Lett., vol.47, no. 10, p.726, 1981.
- [14] Y. Yamamoto, T. Itoh, Y. Hirose and H. Hirose, "Backscattering measurements on Ag photodoping effect in As_2S_3 glass", J. of Appl. Phys., vol. 47, no. 8, p.3603, 1976.
- [15] C. H. Chen and K. L. Tai, "Electron diffraction studies of Ag photodoping in Ge_xSe_{1-x} glass films", Appl. Phys. Lett. 37, 605 (1980).
- [16] M. Janai, "The kinetics of the photodissolution of silver in amorphous As_2S_3 ", Proc. of ECS, vol. 82-9, p.239, 1982.
- [17] S. Zembutsu, "X-ray photoelectron spectroscopy studies of Ag photodoping in Se-Ge amorphous films", Appl. Phys. Lett., vol. 39, p.969, 1981.
- [18] K. L. Tai, E. Ong, and R. G. Vadimsky, "Inorganic resist systems for microlithography", Proc. of ECS, vol. 82-9, p.9, 1982.
- [19] J. C. Phillips, "Phase separation and submicrostructure in semiconductive glasses", Proc. of ECS, vol. 82-9, p.147, 1982.
- [20] V. E. Lamberti, S. M. Vincent, C. T. Kemmerer and R. G. Vadimsky, "Growth of $c-Ag_2Se$ on $g-Ge_{0.1}Se_{0.9}$ inorganic photoresist: The effect of its thickness on lithographic performance", Proc. of ECS, vol. 82-9, p.191, 1982.
- [21] K. L. Tai, R. G. Vadimsky, and V. E. Lamberti, "Edge-sharpening effect in $Ag_2Se / GeSe$ inorganic resist" ECS Extended Abstract, vol. 80-2, p.826, 1980.
- [22] K. J. Polasko, D. J. Ehrlich, J. Y. Tsao, R. F. W. Pease and E. E. Marinero, "Deep UV exposure of $Ag_2Se / GeSe_2$ utilizing an excimer laser", J. of Vac. Sci. Technol., vol. 3, no.1, p. 319, 1985.

- [23] K. L. Chopra, L. K. Malhotra, K. S. Harshvardhan and Bhanwar Singh, "Radiation-induced microlithographic effects in amorphous chalcogenide films", Proc. of ECS, vol. 82-9, p.129, 1982.
- [24] D. E. Carlson, "An overview of amorphous Si solar cell development", Conference Record, 14th IEEE Photovoltaic Specialists Conference, San Diego, p.291, 1980.
- [25] K. L. Tai, R. G. Vadimsky, C. T. Kemmerer, J. S. Wagner, V. E. Lamberti, and A. G. Timko, "Submicron optical lithography using an inorganic resist/polymer bilevel scheme", J. of Vac. Sci. Technol., vol. 17, p.1169, 1980.
- [26] B. Y. Pines, I. P. Grebennick, R. I. Bazyura and G. V. Zozulya, "Surface and volume diffusion in thin films of the system Ag-Se", Phys. Stat. Sol., vol. 20, p.213, 1967.
- [27] D. B. Johnson and L. C. Browns, "Lateral Diffusion in Ag-Se thin-film couples", J. of Appl. Phys., vol. 40, p.149, 1968.

Figure Captions

Fig. 3.1 The $Ag_2Se / Ge_{0.1}Se_{0.9}$ system under exposure.

Fig. 3.2 Processing sequence of the experiments for the studies of Ag photodoping.

Fig. 3.3 SEM micrograph of a square pattern showing the diffusion of Ag after 3 min exposure (a) and 6 min exposure (b). w^2 is plotted as a function of exposure time (c).

Fig. 3.4 (a) RBS yield-energy profiles for samples with 0 and 130 sec exposures. (b) σ_{RBS}^2 as a function of t .

Fig. 3.5 SEM picture of (a) the resultant pattern of a sample and (b) its cross-section.

Fig. 3.6 w^2 / t as a function of $1 / T$.

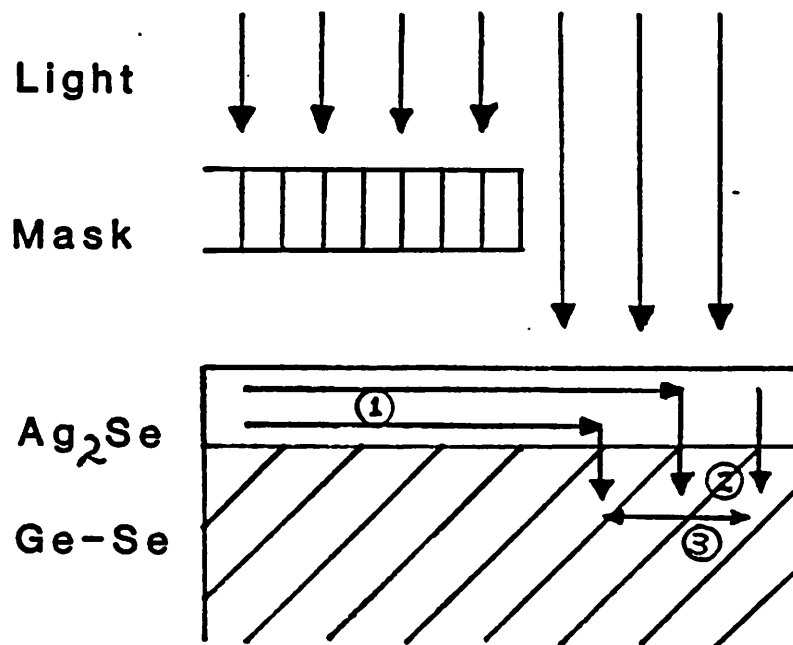
Fig. 3.7 w^2 / t as a function of I .

Fig. 3.8 (a) Schematic to illustrate a sample under photodoping induction exposure in experiment 3. (b) w as a function of the separation distance between the Ag_2Se and the irradiated region (Xa).

Fig. 3.9 A double-exposed pattern to illustrate the lateral diffusion of Ag.

Table caption

Table 3.1 Calculated lateral diffusivity values for different normalized development thresholds.



① Lateral Diffusion

② Photodoping

Fig. 3.1

Procedure of the Experiments

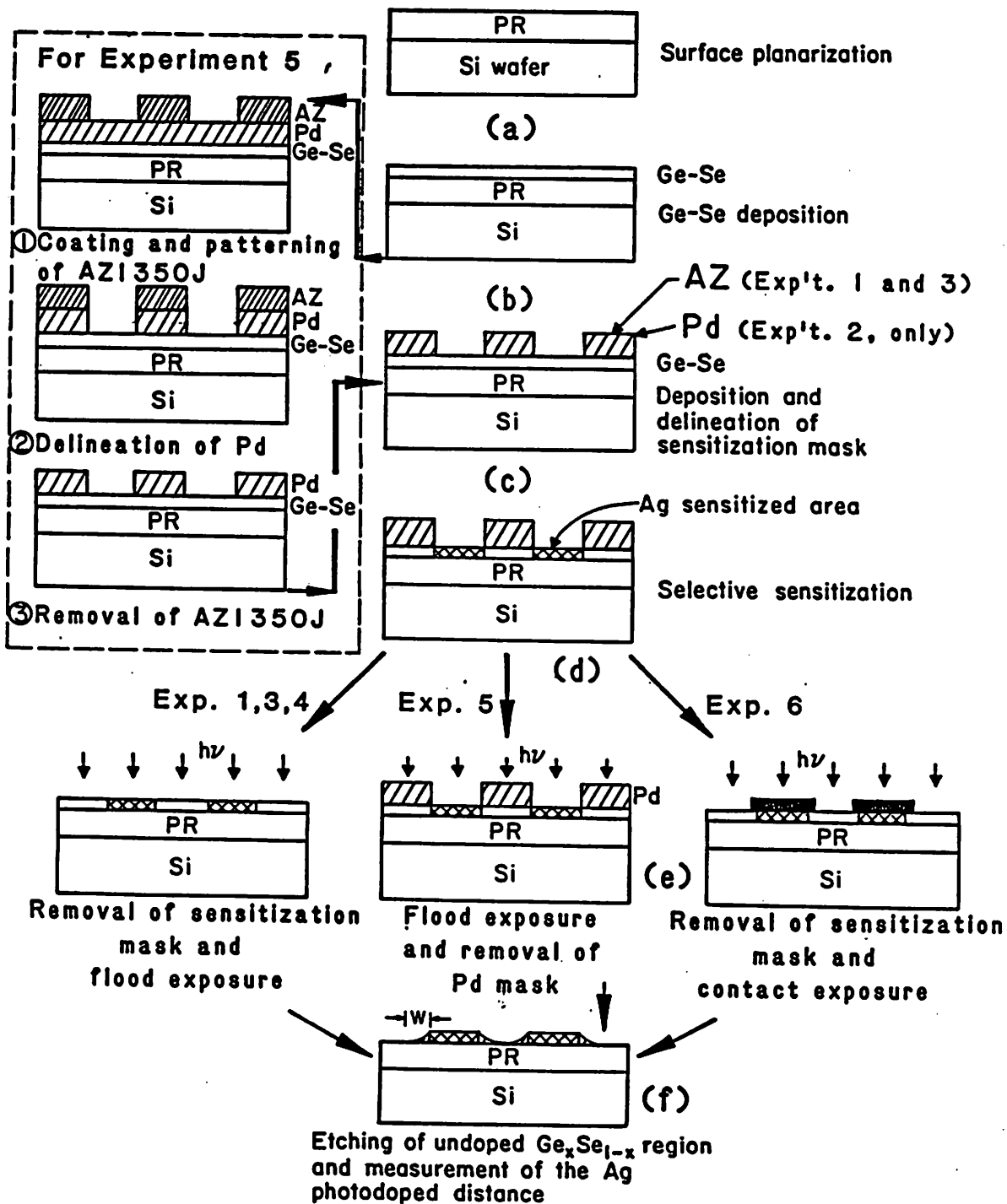


Fig. 3.2

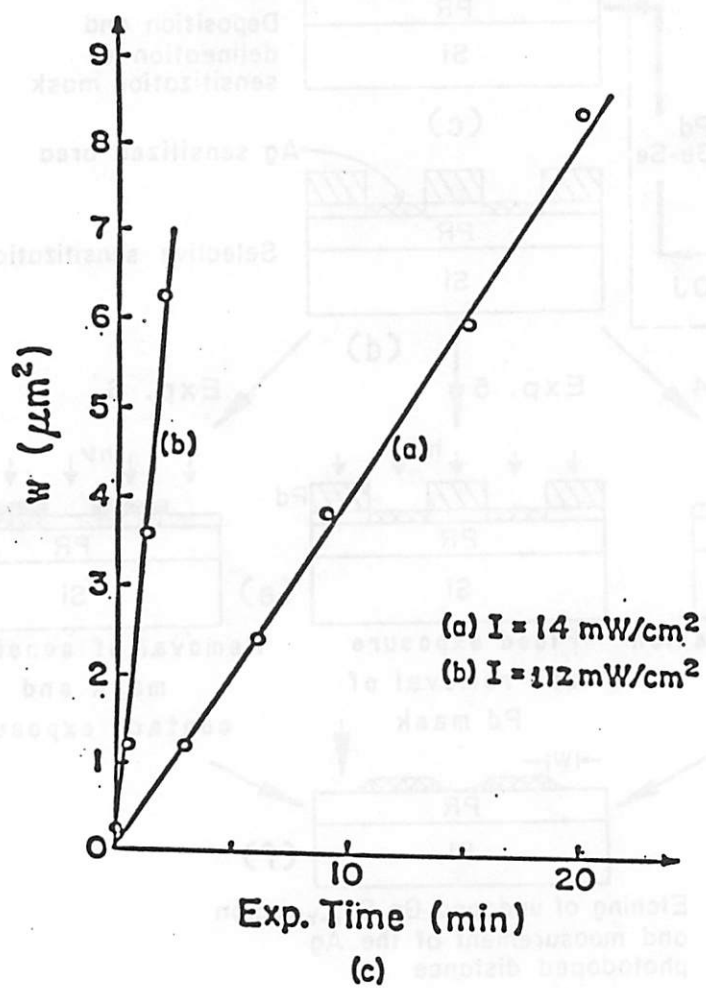
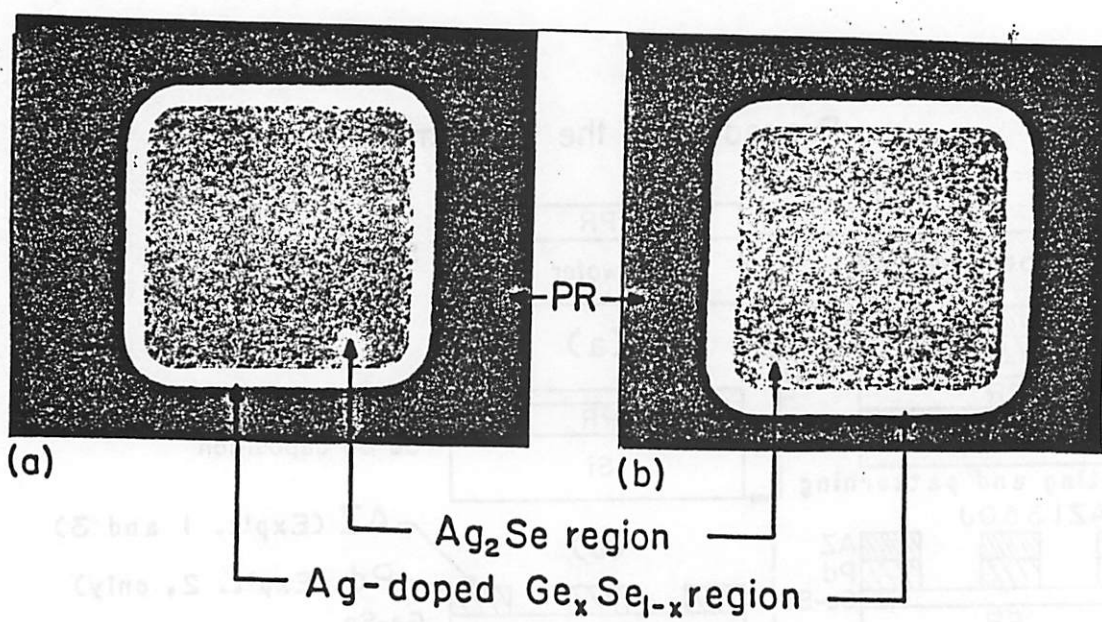
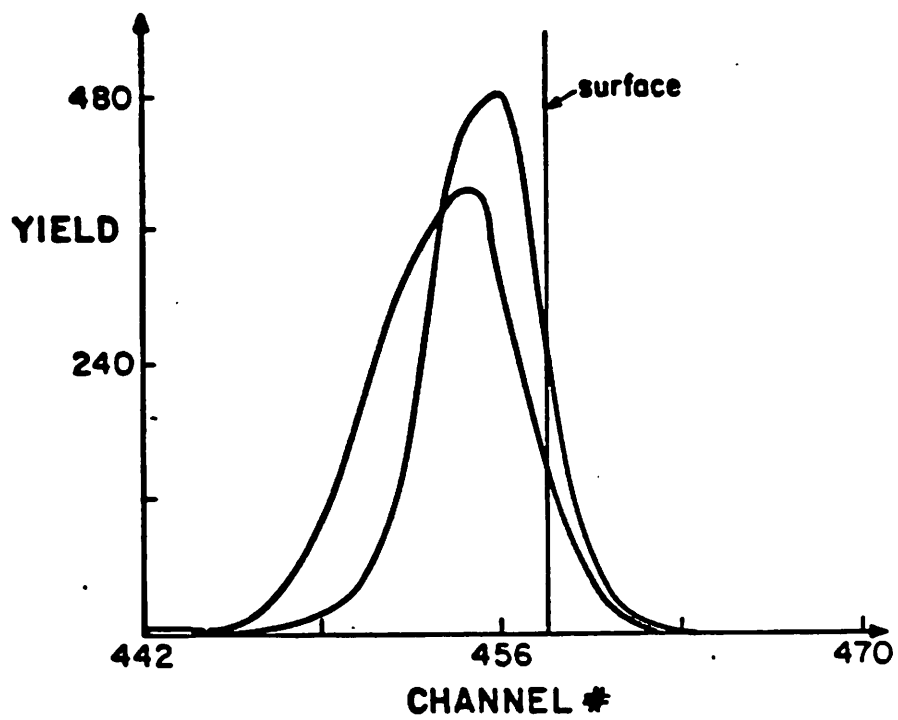
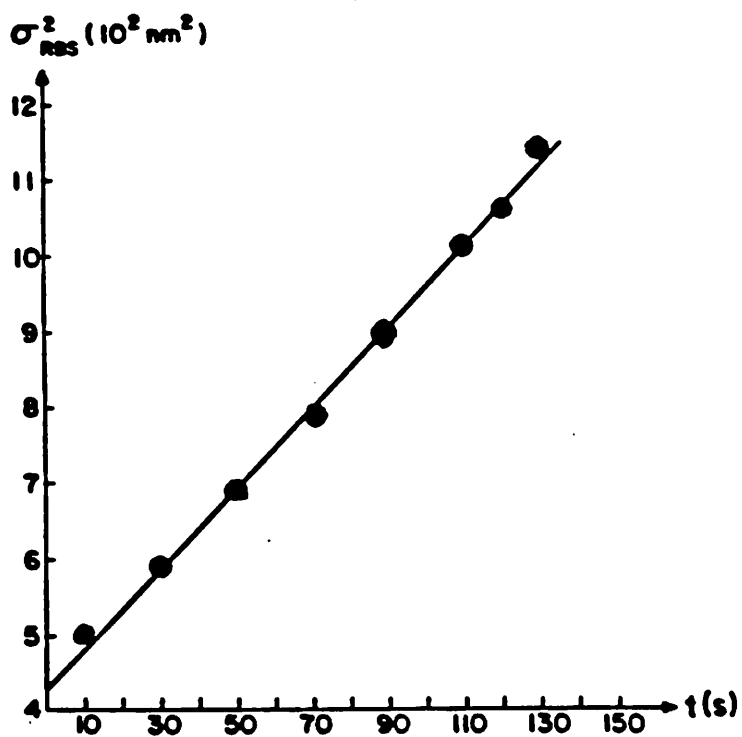


Fig. 3.3

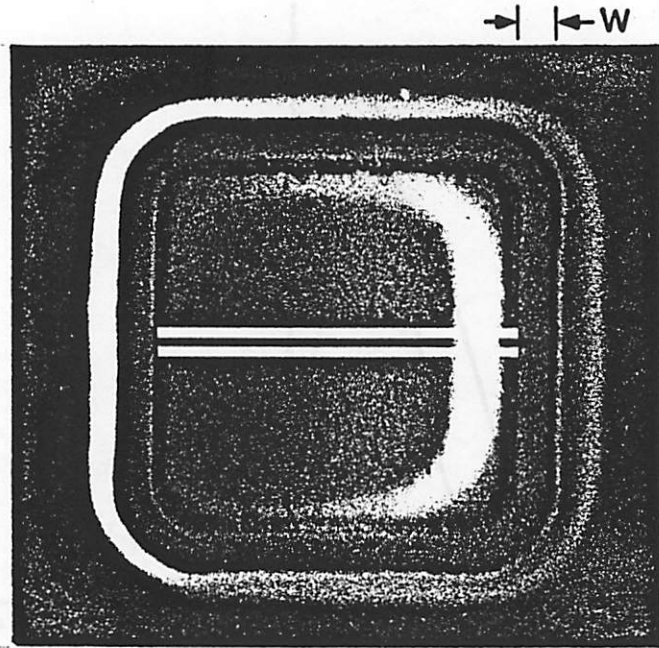


(a)

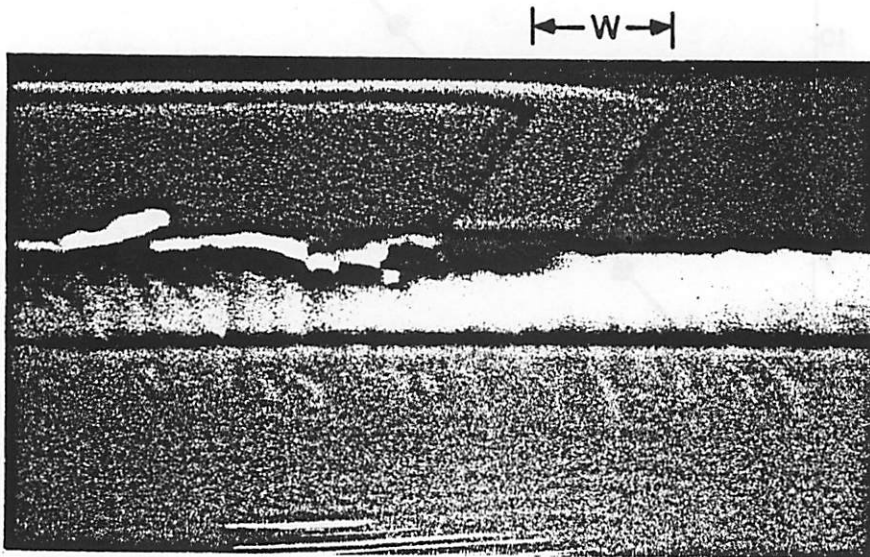
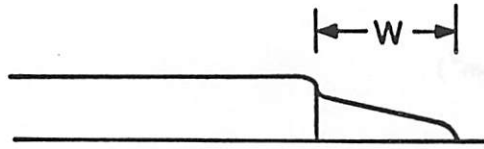


(b)

Fig. 3.4



(a)



(b)

Fig. 3.5

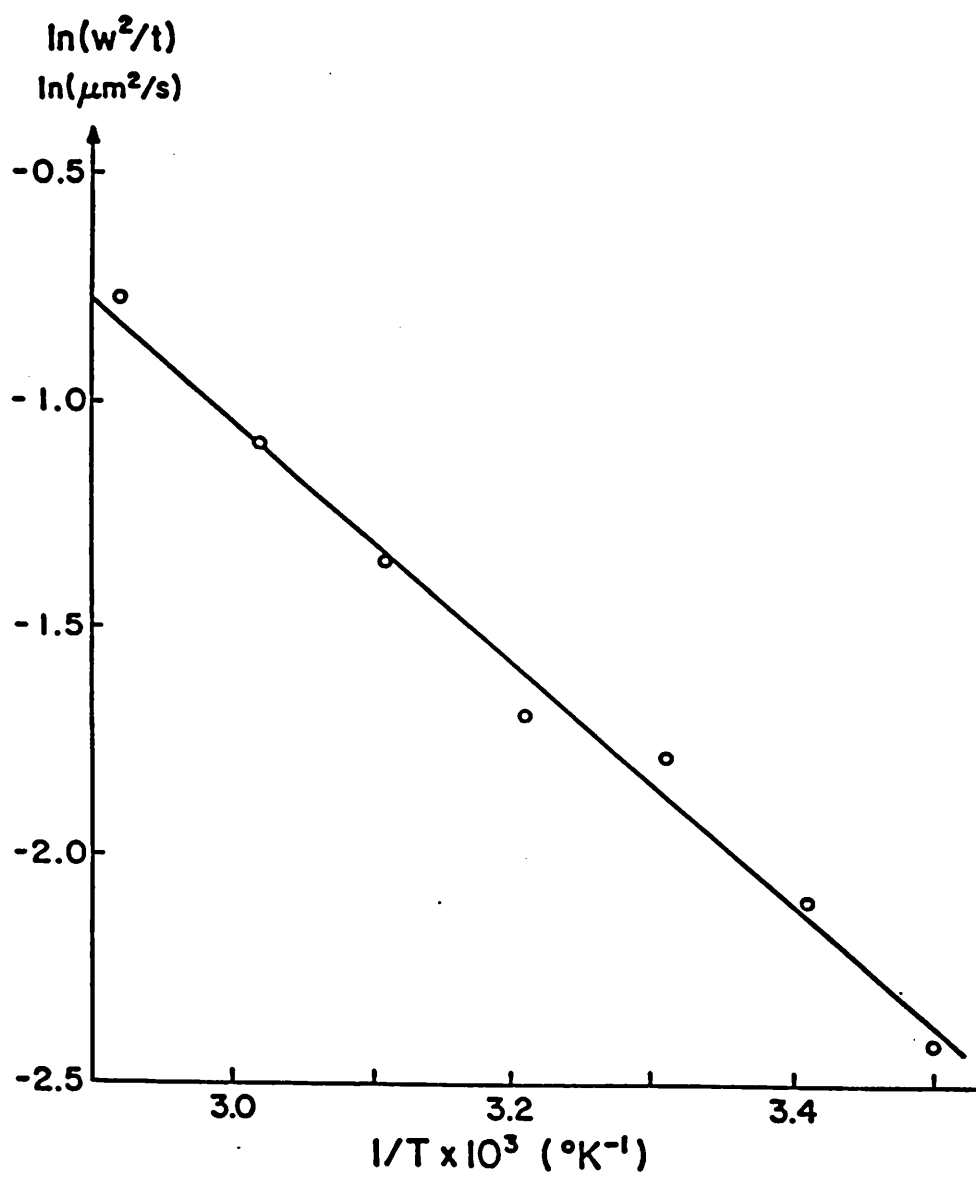


Fig. 3.6

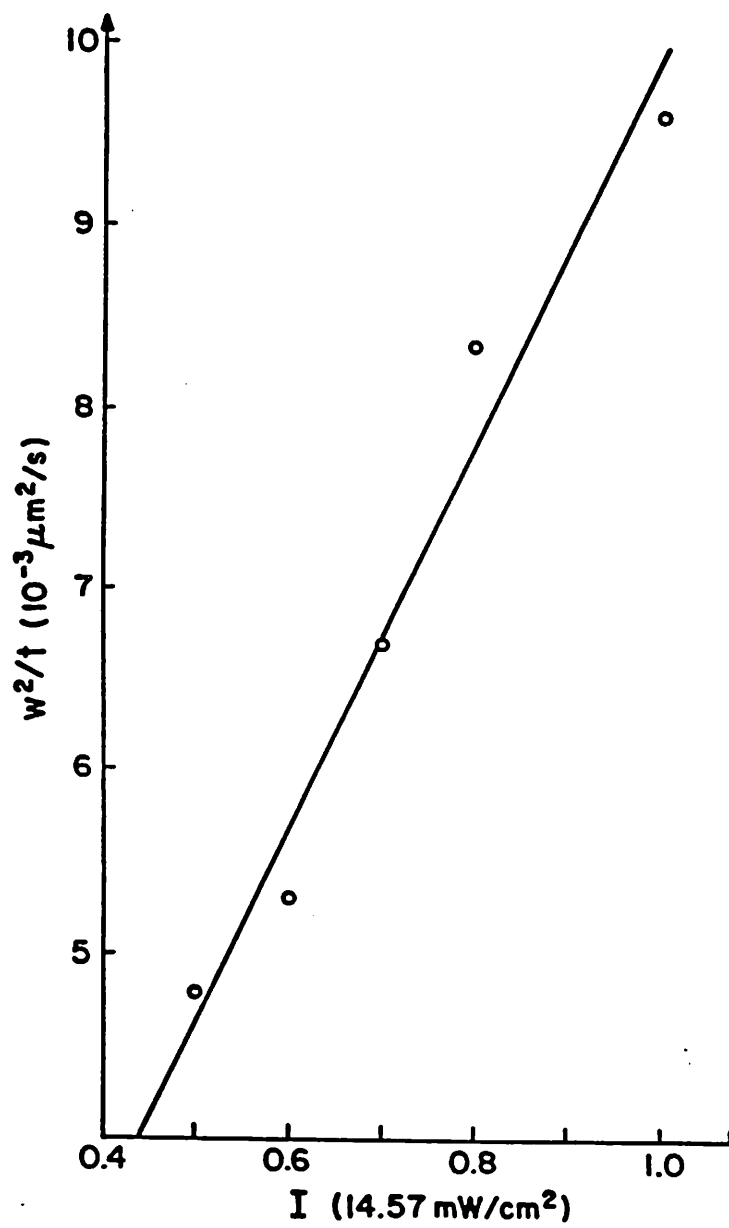


Fig. 3.7

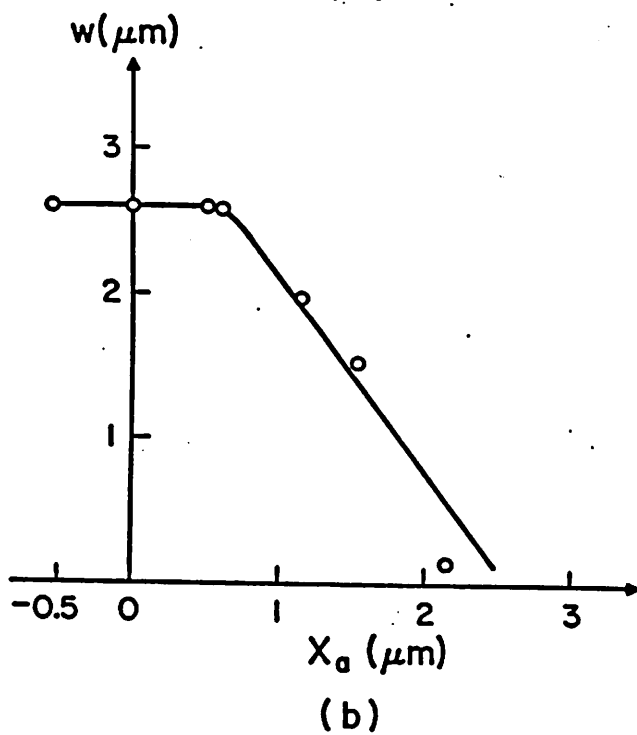
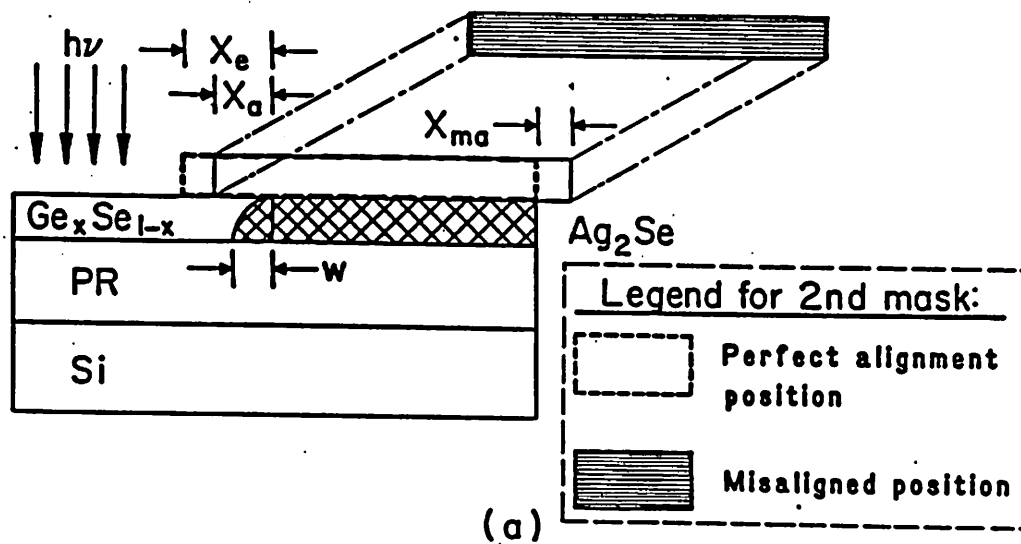


Fig. 3.8

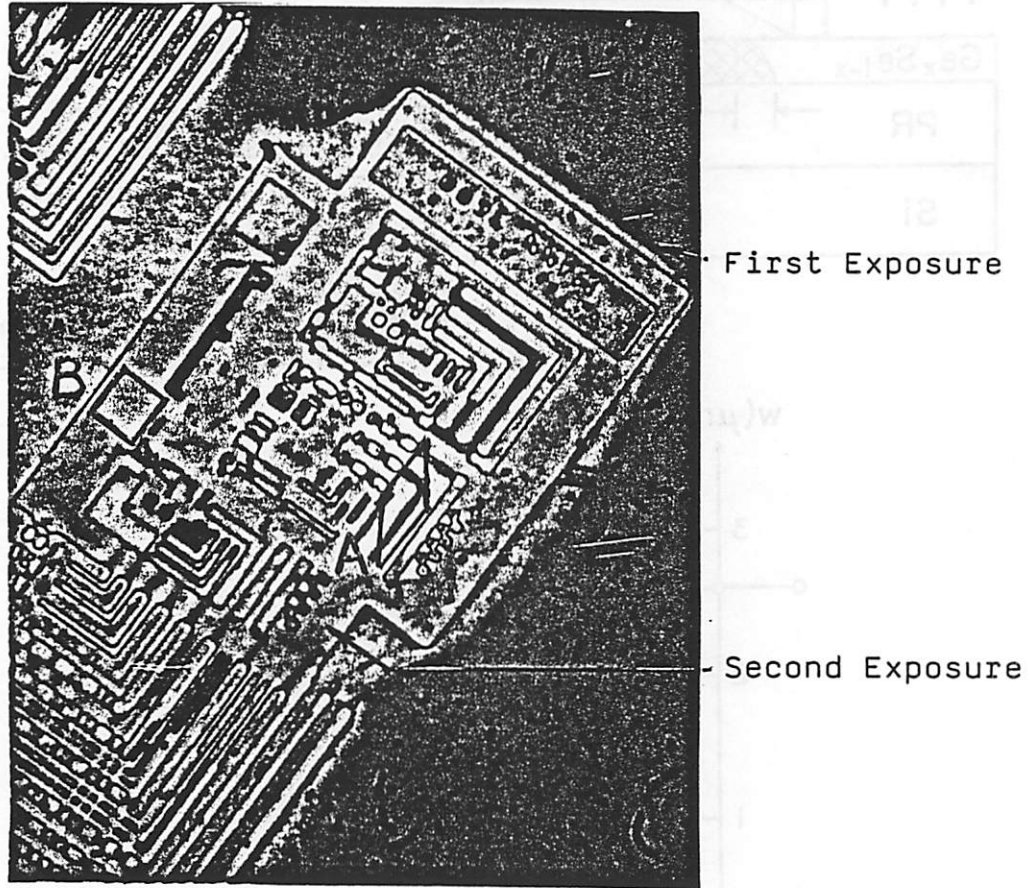


Fig. 3.9

Table 3.1

$\frac{C(w)}{C_0}$	$\frac{w}{2\sqrt{Dt}}$	$D(\text{nm}^2/\text{s})$
0.2	0.92	2130
0.1	1.17	1320
0.05	1.39	933
0.02	1.63	676
0.01	1.81	550

Chapter 4: THE RESIST MODEL AND ITS PARAMETERS

§ 4.1 The resist model

§ 4.1.1 The continuous time model

Work on the exposure model of $Ge_{0.1}Se_{0.9}$ resist was pioneered by Tai and coworkers [1]. Among their results are equations which describe the transport of Ag during the exposure process. These equations are the basis for the simulation model which is developed in this chapter.

For convenience the resist system is assumed to have the surfaces of its layers lie in the x and y coordinates and perpendicular to the z coordinate. Generally, the aerial image which exposes the resist is assumed to have no variation in the y coordinate. However, in the study of defects, circular symmetry and radial diffusion is used.

Implicit in the resist model are the following physical assumptions: (1) The Ag_2Se layer thickness is very thin so that Ag concentration in this layer in the thickness dimension is uniform. (2) Photodoped Ag congregates at the surface of the $Ge_{0.1}Se_{0.9}$ layer and may be modeled as a zero thickness layer. (3) The reflectivity of the resist layers does not change during the exposure. Assumption (1) is justified when the thickness of the Ag_2Se layer is much smaller than the average diffusion distance of Ag in Ag_2Se . Assumption (2) is valid when the Ag photodistance is small ($\approx 20nm$ for typical exposure [1]). The justification of assumption (3) is supported by the experimental result shown in Fig. 4.1 where the normalized intensity of the light reflected from the wafer surface is plotted as a function of exposure time. The data was obtained using an optical system set up by Deok Kim [2]. The intensity measured at the wafer surface was $2mW/cm^2$ and the exposure wavelength was $0.436\mu m$. The result shows that the reflectivity of the $Ge_{0.1}Se_{0.9}$ resist changes by less than 4% through out the exposure of 1300 seconds. The exposure ($2600mJ/cm^2$) is much higher than the normal exposure of the resist ($100mJ/cm^2$).

Letting M be the normalized Ag concentration distribution in the Ag_2Se layer, Ag transport in this layer is described by a continuity equation:

$$\frac{\partial M}{\partial t} = D \frac{\partial^2 M}{\partial x^2} - I_0 I(x) C M e^{-(AM+B)} \quad (1)$$

Letting S be the normalized Ag concentration distribution in the $Ge_x Se_{1-x}$ layer, photodoping of Ag in this layer is described by a kinetic equation:

$$\frac{dS}{dt} = I_0 I(x) C M e^{-(AM+B)} \quad (2)$$

The first term on the right hand side of equation (1) describes the lateral diffusion (in the x -direction) of Ag and the second term accounts for the vertical photodoping (in the z -direction) of Ag to the $Ge_{0.1}Se_{0.9}$ layer. The lateral diffusion and vertical photodoping of Ag has been discussed in detail in chapter 3. The parameters A , B , and C are analogous to the corresponding parameters in the positive photo-resist model [3]. Here A is the bleachable absorption coefficient, B is the non-bleachable absorption coefficient, and C is the photodoping sensitivity factor. For simplicity A and B have been normalized to implicitly include the thickness of the Ag_2Se layer and thus are unitless quantities which describe the attenuation of the light in passing through this layer. I_0 is the open field intensity in W/cm^2 , $I(x)$ is the normalized image intensity and D is the diffusivity of Ag in Ag_2Se . The parameters C and D have units of cm^2/J and $\mu m^2/sec$ respectively.

Assuming the resist system has its boundaries lying at $x=0$ and $x=1$, the boundary and initial conditions of the simulation model are described by the following equations:

$$\frac{\partial M(x,t)}{\partial x} = 0 \quad \text{for } x = 0 \text{ and } x = 1 \quad (3)$$

$$M(x,t=0) = 1 \quad (4)$$

$$S(x,t=0) = 0 \quad (5)$$

Equation (3) guarantees the conservation of Ag in the resist system during the exposure process. Equations (4) and (5) assume that the normalized Ag concentration in the Ag_2Se layer before exposure has a value of 1 and that no Ag atom exist in the $Ge_{0.1}Se_{0.9}$ layers before exposure.

§ 4.1.2 The discretization model

Before the exposure model can be described algorithmically, the continuous time model must be discretized. Many well known discretization methods can be used, e.g. explicit, Crank-Nicolson and full implicit. Crank-Nicolson is chosen because the resultant difference equations are computationally simple and their solutions are stable to discretization and rounding errors [4]. The resultant finite-difference equations of the resist model are:

$$\frac{M_i^{j+1} - M_i^j}{\delta t} = \frac{D}{2\delta x^2} \left(M_{i+1}^{j+1} - 2M_i^{j+1} + M_{i-1}^{j+1} + M_{i+1}^j + 2M_i^j + M_{i-1}^j \right) - \frac{I_i C}{2} e^{-AM_i^j - B} \left(M_i^{j+1} + M_i^j \right) \quad (6)$$

$$\frac{S_i^{j+1} - S_i^j}{\delta t} = \frac{I_i C}{2} e^{-AM_i^j - B} \left(M_i^{j+1} + M_i^j \right) \quad (7)$$

$$M_{-1}^j = M_1^j \quad (8)$$

$$M_{n+1}^j = M_{n-1}^j \quad (9)$$

$$M_i^{j=0} = 1 \quad (10)$$

$$S_i^{j=0} = 0 \quad (11)$$

where i and j are the x coordinate and time index respectively. Substituting equations (8) and (9) into equation (6), the result can be expressed in the matrix form:

$$AM^{j+1} = BM^j \quad (12)$$

where

$$A = \begin{pmatrix} a_1 & -2p & 0 & 0 & 0 & 0 & 0 \\ -p & a_2 & -p & 0 & 0 & 0 & 0 \\ 0 & -p & a_3 & -p & . & . & 0 \\ . & 0 & -p & a_4 & & & \\ . & . & & & a_{n-2} & -p & 0 \\ 0 & . & . & & -p & a_{n-1} & -p \\ 0 & 0 & 0 & 0 & 0 & -2p & a_n \end{pmatrix} \quad (13)$$

$$B = \begin{pmatrix} b_1 & 2p & 0 & 0 & 0 & 0 & 0 \\ p & b_2 & p & 0 & 0 & 0 & 0 \\ 0 & p & b_3 & p & . & . & 0 \\ . & 0 & p & b_4 & & & \\ . & . & & & b_{n-2} & p & 0 \\ 0 & . & . & & p & b_{n-1} & p \\ 0 & 0 & 0 & 0 & 0 & 2p & b_n \end{pmatrix} \quad (14)$$

$$M^{j+1} = \begin{bmatrix} M_0^{j+1} \\ M_1^{j+1} \\ M_2^{j+1} \\ \vdots \\ M_n^{j+1} \end{bmatrix} \quad (15)$$

$$p = \frac{D \delta t}{2 \delta x^2} \quad (16)$$

$$a_i = 1 + \frac{D \delta t}{\delta x^2} + \frac{\delta t I_i C}{2} e^{-AM_i + B} \quad (17)$$

$$b_i = a_i \quad (18)$$

Since A is a tri-diagonal band-matrix, equation (12) can be solved directly using Gaussian elimination method and backward substitution. The method is chosen over, for instance, matrix-inversion because the computation in Gaussian elimination method involves only non-zero elements. This means zero elements, which are the majority of entries in the matrix, do not occupy any core memory in the computer during the simulation. Non-pivoting technique is used because pivoting destroys the tri-diagonal structure of the matrix and results in a much more complicated computation algorithm [2]. After the M_i^{j+1} values are calculated, equation (7) can be solved by direct substitution.

§ 4.1.3 The simulation program

The simulation program for the exposure model has been written in Fortran for incorporation to the SAMPLE program. Fig. 4.2 shows the block diagram of the complete simulation model. The optical machine in SAMPLE [5] takes the mask description and projection printer specifications as the input parameters, and generates the aerial image $I(x)$. The inorganic resist simulator uses $I(x)$ and the resist parameters as its input and computes the Ag concentration distributions $M(x)$ and $S(x)$ in the top and bottom layer of the resist system. The distributions are fed back to the simulator for computing the distributions of next time step. Typically, the program takes 60 seconds of CPU time on the VAX 11/780 with UNIX for 3 second exposure. Error messages are generated by the program if any erroneous input statements are encountered. The source code of the $Ge_{0.1}Se_{0.9}$ resist simulator is listed in Appendix I.

§ 4.2 Resist parameter extraction

As described in equations (1) and (2), a $Ge_{0.1}Se_{0.9}$ resist system under exposure can be characterized by four parameters: the bleachable absorption coefficient A , the non-bleachable absorption coefficient B , the photodoping sensitivity factor C , and the diffusion coefficient of Ag in Ag_2Se . In order to obtain meaningful simulation result, nominal values of these parameters need to be determined.

By isolating the photodoping effect from the lateral diffusion effect using uniform exposure, the photodoping parameters A , B and C can be determined from the experimental data shown in Fig. 4.3. Published by Lamberti et al [6], the figure shows the photodoped Ag concentration as a function of exposure time (t) and resist thickness (T). Assuming the product of A and M is much greater than B at the beginning of the exposure, the parameters A and C can be determined from the slope of any two curves at zero exposure. The effect of B is most pronounced at high exposure dose when M has approached to zero and the effect of A can be neglected. Therefore, the value of B can be estimated from the slope of the curves at the exposure time when photodoping saturation begins to occur. Using this method, the A , B , C parameters for a $Ge_{0.1}Se_{0.9}$ system with a $9nm$ -thick Ag_2Se layer have the estimated values of 1.5 , 0.15 and $20.8cm^2/J$ respectively.

The parameter D was estimated by Tai et al [7] to be $1\mu m^2/s$ using the edge sharpening effect and the data published by Pines et al [8] and Johnson et al [9]. More details on the diffusivity of Ag in Ag_2Se can also be found in section 3.3 of Chapter 3.

References

- [1] K. L. Tai, E. Ong, R. G. Vadimsky, C. T. Kemmerer and P. M. Bridenbaugh, "Modeling of image formation in $Ag_2Se/Ge-Se$ resist systems: Implications for microlithography", Proc. of ECS, vol. 82-9, pp.49, 1982.
- [2] D. J. Kim, Doctoral Dissertation, EECS, University of California at Berkeley, 1984.
- [3] F. H. Dill, W. P. Hornberger, P. S. Hauge and J. M. Shaw, "Characterization of Positive Photoresist", IEEE Trans. on Electron Devices, vol. ED-22, no. 7, p. 445, 1975.
- [4] G. D. Smith, "Numerical solution of partial differential equation: finite difference method", 2d. ed., Oxford U., 1978.
- [5] W. G. Oldham, S. N. Nandgaonkar, A. R. Neureuther and M. M O'Toole, "A general simulator for VLSI lithography and etching processes: Part I - Applications to projection lithography", IEEE Trans. on Electr. Dev., vol. ED-26, no. 4, pp.717, 1979.
- [6] V. E. Lamberti, S. M. Vincent, C. T. Kemmerer, and R. G. Vadimsky, "Growth of $c-Ag_2Se$ on $g-Ge_{0.1}Se_{0.9}$ inorganic resist: The effect of its thickness on lithographic performance", Proc. of ECS, vol. 82-9, pp.191, 1982.
- [7] K. L. Tai, R. G. Vadimsky, C. T. Kemmerer, J. S. Wagner, V. E. Lamberti, and A. G. Timko, "Submicron optical lithography using an inorganic resist/polymer bilevel scheme", J. of Vac. Sci. Technol., vol. 17, pp.1169, 1980.
- [8] B. Y. Pines, I. P. Grebennick, R. I. Bazyura and G. V. Zozulya, "Surface and volume diffusion in thin films of the system Ag-Se", Phys. Stat. Sol., vol. 20, pp.213, 1967.
- [9] D. B. Johnson and L. C. Browns, "Lateral diffusion in Ag-Se thin-film couples", J. of Appl. Phys., vol. 40, pp.149, 1968.

Figure Captions

Fig. 4.1 Relative intensity of the light reflected from the $Ge_{0.1}Se_{0.9}$ resist surface plotted as a function of exposure time.

Fig. 4.2 Block diagram of the simulation model.

Fig. 4.3 Photodoped Ag as a function of exposure under uniform intensity. (Courtesy of Lamberti et al [4]).

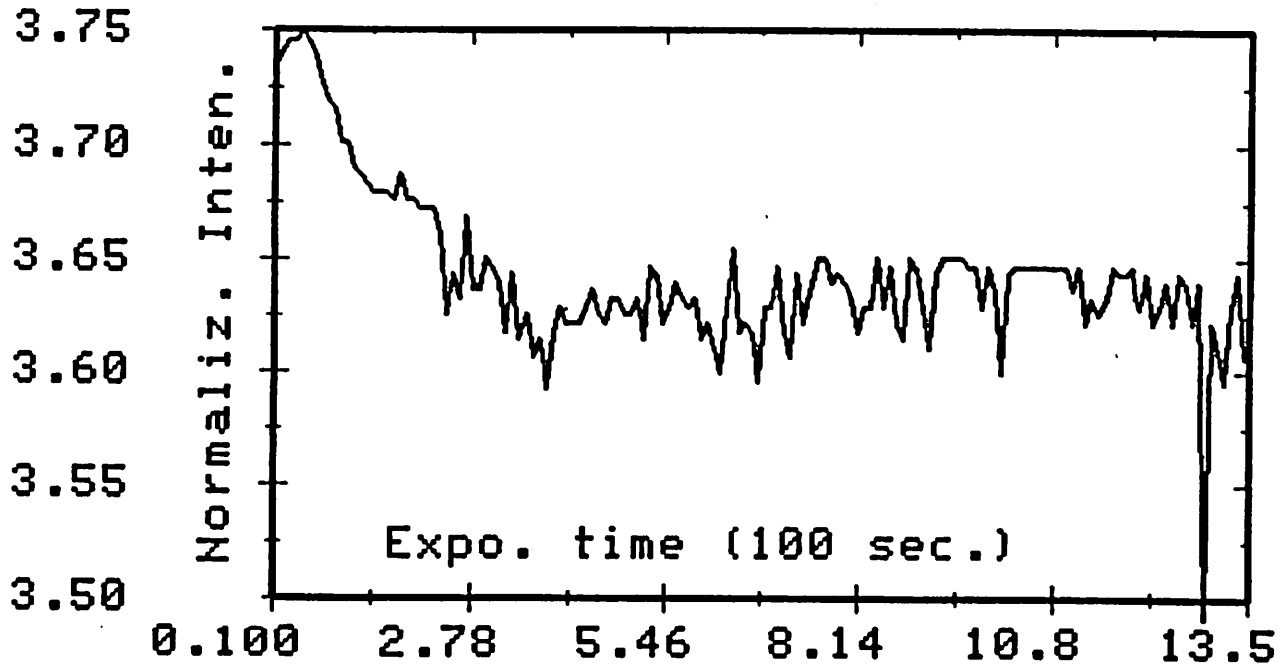


Fig. 4.1

FLOW CHART OF SIMULATION FOR THE EXPOSURE PROCESS OF Ge-Se RESIST

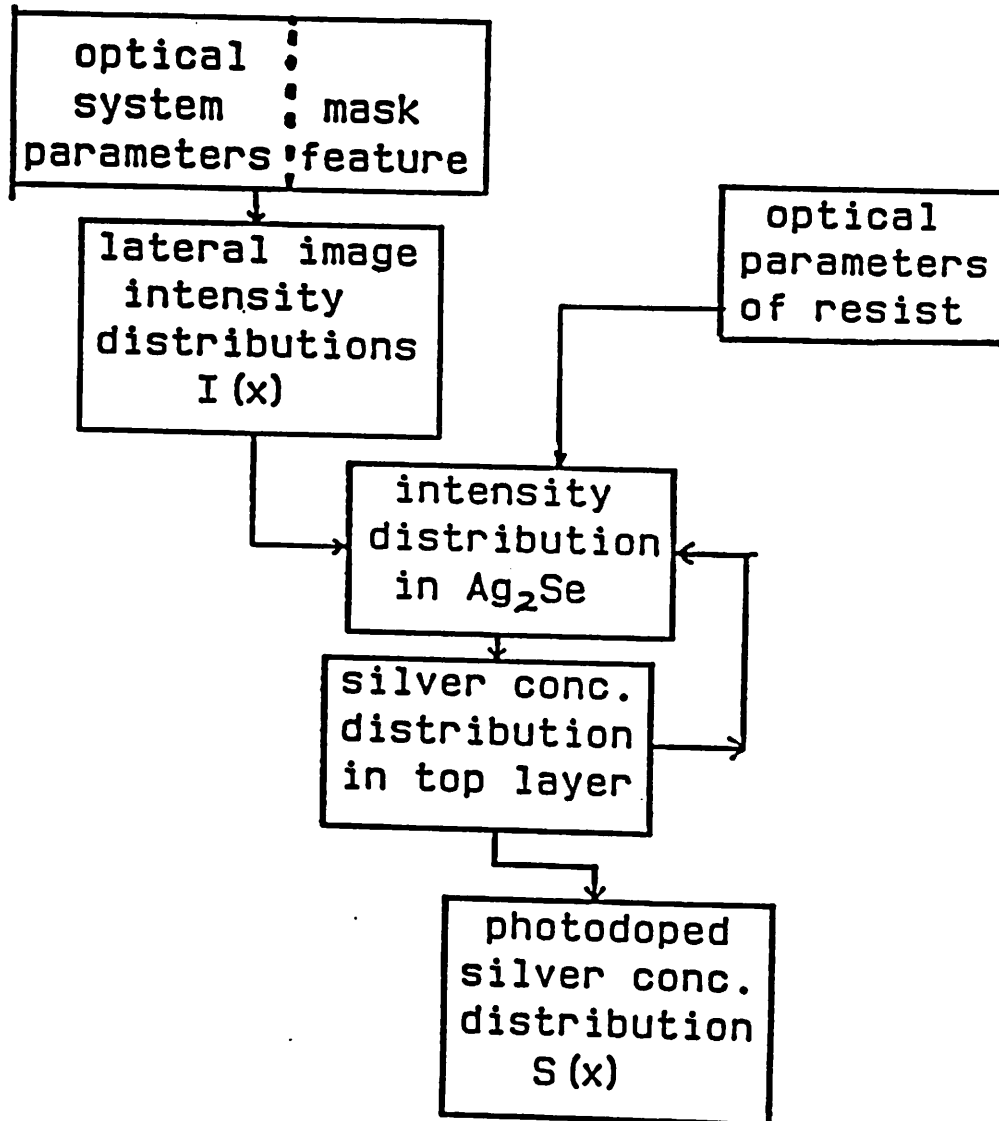


Fig. 4.2

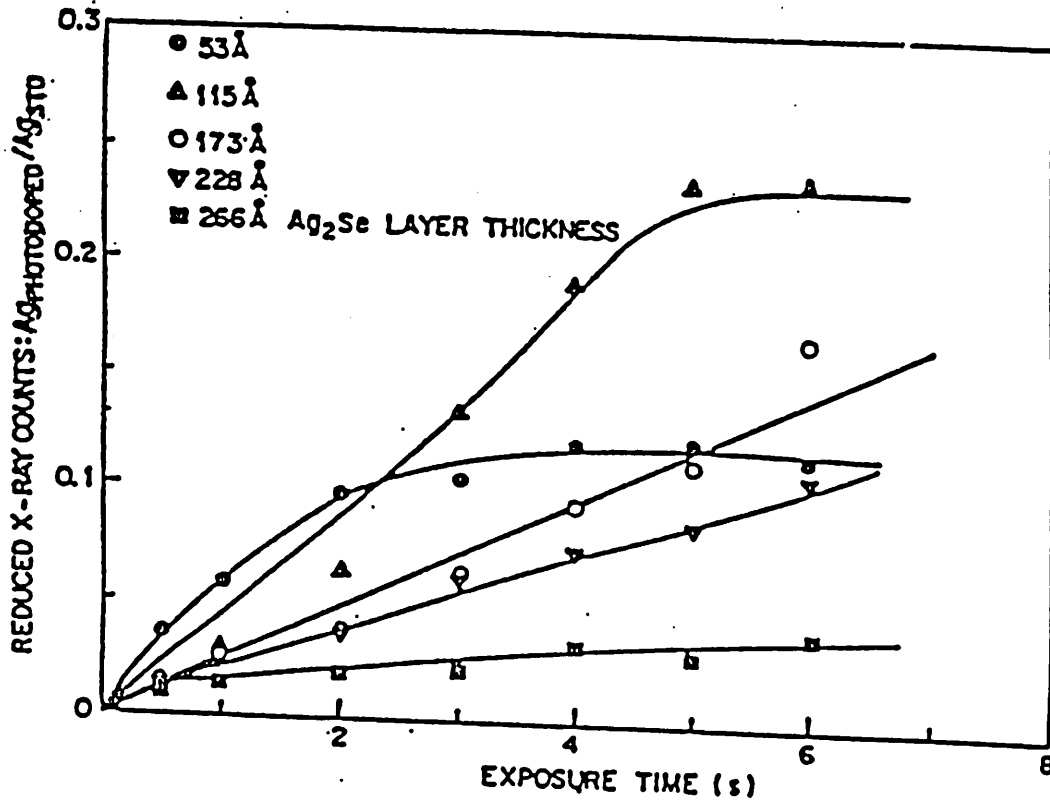


Fig. 4.3

Chapter 5: THE EXPOSURE PHENOMENA

§ 5.1 Introduction

As mentioned in chapter 4, when a $Ge_{0.1}Se_{0.9}$ resist system is under exposure, photodoping and lateral diffusion of Ag take place. These mechanisms cause phenomena such as edge sharpening, contrast enhancement and feature-dependent amplification to occur. These exposure phenomena affects the formation of the latent image (photodoped-Ag-concentration distribution) and therefore have a direct impact on the printing of the final relief image. Understanding these phenomena allows fine tuning of the resist process to meet specific lithographic requirements. The applications of these phenomena for compensating proximity effects and suppressing the printability of open defects will be discussed in chapter 6. This chapter explores experimental and theoretical conditions under which the exposure phenomena occur. The phenomena are first described in detail and then characterized by "Rules of thumb".

§ 5.2 The exposure model

The exposure model of Ge_xSe_{1-x} resist has been elaborated in chapter 4. For convenience of discussion, the equations of the model which describe the transport of Ag in the Ag_2Se and Ge_xSe_{1-x} layer are copied below:

$$\frac{\partial M}{\partial t} = D \frac{\partial^2 M}{\partial x^2} - I_0 I(x) C M e^{-iAM+B} \quad (1)$$

$$\frac{dS}{dt} = I_0 I(x) C M e^{-iAM+B} \quad (2)$$

§ 5.3 Contrast enhancement

The possibility of obtaining contrast enhancement in $GeSe$ resists was first suggested by Tai et al [1]. The mechanisms of contrast enhancement in photobleachable polymer films was first studied and applied to microlithography by Griffing et al [2,3]. In their report, they pointed out that contrast enhancement is associated with the photobleachable characteristic of the material. For $GeSe$ resists, photobleaching in the top

layer is caused by the loss of Ag to photodoping. The rate of photodoping, or equivalently, photobleaching depends on the amount of light that can reach the interface of the Ge_xSe_{1-x} layer and the local Ag concentration in the Ag_2Se layer [4,5]. Ag in the top layer can suppress photodoping by decreasing the intensity at the interface and enhance photodoping by participating in the process. These effects can be observed in the experimental data of Tai et al in Fig. 5.1. The photodoped Ag concentration is plotted as a function of exposure time and the thickness of the Ag_2Se layer when the resist is under uniform exposure. For resists with a thin Ag_2Se layer (curve 1 and 2), the photodoping rate at all exposures is limited by the supply of photodoping Ag which decreases with exposure time. Consequently, the photodoping rate decreases with exposure time. For resists with thicker Ag_2Se layers (curve 3 and 4), the high absorptivity of the Ag_2Se layer at low-dose exposures limits the amount of light that can reach the $Ag_2Se/GeSe$ interface and suppresses photodoping. As the exposure time increases, loss of Ag to photodoping decreases the absorptivity of the Ag_2Se layer and increases the photodoping rate which in turn increases the photodoping of Ag. This positive feedback process can be put to use in imaging. In an area with higher image intensity the photodoping rate increases faster than the rate in an area with lower intensity, effecting a contrast enhancement.

Photobleaching is complicated by the lateral diffusion process. Lateral diffusion of Ag from dark to bright areas tends to offset the photobleaching effects. To obtain contrast enhancement, three criteria need to be satisfied: (1) The initial absorptivity of the top layer must be high so that it suppresses the photodoping in the dark area. (2) The exposure dose must be at a level so that the photodoping rate in the bright area increases faster than the rate in the dark area. (3) The amount of lateral diffusion between the dark and bright area must be small so that the photobleaching process is not compensated by a diffusion flow.

The first criterion (1) is satisfied when A is greater than 2. In practice, the thickness

of the Ag_2Se layer must be greater than $12\mu m$. The exposure doses which satisfy criterion (2) are the doses at which the photodoping rate in the bright area has not reached its maximum value. The photodoping rate is maximum when [6]

$$AM = 1 \quad (3)$$

The exposure dose E as a function of Ag concentration M is given by:

$$E = \int_M^1 \frac{1}{mC} e^{Am+B} dm \quad (4)$$

Equation (4) is obtained by setting D equals to 0 in equation (1) and solving the resultant equation. Assuming a saturation threshold of 0.2, equation (4) has a closed form solution given by:

$$E = \frac{1}{C} e^B \left[\log M + AM + \frac{(AM)^2}{2 \times 2!} + \frac{(AM)^3}{3 \times 3!} + \frac{(AM)^4}{4 \times 4!} + \dots \right]_{0.2}^1 \quad (5)$$

Substituting equation (3) in (5) and assuming that the value of B is very small, the following expression for the exposure dose E_s , at which the maximum photodoping rate occurs is obtained:

$$E_s = \frac{1}{C} \left[\log A + A + \frac{A^2}{4} + \frac{A^3}{18} + \dots \right] \quad (6)$$

For A and C values of 3.0 and 0.02, E_s has a value of $500mJ/cm^2$. Criterion (3) is satisfied if the width of the transition region (T_w) of an image is longer than the lateral diffusion distance (L). A transition region of an image is defined as the region between the dark and bright area where the local image intensity changes from its minimum to its maximum. The lateral diffusion distance is related to the average photodoping rate (\bar{R}) by the following expression:

$$L = \sqrt{\frac{D}{\bar{R}}} \quad (7)$$

\bar{R} can be estimated using equation (8) [6].

$$\bar{R} = \bar{I} \bar{M} C e^{-A\bar{M}-B} \quad (8)$$

where \bar{M} is the average Ag concentration in the Ag_2Se layer in the transition region and \bar{I} is the image intensity at the knife-edge. Using the resist parameters in Fig. 5.2 and

assuming \bar{M} equal to 0.5, \bar{R} has a value of $0.4\mu m$. The simulated images shown in Fig. 5.2 illustrate the case when the criteria are met. An Ag diffusivity of $0.1\mu m^2/s$ is assumed and a contrast enhancement of 7% is obtained. However, the actual Ag diffusivity is about $1\mu m^2/s$ and criterion (2) is normally not satisfied except for projection printers which have a very high open field intensity ($>500mW/cm^2$). Therefore, in normal practice, contrast enhancement does not occur.

§ 5.4 Edge sharpening

The phenomenon of edge sharpening was first observed by Tai et al and was used to explain the high resolution capability of GeSe resist [7]. Non-uniform photodoping sets up a concentration gradient of Ag in the top layer causing Ag to diffuse toward the bright areas from darker areas. This flow increases the net photodoping in the bright areas near edges, in effect preventing the edge slope of a latent image from being degraded by photodoping saturation. Therefore, edge sharpening is caused by lateral diffusion and its effects are to increase the edge slope of a latent image. In the extreme, the normalized edge slope of the latent image can be increased over that associated with the incident aerial image.

Fig. 5.3 shows the simulated aerial and latent image of a $5\mu m$ periodic equal lines-and-spaces (L/S) pattern. Here, the lateral diffusion distance of Ag ($\approx 1\mu m$) is smaller than the width of the transition region (T_w). Therefore, most of the Ag diffused from the dark area is photodoped in the transition zone at the edge of the bright region. As a result, photodoped Ag concentration at the edge is higher than that at the central part of the bright region. The normalized edge slope of an aerial image can be defined as:

$$\Theta_a = \frac{I_{\max} - I_{\min}}{T_w} \quad (9)$$

where I_{\max} and I_{\min} are the maximum and minimum normalized intensity in the transition region respectively. Similarly, the normalized edge slope of a latent image can be defined as:

$$\Theta_l = \frac{S_{\max} - S_{\min}}{T_{wl}} \quad (10)$$

where S_{\max} and S_{\min} are the maximum and minimum normalized Ag concentration in the transition region respectively, and T_{wl} is the transition region width of the latent image. In Fig. 5.3 Θ_l is larger than Θ_a because T_{wl} is smaller than T_w . This result, however, does not occur in the printing of features less than $1.5\mu m$ because the aerial image of these features have a T_w value less than the lateral diffusion distance of Ag [6].

Fig. 5.4 shows the simulated latent image of a $0.75\mu m$ L/S pattern printed in GeSe resist with two different values of assumed Ag diffusivity (D), 0 and $1\mu m^2/s$, and using the parameters appropriate for a GCA stepper. For exposures shorter than 0.6 second, the corresponding latent images of the resists are the same and the effect of edge sharpening cannot be observed. For exposures longer than 0.6 second, exposure saturation occurs in the resist with a D value of zero and the edge slope begins to decrease with exposure time. In practice, GeSe resists have a D value about $1\mu m^2/s$, and lateral diffusion prevents exposure saturation. Consequently, the absolute slope of the latent image continues to increase with exposure time. When the Ag in the top layer is exhausted, exposure saturation occurs simultaneously in both the dark and bright areas.

Edge sharpening occurs when photodoping saturation appears in the resist. We may solve for the exposure dose E_s at which 80% of the Ag is photodoped, using equation (6). The exposure time at which edge sharpening begins to occur can then be calculated using equation (11):

$$t_s = \frac{E_s}{I_0 I_M} \quad (11)$$

where I_M is the normalized local maximum intensity. For typical values of A, B and C of 1.5, 0.15 and 0.02 respectively [5], E_s is about $200mJ/cm^2$. For the printing of a $0.75\mu m$ L/S pattern using the GCA stepper, the values of I_M and I_0 are 0.6 and $500mW/cm^2$ respectively. Under these conditions, edge sharpening occurs at a dose greater than $330mJ/cm^2$ or an exposure time longer than 0.7 second. This value agrees with

the simulation result shown in Fig. 5.4 and it is higher than the normal exposure dose ($250\text{mJ} / \text{cm}^2$).

§ 5.5 Feature-dependent amplification

Feature-dependent amplification is another phenomenon associated with the lateral diffusion of Ag. When the lateral diffusion distance (L) is longer than the width of the transition region (T_w) of an image, the Ag concentration in the top layer and in the transition region is kept quite uniform during the exposure. Consequently, the latent image at the transition area is simply a linear amplification of that of the aerial image. The amplification factor however is a function of the exposure time (t) and the supply of Ag. The supply in a bright area depends not only on the local Ag concentration but, because of lateral diffusion, also on the Ag concentration in the surrounding dark area. Therefore, latent image amplification is feature dependent.

In an imaging process, when patterns with different sizes and therefore different intensity levels are printed, the feature-dependent amplification effect can be used to advantage. It compensates for the feature-dependent bias of the optical imaging system so that aerial images with small intensity levels are amplified by a large multiplication factor and vice versa. The importance of this effect can be demonstrated by simulation. In Fig. 5.5 the aerial images and resultant latent images of three different features are shown. The relatively smaller modulation of the $0.5\mu\text{m}$ isolated space and the lines and spaces (L/S) are increased in the formation of the latent image. In effect the modulation of the isolated space and periodic L/S features "catches up" with that of the isolated line, so that all the patterns can be printed simultaneously with little linewidth variation.

In order for the effect of feature-dependent amplification to occur, two criteria must be satisfied: (a) the lateral diffusion distance of Ag should be larger than the width of the transition region (T_w) so that the edge slope and contrast of the latent image is not degraded by photodoping saturation and, (b) the exposure dose (E_s) should be high enough so that photodoping saturation occurs in large bright regions allowing

photodoping in small bright region to catch up with that in large bright regions. The value of E_c can be estimated using equation (6). The lateral diffusion distance of Ag is dependent on the image intensity. For the 10X camera which has an open field intensity of $2mW/cm^2$, the diffusion distance is approximately $12\mu m$. For the typical *GeSe* resist parameters and the aerial images shown in Fig. 5.5 (a), feature dependent amplification occurs at doses higher than $200mW/cm^2$, consistent with our computer simulation.

§ 5.6 Feature-dependent photodoping suppression

Lateral diffusion can also suppress the photodoping mechanism on a feature-dependent basis. As discussed in section 5.2.2, in resists with a thick Ag_2Se layer, the positive feedback process of photobleaching can enhance the image contrast. However, lateral diffusion of Ag can suppress the photobleaching effect. Silver can diffuse from dark areas to replace bleached Ag in bright areas, in effect suppressing bleaching. Photobleaching in bright areas is reduced and the positive feedback aspect of photobleaching is inhibited. Since the suppression depends on the supply of Ag from the nearby dark areas, the suppression is feature dependent.

Fig. 5.6 gives an example of this effect. Fig. 5.6 (a) shows the aerial image of a $0.75\mu m$ line for three different cases: the line by itself, the line $0.5\mu m$ away from a large opening, and the line in proximity of two large openings. Due to diffraction effects, the local intensity of the line in proximity of large openings is lower than the intensity of the isolated line [8]. Fig. 5.6 (b) shows the developed pattern printed in a resist with normal Ag_2Se layer thickness ($9nm$). Without the effect of feature-dependent photodoping suppression, photodoping in the isolated region is higher than that in the proximity region. However, the contrary is observed in Fig. 5.6 (c) where the pattern printed in a resist with a ($15nm$)-thick Ag_2Se layer is shown. The result can be explained by the diffusion of Ag from the dark regions of Fig. 5.6 (c) into the bright regions. The persistent high Ag concentration causes excessive absorption and the photodoping process never becomes efficient.

For feature-dependent photodoping suppression to occur, the absorptivity of the Ag_2Se layer must be high so that it can suppress the photodoping process. This condition can be satisfied using a resist with an A value larger than 2 or, equivalently, a Ag_2Se layer thicker than $9nm$.

§ 5.7 Summary of exposure phenomena

The conditions for the occurrence of the exposure phenomena can be summarized as follow: All the phenomena occur at dose levels higher than the normal exposure ($140mJ / cm^2$). Contrast enhancement occurs when the diffusion length L is smaller than the transition width T_w and the bleachable absorption coefficient A is larger than $2 \mu m^{-1}$. Edge sharpening occurs when L is in the same order of T_w . Feature-dependent amplification occurs when L is greater than T_w and A is less than $2 \mu m^{-1}$. Feature-dependent photodoping suppression occurs when L is greater than T_w and A is greater than $2 \mu m^{-1}$. Fig. 5.7 shows the different regions of L and A values at which the exposure phenomena can occur. The operating conditions for Figs. 5.2, 3, 4(b), 5 and 6 are also indicated.

References

- [1] K. L. Tai, E. Ong, R. G. Vadimsky, C. T. Kemmerer and P. M. Bridenbaugh. "Model of Image Formation in $Ag_2Se/Ge-Se$ Resist Systems: Implications for Microlithography", Proc. of ECS, vol. 82-9, p. 49, 1982.
- [2] B. F. Griffing and P. R. West. "Contrast Enhanced Photoresists - Processing and modeling", Proc. Reg. Tech. Conf. on Photopolymers, Principles, Processes, and Materials, Midhudson section, SPE, Ellenville, N.Y., p. 185, 1982.
- [3] B. F. Griffing and P. R. West. "Contrast Enhanced Photolithography", IEEE Electron Dev. Lett., vol. EDL-4, no. 1, p. 14, 1983.
- [4] K. L. Tai, E. Ong and R. G. Vadimsky, "Inorganic Resist Systems for VLSI Microlithography", Proc. of ECS, vol. 82-9, p. 9, 1982.
- [5] W. Leung, N. W. Cheung and A. R. Neureuther. "Studies of Ag Photodoping in $GeSe$ Glass Using Microlithography techniques", Appl. Phys. Lett., vol. 46, no. 5, p.48, 1985.
- [6] W. Leung, A. R. Neureuther and W. G. Oldham. "Edge Sharpening, Contrast Enhancement, and Feature Dependent Amplification in Inorganic Resist - A Simulation Study", Proc. of SPIE, vol. 394, p.134, 1983.
- [7] K. L. Tai, R. G. Vadimsky and V. E. Lamberti. "Edge-sharpening Effects in $Ag_2Se/GeSe$ Inorganic Resist", ECS Ext. Abst., 80-2, p. 826, 1980.
- [8] P. D. Robertson, F. W. Wise, A. N. Nasr, A. R. Neureuther and C. H. Ting. Proximity Effects and Influences of Nonuniform Illumination in Projection Lithography, Proc. of SPIE, 334, p.37-43, 1982.

Figure Captions

Fig. 5.1 Measured photodoped Ag as a function of exposure time and initial Ag_2Se film thickness. (Courtesy of Tai et al [3])

Fig. 5.2 Simulated aerial and latent image of $0.75\mu m$ L/S projected by the GCA stepper.

Fig. 5.3 Simulated aerial and latent image of $5.0\mu m$ L/S projected by the GCA stepper.

Fig. 5.4 Simulated latent images of $0.75\mu m$ L/S printed by the GCA stepper on $GeSe$ with a Ag diffusivity of (a) 0 and (b) $1 \mu m^2 / s$.

Fig. 5.5 Simulated (a) aerial and (b) latent images of $0.5\mu m$ L/S, isolated line and isolated space projected by the 10X camera.

Fig. 5.6 (a) Simulated aerial images of the three regions of the proximity-effect pattern. (b),(c) SEM micrograph of the developed pattern printed by the GCA stepper with a dose of (b) 250 and (c) $560 mJ / cm^2$.

Fig. 5.7 Chart to show the different regions of L and A values at which the exposure phenomena can occur.

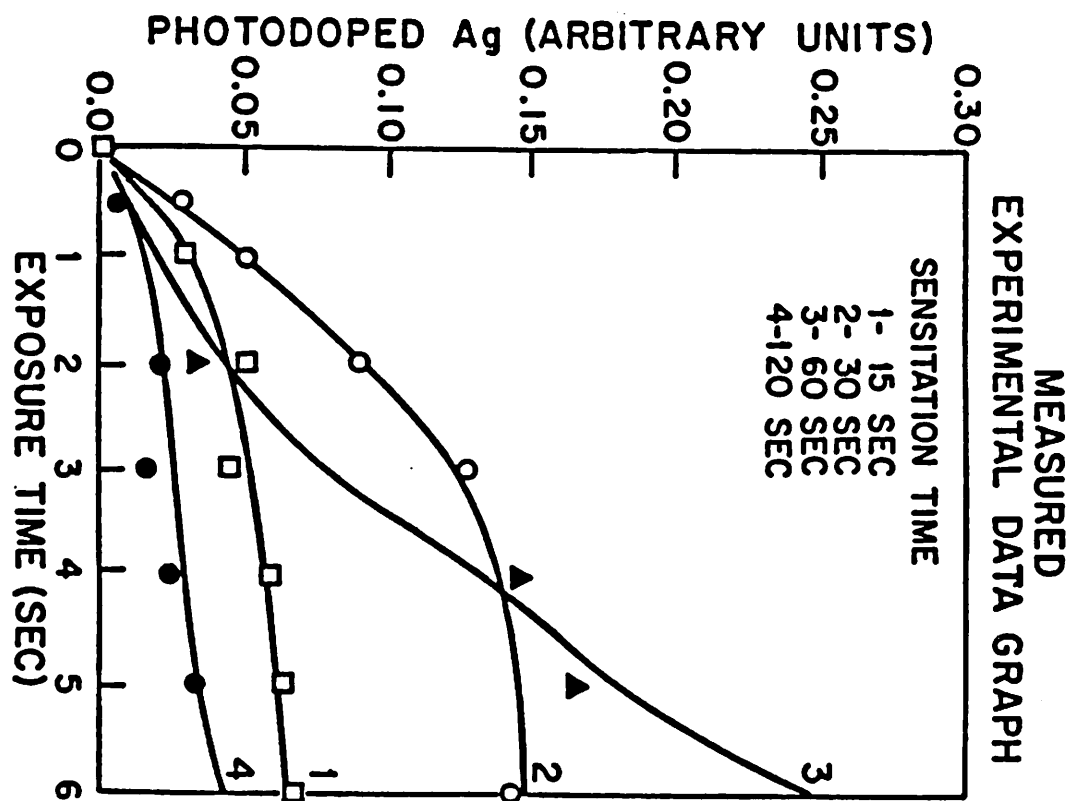


Fig. 5.1

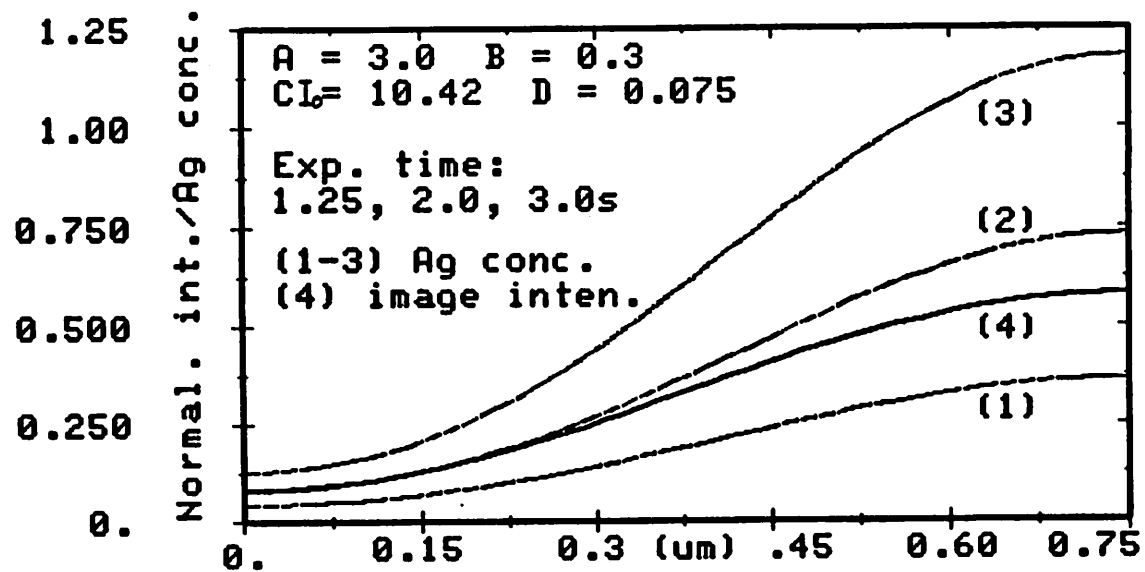


Fig. 5.2

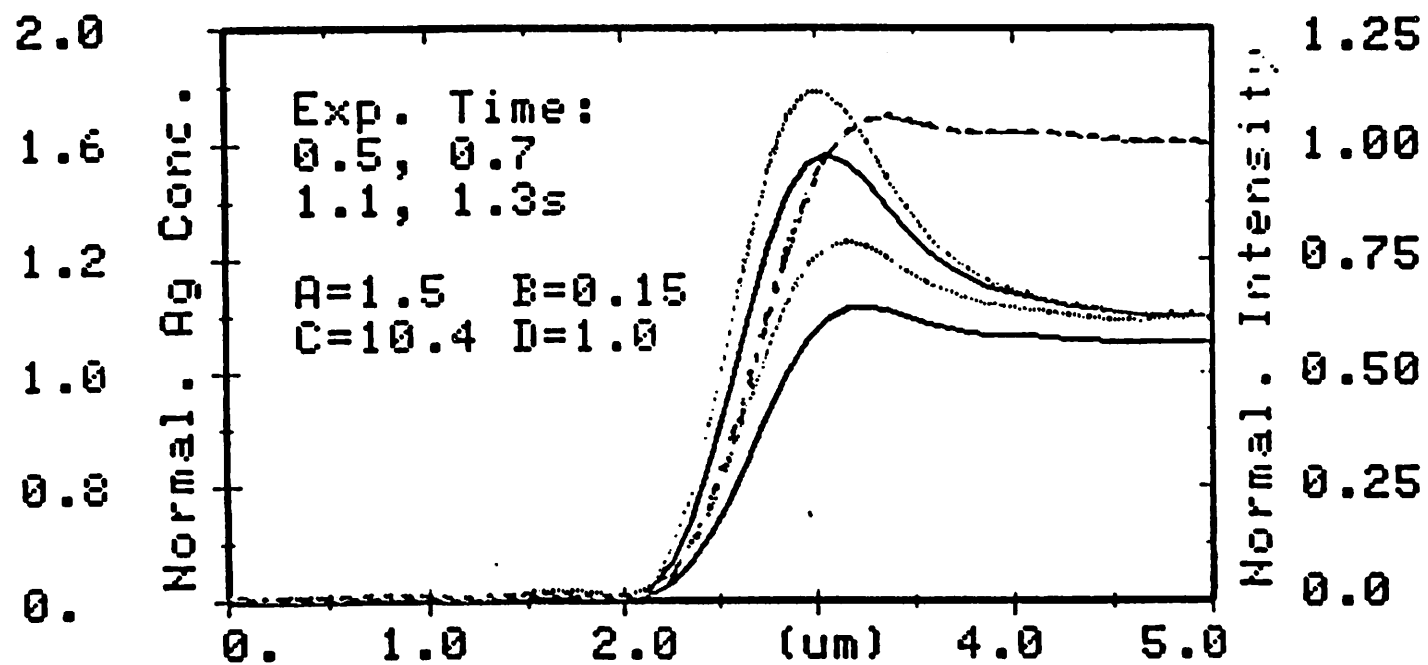


Fig. 5.3

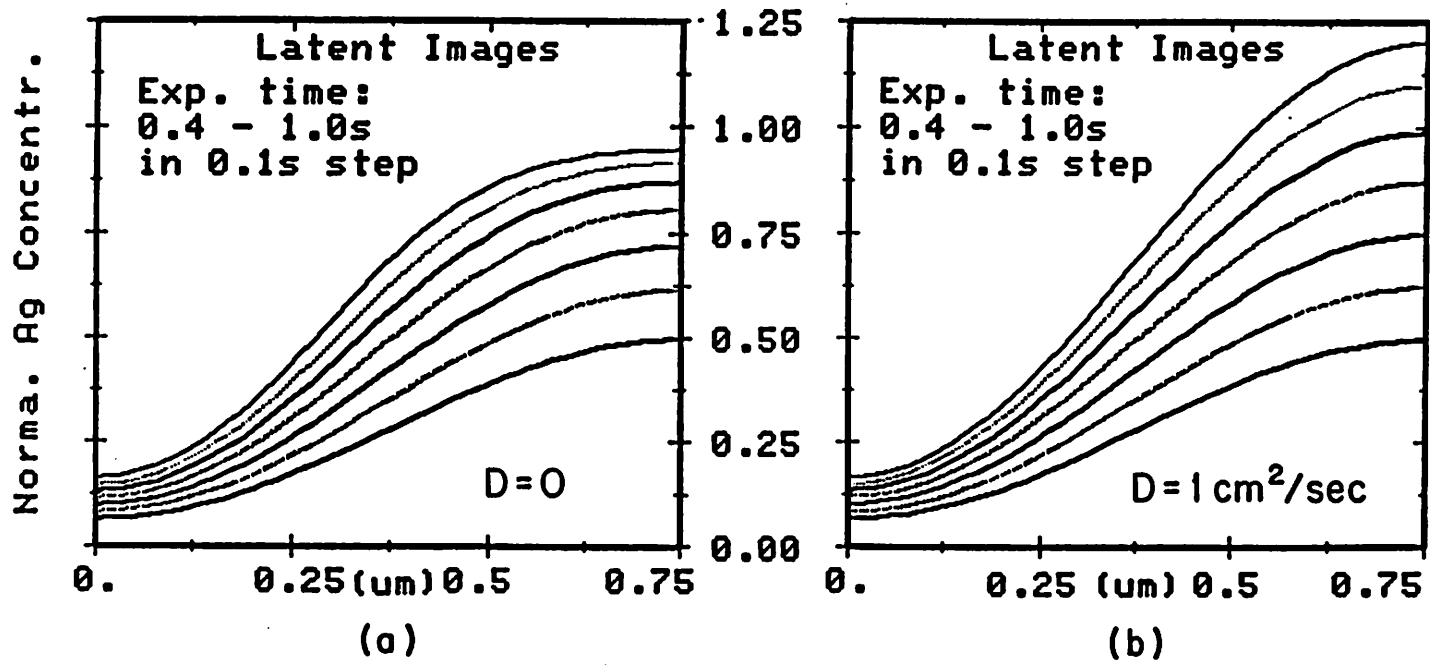


Fig. 5.4

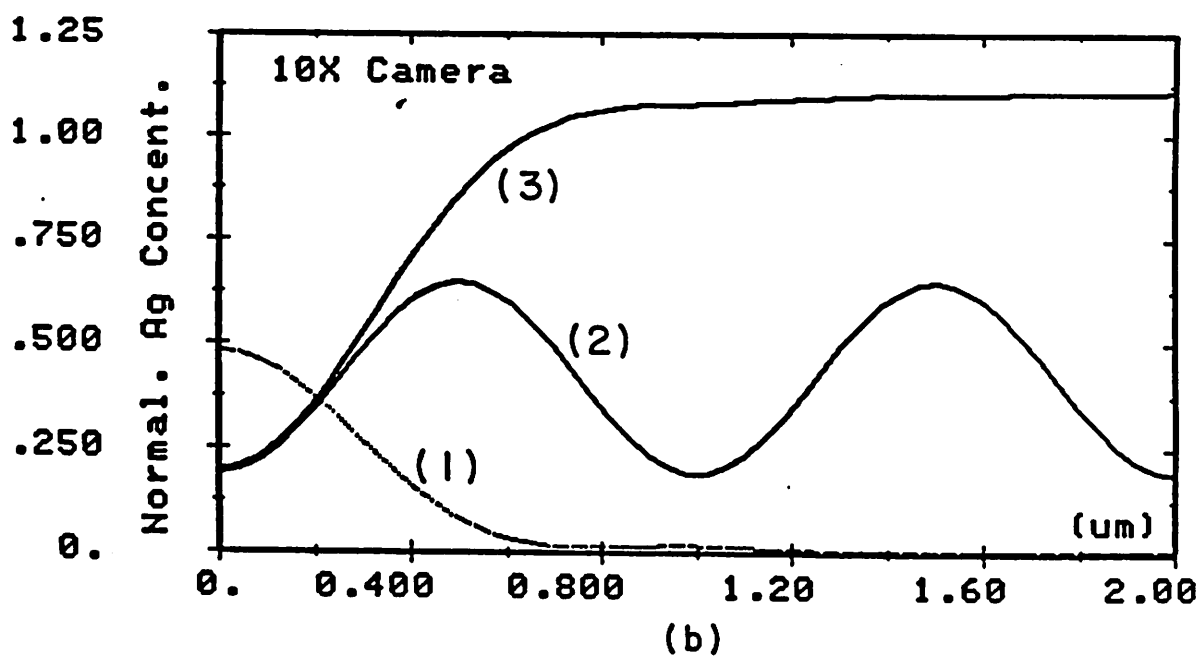
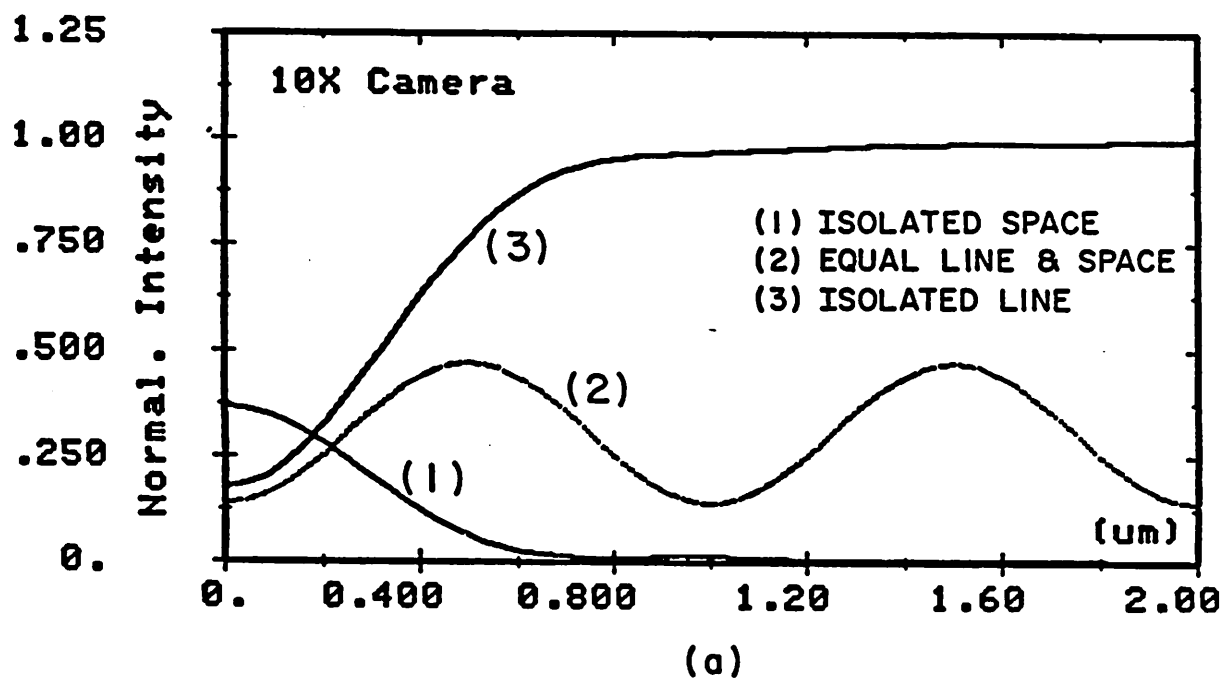
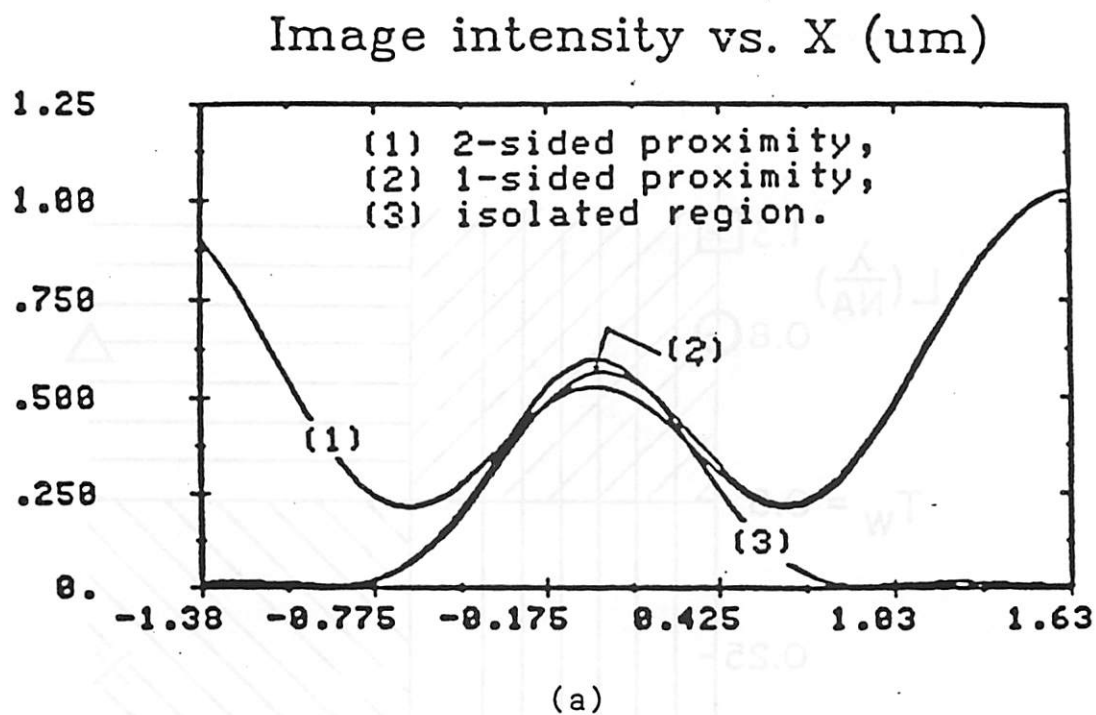
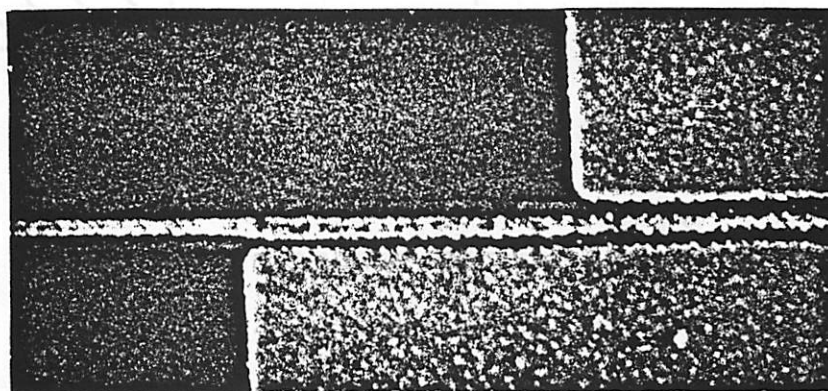


Fig. 5.5



(b)



(c)

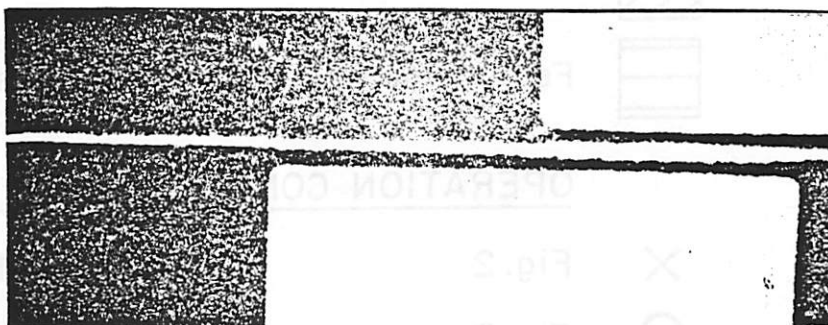
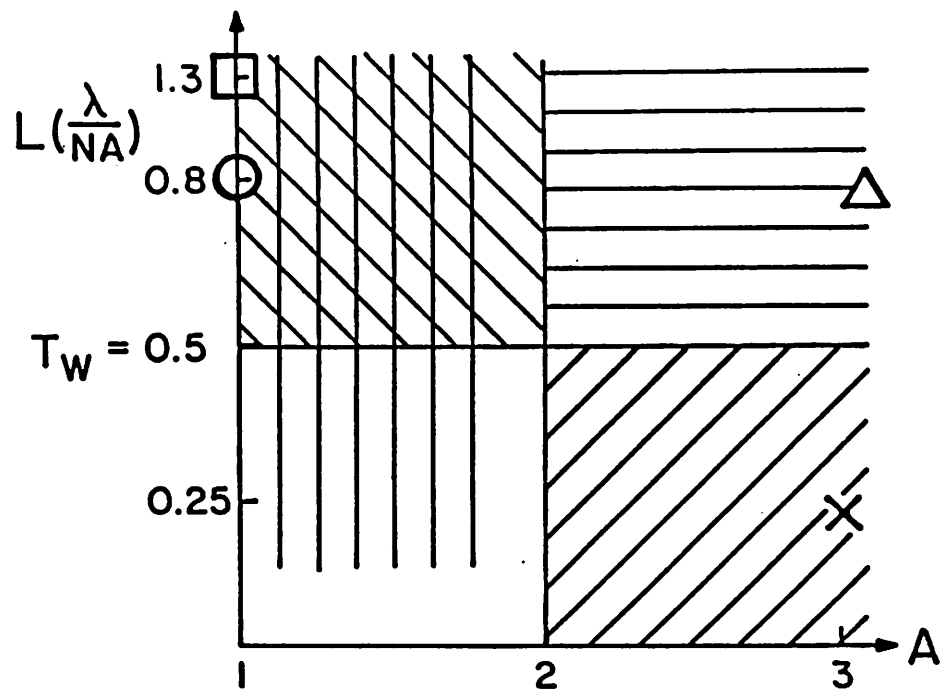


Fig. 5.6



LEGEND:

- | | |
|---|---|
|  | Contrast enhancement |
|  | Edge sharpening |
|  | Feature-dependent amplification |
|  | Feature-dependent photodoping suppression |

OPERATION CONDITION OF FIGURES:

- | | | | |
|---|--------|---|-----------------|
| × | Fig. 2 | □ | Fig. 4b, Fig. 5 |
| ○ | Fig. 3 | △ | Fig. 6 |

Fig. 5.7

Chapter 6: LITHOGRAPHIC APPLICATIONS

§ 6.1 Introduction

The $Ge_{0.1}Se_{0.9}$ resist system, with its unique material characteristics, offers many advantages in microlithographic applications over polymer resists. The advantages are high resolution, high dry-etch resistance, dry development capability, resist-profile shaping and image effect compensation. With these advantages, $Ge_{0.1}Se_{0.9}$ resist has a good potential of extending the limits of optical lithography.

§ 6.2 Resolution

As discussed in chapter 1, the theoretical minimum linewidth (L) that can be attained by an optical system is related to the exposure wavelength (λ) and numerical aperture (NA) of the printer by the equation:

$$L = k \frac{\lambda}{NA} \quad (1)$$

where k is a proportionality constant whose value depends on the photoresist material, substrate reflectivity and surface topography. By using a high resolution resist material and a resist system which minimizes the effects of substrate reflectivity and surface topography, the resolution limit of the optical system can be extended. For the existing single- and multi-layer positive resist systems, k is approximately equal to 0.6 and 0.45 respectively [1,2]. Using a layer of highly-absorptive polymer resist to minimize the topography and light interference effects and a thin layer of $Ge_{0.1}Se_{0.9}$ resist material, the bi-level $Ge_{0.1}Se_{0.9}$ resist system has attained a minimum k value of 0.33 [3]. This is the smallest value reported for any optical resist system. The SEM micrographs shown in Fig. 6.1 illustrates the high resolution capability of the bi-level resist system developed at Berkeley. Equal lines-and-spaces (L/S) patterns with critical dimensions of 0.5 and $0.75\mu m$ were printed using the 10X camera and the GCA stepper respectively. Resolution of submicron features using commercially available printers is clearly demonstrated.

As described by equation (1), the resolution limit of optical lithography can also be extended by decreasing the radiation wavelength of the optical system. However, commercially available positive resist, such as Kodak 820 and AZ1350J, has a spectral response limited to the near UV (350–436nm) region [4] and they are not suitable for lithography applications in the spectral region of mid to deep UV (200–300nm). Ge_xSe_{1-x} resists, with its broad spectral response, can be used as a near UV, mid UV as well as deep UV resist. The transmission spectrum of the Ag_2Se / Ge_xSe_{1-x} system reported by Tai et al [5] is reproduced in Fig. 6.2. It shows that Ge_xSe_{1-x} resist is more sensitive to radiation at deep and mid UV frequencies than those at near UV.

The high sensitivity of $Ge_{0.1}Se_{0.9}$ resist to deep UV radiation has been demonstrated by Tai et al [6]. Using a projection system with a NA of 0.16 and exposure wavelengths at $260 \pm 40nm$, L/S features with linewidths as small as $0.75\mu m$ were resolved with a dose of $50mJ / cm^2$. This dosage is only one tenth of that required for PMMA resist. For a system with a NA of 0.35 and λ at $220nm$, the extrapolated resolution limit of $Ge_{0.1}Se_{0.9}$ is $0.25\mu m$. The high resolution of $Ge_{0.1}Se_{0.9}$ resist has the capability of putting optical in direct competition with x-ray and e-beam lithography for applications in the submicron regime.

§ 6.3 Dry development

As discussed in chapter 2, Ge_xSe_{1-x} resist can be developed in an SF_6 plasma. The advantages of using dry development include chemical savings, compatibility with process automation, higher resist sensitivity and development contrast. The first two are associated with the characteristics of the dry-etching process, and the last two are associated with the properties of the material.

One of the major concerns in using Ge_xSe_{1-x} resist for IC manufacturing is the low sensitivity ($130mJ / cm^2$) of the resist to UV radiation compared to that ($60mJ / cm^2$) of positive resists. Low photo-sensitivity reduces the through-put of the expensive projec-

tion printer and increases the cost of each IC manufactured. The concern was alleviated when Huggett et al showed that the sensitivity of $Ge_{0.1}Se_{0.9}$ resist can be increased by a factor of two using dry development instead of wet [7]. With the development carried out in SF_6 plasma, submicron features exposed with a dose of $50mJ/cm^2$ were well resolved. The exposure dose is almost comparable with that of positive polymer resist. The increased in photo-sensitivity is a result of the high dry-etching selectivity (500:1) between Ag-doped and undoped $Ge_{0.1}Se_{0.9}$. The high dry-etching selectivity also translates into high development contrast (γ). Using dry development, Huggett et al reported a development contrast of 8 [7] which is considerably higher than the contrast value of 6 obtained using wet development [8].

Development of the $Ge_{0.1}Se_{0.9}$ resist using SF_6 plasma has also been carried out successfully using the Plasma Therm plasma reactor in Berkeley microfabrication lab. Using the etching condition described in chapter 2, submicron features were printed with considerably lower exposure energy. Fig. 6.3 shows the SEM micrograph of the developed pattern printed with an exposure dose of $150mJ/cm^2$ using the GCA stepper. L/S features with linewidths of 0.8 to $10\mu m$ were resolved simultaneously within 10% linewidth variation. Table 6.1 compares the exposure dosages normally used at Berkeley for the GCA stepper for the resists listed. The sensitivity of the $Ge_{0.1}Se_{0.9}$ resist developed in SF_6 plasma is comparable to that of Kodak 820 and AZ1350J resist.

§ 6.4 Shaping of the resist profile

As discussed in chapter 2, the polymer layer in a bi-level Ge_xSe_{1-x} resist system can be delineated using reactive ion etching in an oxygen plasma. The delineation is possible because of the high etch resistance of the Ge_xSe_{1-x} layer to an oxygen plasma [5]. The two-layer resist structure together with the control offered by plasma etching in shaping the etched profile [9] allow the construction of different resist structures to meet different processing requirements. For examples the vertical profile, as shown in Fig. 6.4 (a), is desirable for dry etching processes and the overhanging profile, as illustrated in

Fig. 6.4 (b), is required for lift-off processes [10]. Fig. 6.4 (a) shows the cross-section of a $1.0\mu\text{m}$ L/S pattern. The polymer layer was delineated using RIE in an oxygen plasma with the process conditions described in chapter 2. Fig. 6.4 (b) shows the cross-section of a $0.8\mu\text{m}$ L/S pattern with the polymer layer purposely over-etched in an oxygen plasma. The overhang structure was used to define palladium (Pd) patterns using lift-off. The results are shown in Fig. 6.5. Pd lines with thickness of $0.5\mu\text{m}$ and linewidths down to $0.8\mu\text{m}$ are clearly defined.

§ 6.5 Image effect compensation

§ 6.5.1 Proximity effect compensation

The proximity of large features affects the printing of small ones through two mechanisms: diffraction effects in forming the local image intensity and the lateral Ag diffusion in extending the supply of photodoping Ag. These effects have been studied in detail in [11]. Depending on the filling factor of the illuminator, light diffracted from nearby large openings can decrease or increase the local image intensity of a line with respect to that of the line with no neighbor. The two cases are illustrated in Fig. 6.6 (a) and Fig. 6.6 (b) respectively. Using conventional resist systems, a small line under the strong influence of the proximity effect cannot be printed simultaneously with an isolated line of the same width without sacrificing linewidth variation. However, using $\text{Ge}_{0.1}\text{Se}_{0.9}$ resists, compensation of the proximity effect is possible by controlling the diffusion and photobleaching effects.

The effect of feature-dependent amplification can be used to compensate for the image effect. Fig. 6.6 (b) shows the aerial images of a $0.5\mu\text{m}$ line in the 2-sided proximity, one-sided proximity and isolated region projected by the 10X camera with a σ value of 1. The proximity distance, the distance between the line and the large openings, is also $0.5\mu\text{m}$. Notice that diffraction effects cause the local intensity of the line to be higher in the proximity regions than in the isolated regions. Fig. 6.7 (a) and (b) show

the SEM micrographs of the developed pattern. As shown by the width of the line, diffraction effects dominate at low-dose exposure and the line has more photodoped Ag in the proximity regions than in the isolated region. At high-dose exposure, the effect of feature-dependent amplification dominates and the line has more photodoped Ag in the isolated region than in the proximity regions. The results suggest that by varying the exposure dose, the effect of feature-dependent amplification can be adjusted to offset the image effect. Fig. 6.8 shows the result of using this compensation technique. The simulated latent image of the line in the three regions is shown in Fig. 6.8 (a). If a threshold development model is assumed, at a threshold of 0.5, the line in the three regions can be printed with linewidth constant to better than 5%. The experimental results are shown in Fig. 6.8 (b) and (c).

Diffraction effects can also cause the local intensity of the line to be smaller in the proximity regions than in the isolated region. This effect is illustrated by the image intensities shown in Fig. 6.6 (a). In this case, both the image and the feature-dependent amplification effect cause the line to have more photodoped Ag in the isolated region than in the proximity regions. These effects are confirmed by the developed patterns shown in Fig. 6.9. The line is $0.75\mu m$ wide and the proximity distance is $0.5\mu m$. At low-dose exposure, thinning of the line in the proximity regions is caused mainly by the aerial image effect. At high dose, feature-dependent amplification aggravates the thinning. To compensate for these proximity effects, a mechanism is needed to increase photodoping in the proximity region or to suppress photodoping in the isolated region. Fig. 6.10 (a) shows that when the pattern is printed on a resist with a $15nm$ thick Ag_2Se layer, the effect of feature-dependent photodoping suppression results in a line which has more photodoping in the proximity regions than in the isolated region. By adjusting the exposure time, this effect can be used to compensate for the aerial image effects. This compensation method is used to obtain the developed images shown in Fig. 6.10 (b) and (c). They are printed on a $Ge_{0.1}Se_{0.9}$ resist which has a $15nm$ thick Ag_2Se layer. Only the

isolated and 2-sided proximity region of the pattern are shown. The widths of the line in the two regions are approximately equal indicating the effectiveness of the compensation. (The exposure is chosen to compensate for the proximity effects in the 2-sided proximity region only.)

§ 6.5.2 Printing of small isolated features

By controlling the exposure dose, small complementary features, which cannot be printed simultaneously using any existing polymer resist system, can be printed simultaneously using $Ge_{0.1}Se_{0.9}$ resists. Examples of these features are a hole and a pad, and an isolated line and a space with the characteristic that the maximum image intensity of the small bright feature is lower than the minimum intensity of the small dark feature. In Fig. 6.11, the simulated intensity at the center of isolated features is plotted as a function of normalized critical dimension [12]. For the GCA stepper, image intensities of isolated lines and spaces with linewidth of $0.44\mu m$ ($0.28x\lambda/NA$) or less have the image characteristic stated above. These complementary features normally cannot be resolved simultaneously in a polymer resist system. However, in $Ge_{0.1}Se_{0.9}$ resists, the effect of feature-dependent amplification can cause the latent image of a small bright feature to be amplified much larger than that of the complementary feature. Consequently, the features can be printed simultaneously. Fig. 6.12 (a) and (b) show the SEM micrographs of the developed image of $0.48\mu m$ ($0.31\lambda/NA$) isolated space (small line opening in the mask) and $0.38\mu m$ ($0.24\lambda/NA$) line printed by the GCA stepper. The simulated intensities at the centers of the features are shown in Fig. 6.11. The developed image of the space and line has a critical dimension of 0.5 and $0.35\mu m$ respectively. The experiment is repeated with $0.7\mu m$ ($0.45\lambda/NA$) square holes and pads and the results are shown in Fig. 6.12 (c) and (d). In both cases the features are clearly resolved showing that $Ge_{0.1}Se_{0.9}$ is capable of printing simultaneously small complementary features which cannot be printed by any existing polymer resist systems.

§ 6.5.3 Defect printability suppression

During the printing of regular features, defects on the mask may also be printed. It is desirable to suppress the printing of defects without affecting the printing of regular features. Fig. 6.13 shows the simulated aerial and latent images of a pair of $0.78\mu m$ complementary square features printed by the GCA stepper on resists with different Ag_2Se layer thicknesses. The exposure time in each case is chosen so that photodoping saturation occurs at large bright areas. As the Ag_2Se layer thickness increases, the relative photodoped-Ag concentration of the small bright feature decreases. The decrease is caused by the effect of feature-dependent photodoping suppression which suppresses Ag photodoping of the small bright feature and the suppression is larger with thicker Ag_2Se layer. The results suggest that the printability of small bright defects can be suppressed using the effect of feature-dependent photodoping suppression.

The effectiveness of applying this technique to suppress the printability of open defects is further illustrated by the experimental results shown in Fig. 6.14 where the size of the printed square features is plotted against their size on mask for different Ag_2Se layer thickness. The open features are defined as small openings on the mask and they are simulated defects in this experiment. The square pads (chrome pads in the mask) are regular features. The developed images are printed with the same development time on the same wafer which has two regions Ag sensitized for 60 and 75 seconds. The exposure time in each case is chosen so that the regular features of sizes down to $1\mu m$ are printed with less than 10% size variations. As shown in Fig. 6.14 (a), small open defects are printed as well as regular features in the region sensitized for 60 seconds. However, Fig. 6.14 (b) shows that in the region sensitized for 75 second (thicker Ag_2Se layer), the size of printed defects is much smaller than their size in the mask. Open defects with size less than $0.75\mu m$ are not printed at all.

§ 6.6 Conclusions

The bi-level $Ge_{0.1}Se_{0.9}$ resist system offers many advantages over polymer resist systems in microlithographic applications. The $Ge_{0.1}Se_{0.9}$ resist has a resolution and development contrast unmatched by any reported resist material. The high etch resistance to oxygen plasma enables the planarization layer to be delineated using RIE as well as PCM. Reactive ion etching allows the etched resist profile to be tuned to meet different process requirements. By controlling the Ag_2Se layer thickness and exposure time, the effects of the exposure phenomena can be adjusted to compensate proximity effects caused by light diffraction, to print simultaneously small complementary features whose image intensities do not cross each other, or to suppress the printability of open defects.

References

- [1] V. Miller and H. L. Stover, "Submicron optical lithography: I-line wafer stepper and photoresist technology", *Solid State Technology*, vol. 28, no. 1, p.127, 1985.
- [2] C. H. Ting, K. L. Liauw, "An improved DUV multi-layer resist process for high resolution lithography", *Proc. of SPIE*, vol. 469, p.24, 1984.
- [3] E. Ong, K. L. Tai and R. G. Vadimsky, "Ge-Se based resist system for submicron VLSI applications", *Proc. of SPIE*, vol. 394, p.39, 1983.
- [4] G. Willson, R. Miller, D. McKean, N. Clecak, T. Tompkins and D. Hofer, "Design of a positive resist for projection lithography in the mid UV", *Proc. Regional Tech. Conf. on Photopolymer, Principles, Processes and Materials*, Midhuson section, SPE, Ellenville, N. Y., p.111, Oct., 1982.
- [5] K. L. Tai, W. R. Sinclair, R. G. Vadimsky and J. M. Moran, "Bi-level high resolution photolithographic technique for us with wafers with stepped and/or reflecting surfaces", *J. of Vacc. Sci. Technol.*, vol. 16, no. 6, p.1977, 1979.
- [6] E. Ong, K. L. Tai and R. G. Vadimsky, "Application of GeSe as a deep UV resist for submicron lithography", *Proc. of ECS*, vol. 82-9, p.71, 1982.
- [7] P. G. Huggett, K. Frick and H. W. Lehmann, "Development of silver sensitized Germanium Selenide photoresist by reactive sputter etching in SF_6 ", *Appl. Phys. Lett.*, vol. 42, no. 7, p.592, 1983.
- [8] K. L. Tai, R. G. Vadimsky, C. T. Kemmerer, J. S. Wagner, V. E. Lamberti, and A. G. Timko, "Submicron optical lithography using an inorganic resist/polymer bilevel scheme", *J. of Vac. Sci. Technol.*, vol. 17, no. 5, p.1169, 1980.
- [9] J. L. Reynolds, "Characterization of plasma etched structures in IC processing", PhD dissertation, EECS dept., Univ. of Cal at Berkeley, 1983.
- [10] B. J. Lin, E. Bassous, V. W. Chao, and K. E. Petrillo, "Practicing the Novolac deep-UV portable conformable masking technique", *J. of Vac. Sci. Technol.*, vol. 19, no.

4, p.1313, 1981.

- [11] W. Leung, A. R. Neureuther and W. G. Oldham, "Proximity Effects and Printability of Defects in GeSe Resist", Journal of Vacc. Sci. and Technol., vol.3, no.1, p.310, 1985.
- [12] M. D. Prouty, "Addition to The Imaging of SAMPLE", M. S. Project Report, University of California, Berkeley, 1984.

Figure Captions

Fig. 6.1 SEM micrography of equal lines-and-spaces features with critical dimension of (a) $0.5\mu m$ and (b) $0.75\mu m$.

Fig. 6.2 Transmittance as a function of radiation wavelength for Ge_xSe_{1-x} films. (Courtesy of Tai et al [5]).

Fig. 6.3 SEM micrographs of developed L/S features with linewidths of (a) $10-1\mu m$ and (b) $0.8\mu m$ printed by the GCA stepper with exposure time of 0.3 second.

Fig. 6.4 Cross-section of (a) $1\mu m$ L/S and (b) $0.8\mu m$ equal lines-and-spaces with the polymer layer delineated using RIE in oxygen plasma.

Fig. 6.5 SEM micrographs of 0.8 and (b) $1.25\mu m$ equal lines-and-spaces defined using by the lift-off process.

Fig. 6.6 Simulated aerial images of the three regions of the proximity-effect pattern projected by the (a) GCA stepper and (b) 10X camera.

Fig. 6.7 SEM micrographs of the developed pattern printed by the 10X camera with doses of (a) $120mJ/cm^2$ and (b) $500mJ/cm^2$.

Fig. 6.8 (a) Simulated latent images of the three regions of the proximity-effect pattern printed by the 10X camera. (b) and (c) Experimental results printed with a dose of $300mJ/cm^2$.

Fig. 6.9 SEM micrographs of the developed pattern printed by the GCA stepper with doses of (a) $250mJ/cm^2$ and (b) $550mJ/cm^2$.

Fig. 6.10 SEM micrographs of the developed pattern printed by the GCA stepper with (a) 560, (b) and (c) $1000mJ/cm^2$ dose.

Fig. 6.11 Simulated intensity at the center of complementary 1- and 2-dimensional features as a function of normalized feature size. The projection printer simulated has a filling factor of 0.7.

Fig. 6.12 SEM micrographs of developed image of (a) $0.5\mu m$ isolated gap, (b) $0.5\mu m$ isolated line, (c) $0.7\mu m$ square hole and (d) $0.7\mu m$ square pad. The 1- and 2-dimensional features are printed with a dose of 250 and $500mJ/cm^2$ respectively.

Fig. 6.13 Simulated (a) aerial and latent images of $0.78\mu m$ square hole and pad printed by the GCA stepper on *GeSe* resists with Ag_2Se layer thickness of (b) 90, (c) 150 and (d) 200 nm.

Fig. 6.14 The feature size of square features as a function of mask feature size. The features are printed by the GCA stepper on a *GeSe* resist with a sensitization time of (a) 60 (b) 75s.

Table caption

Table 6.1 Normal dosages for the GCA stepper for the exposure of different resists on silicon substrate.

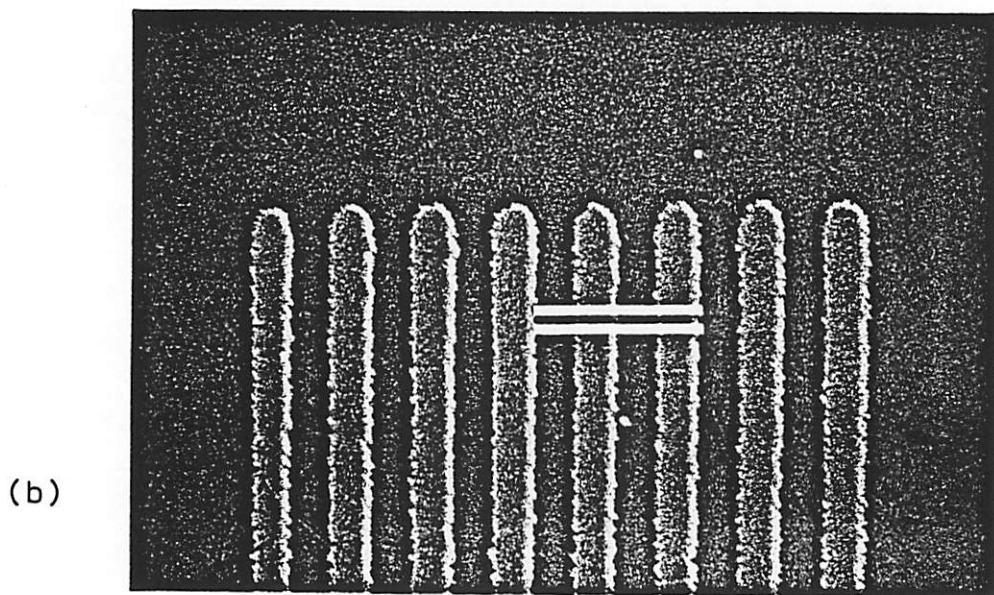
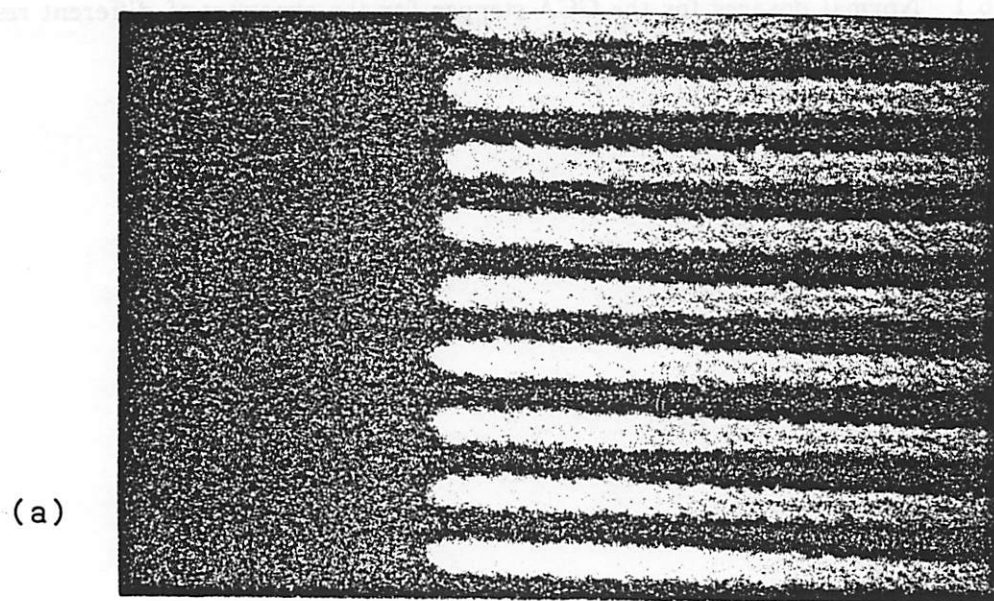


Fig. 6.1

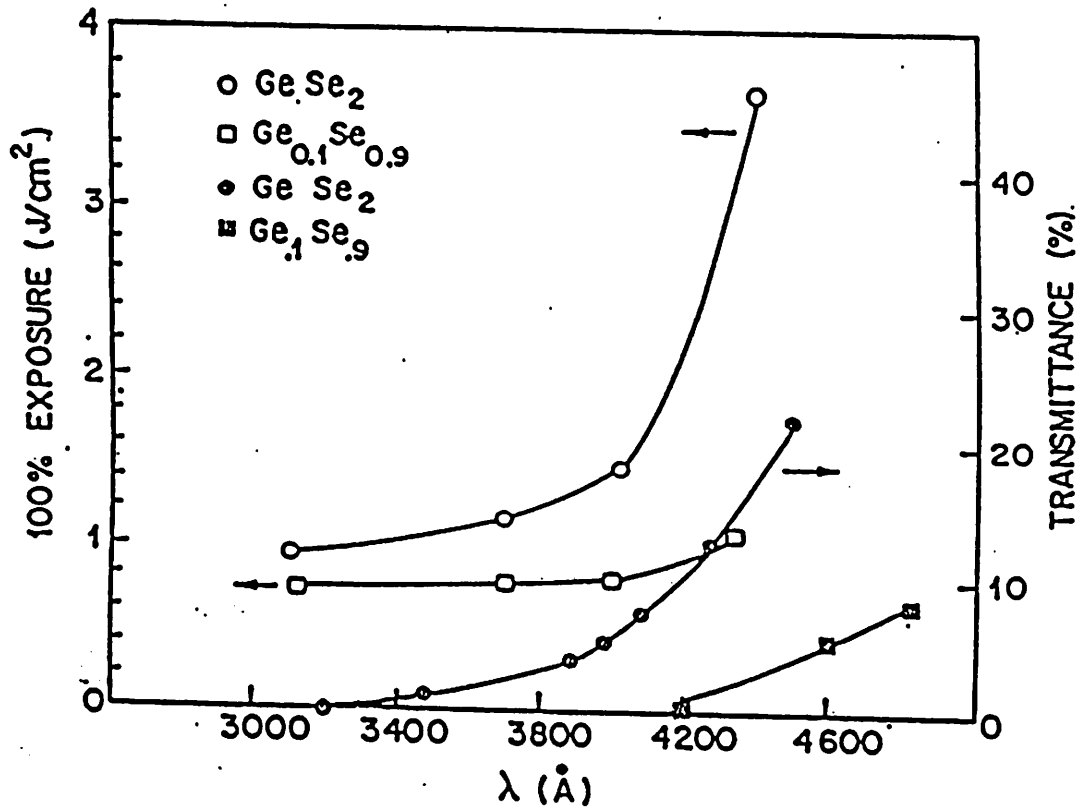


Fig. 6.2

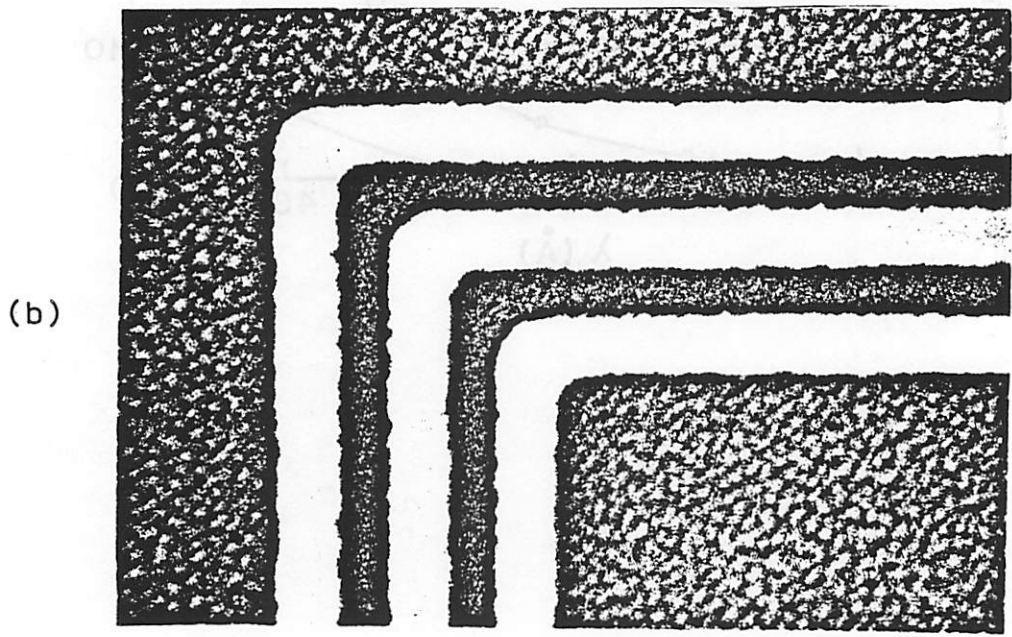
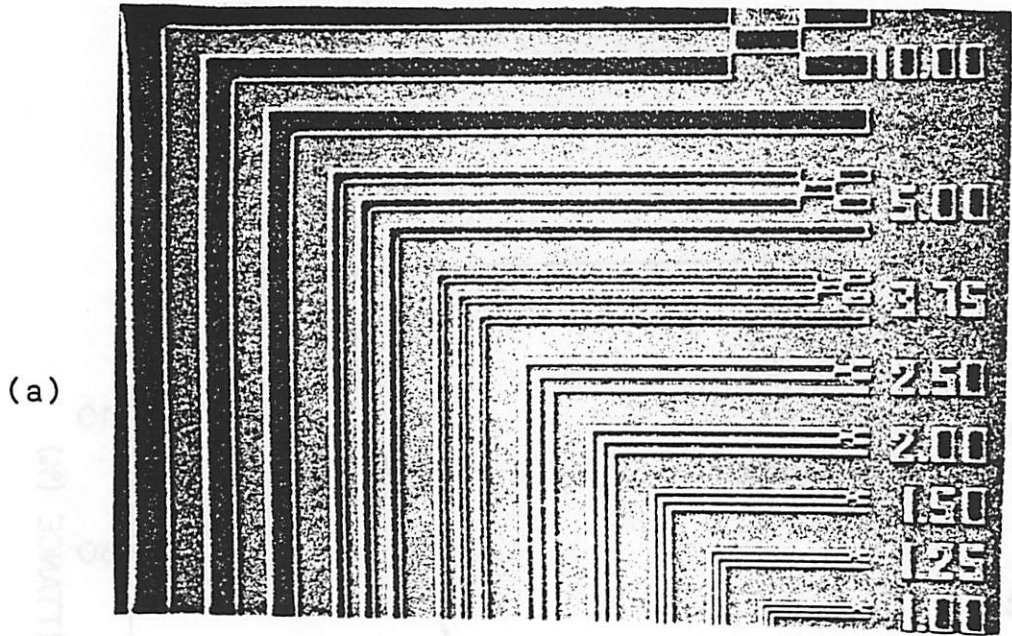


Fig. 6.3

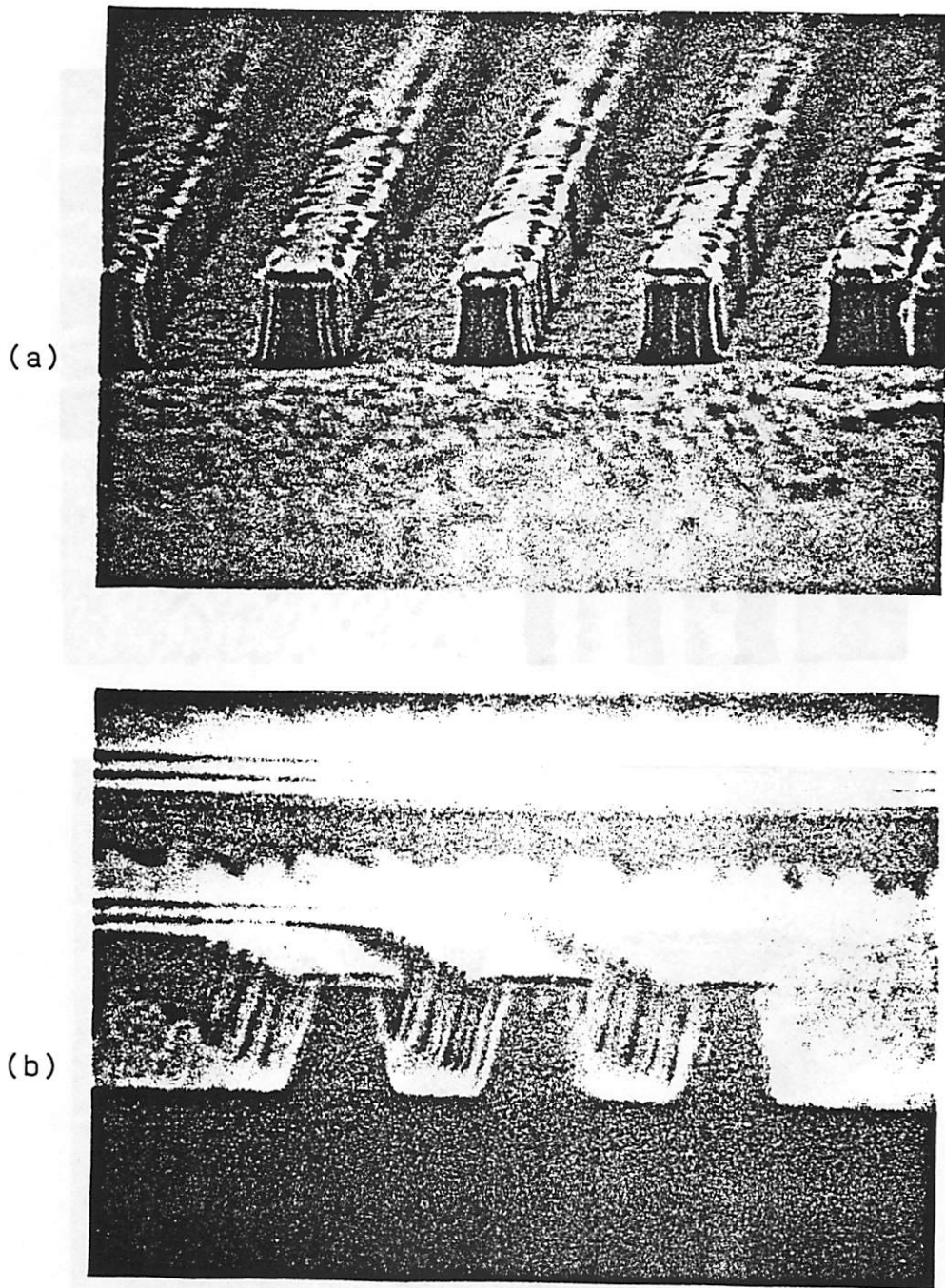


Fig. 6.4

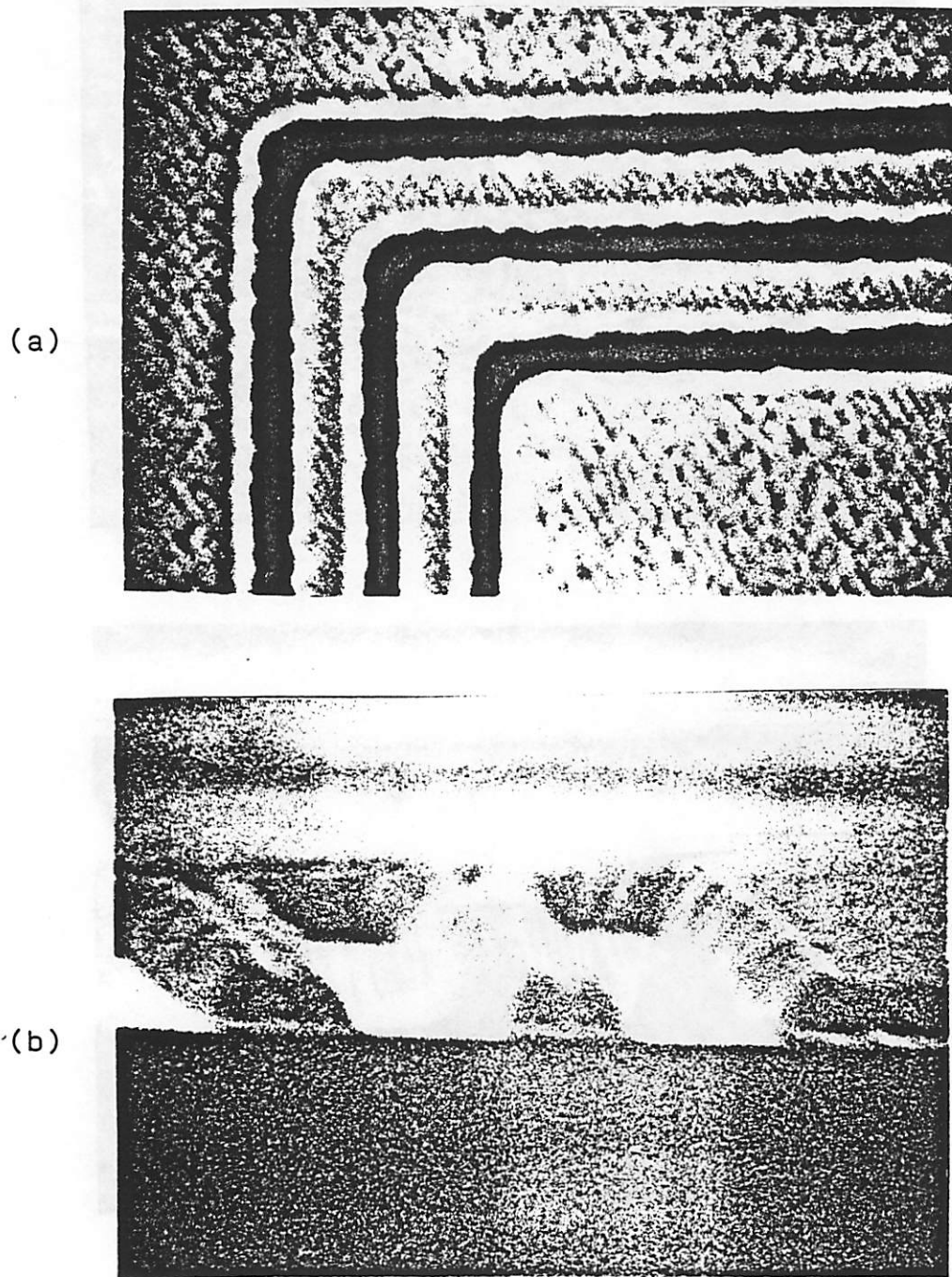


Fig. 6.5

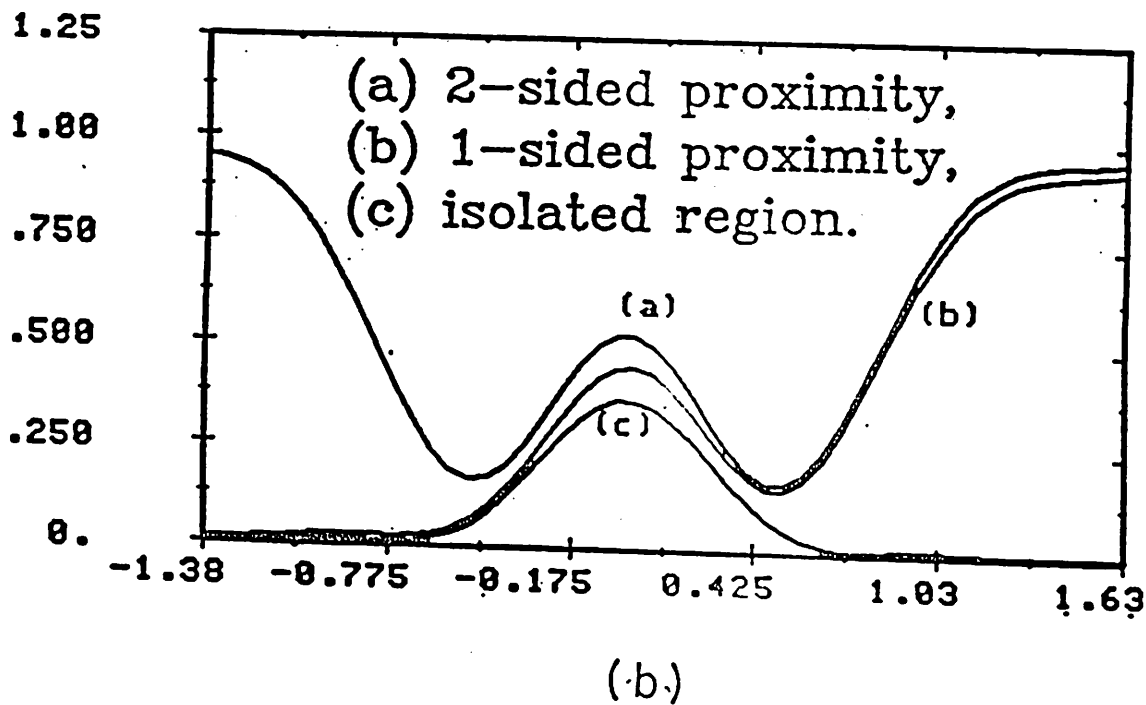
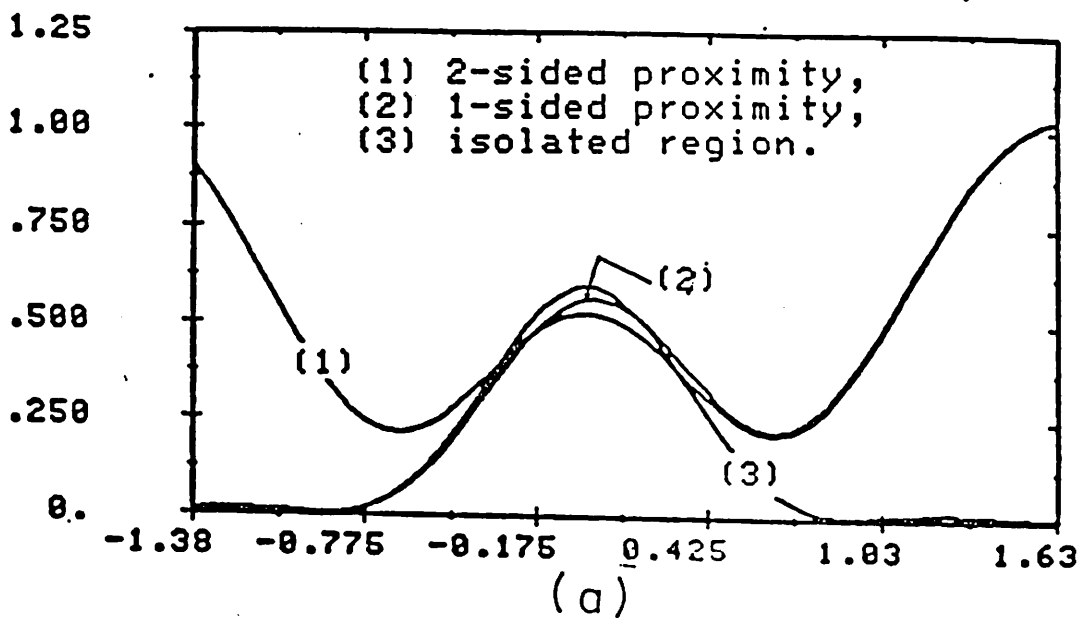
Image intensity vs. X (μm)

Fig. 6.6

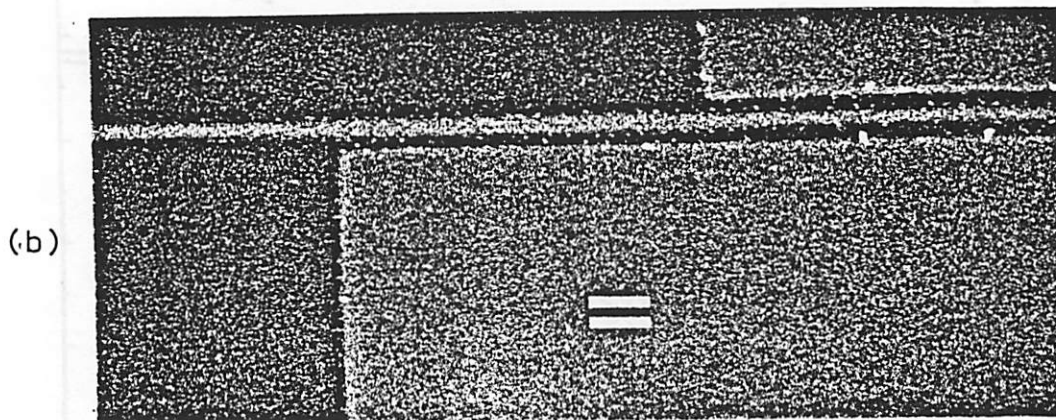
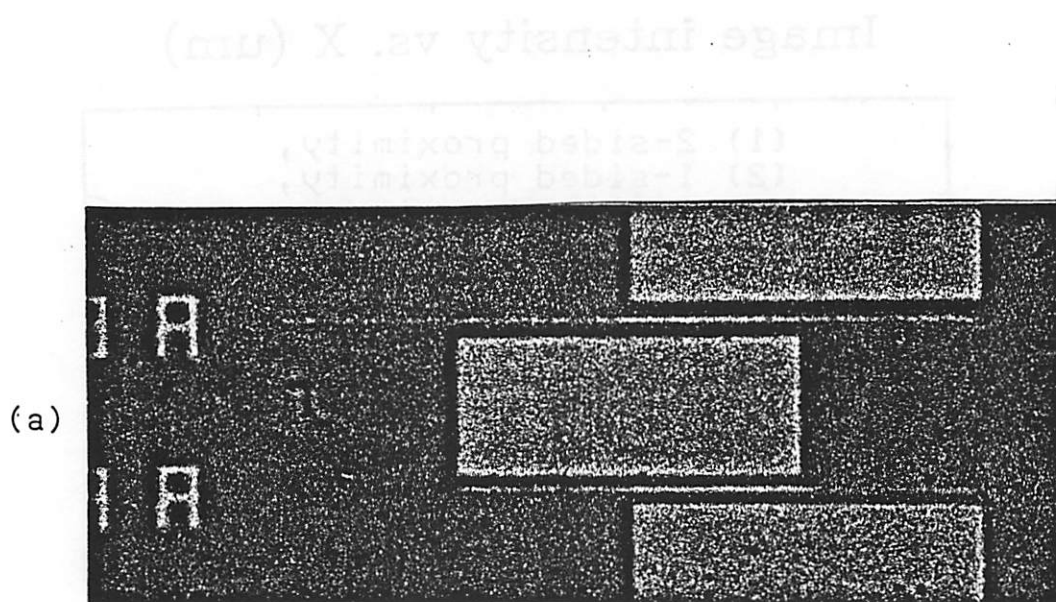
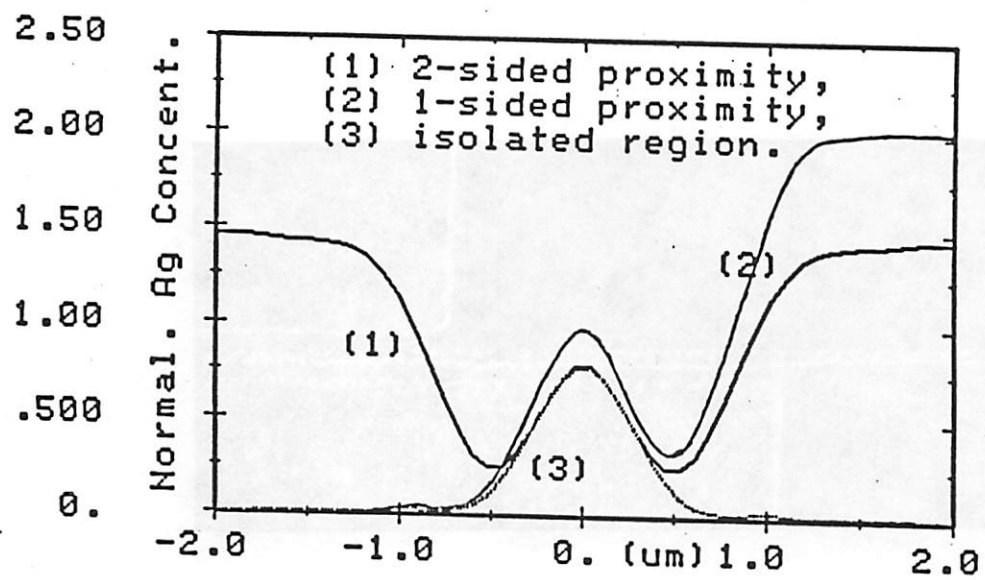
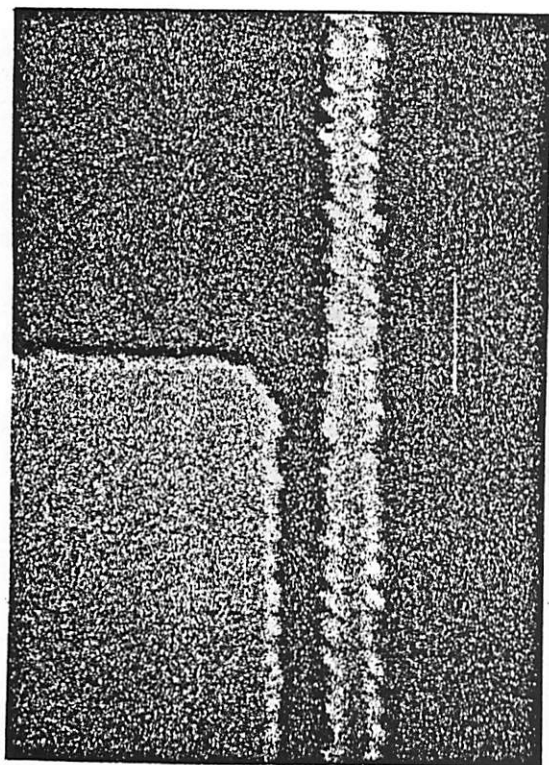


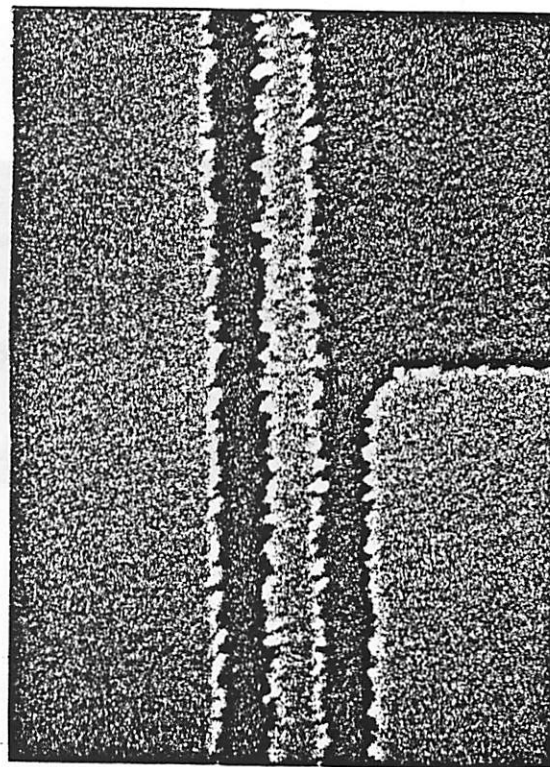
Fig. 6.7



(a)

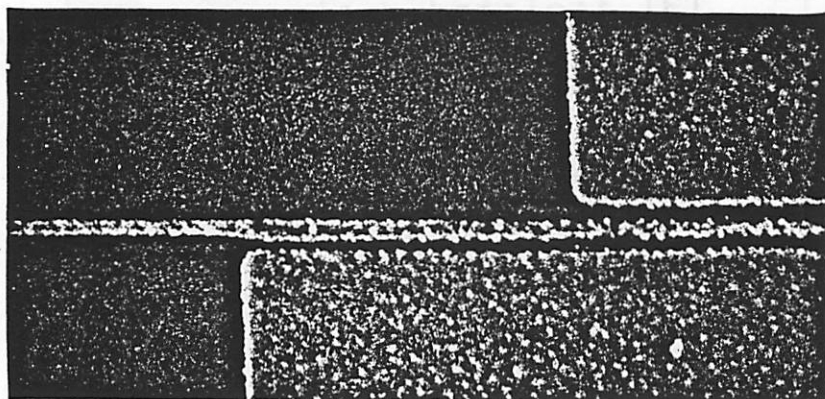


(b)

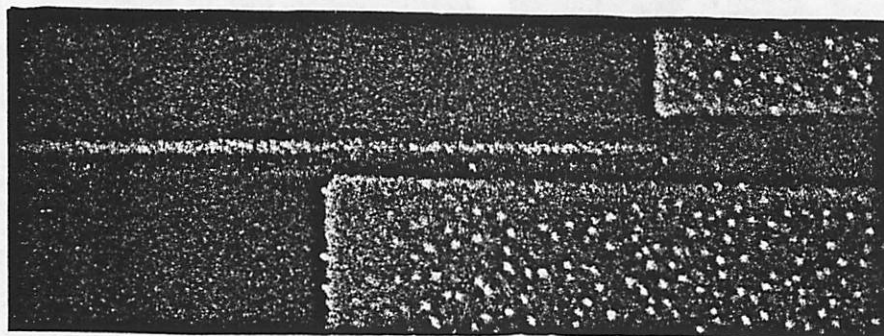


(c)

Fig. 6.8

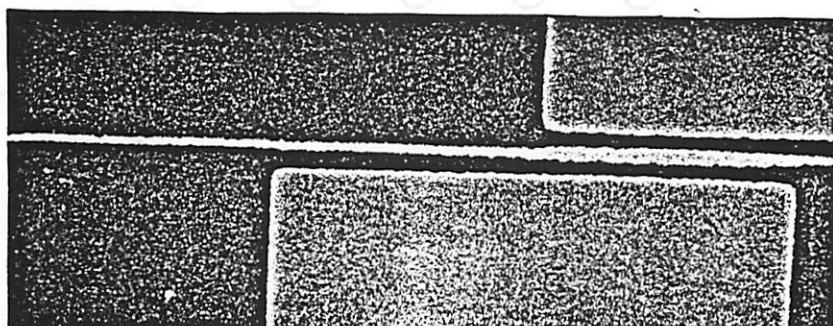


(a) (b)

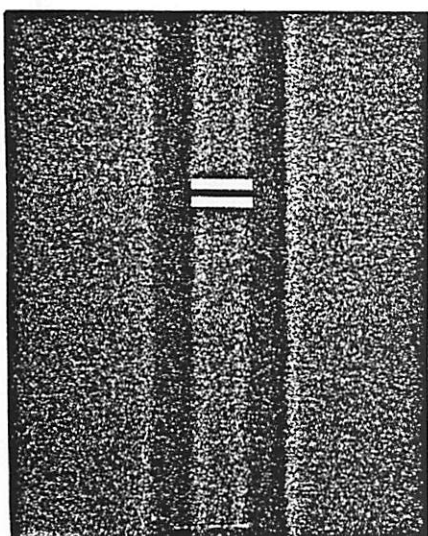


(b)

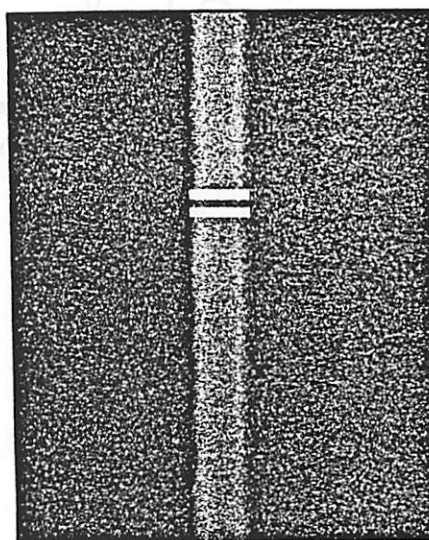
Fig. 6.9



(a)



(b)



(c)

Fig. 6.10

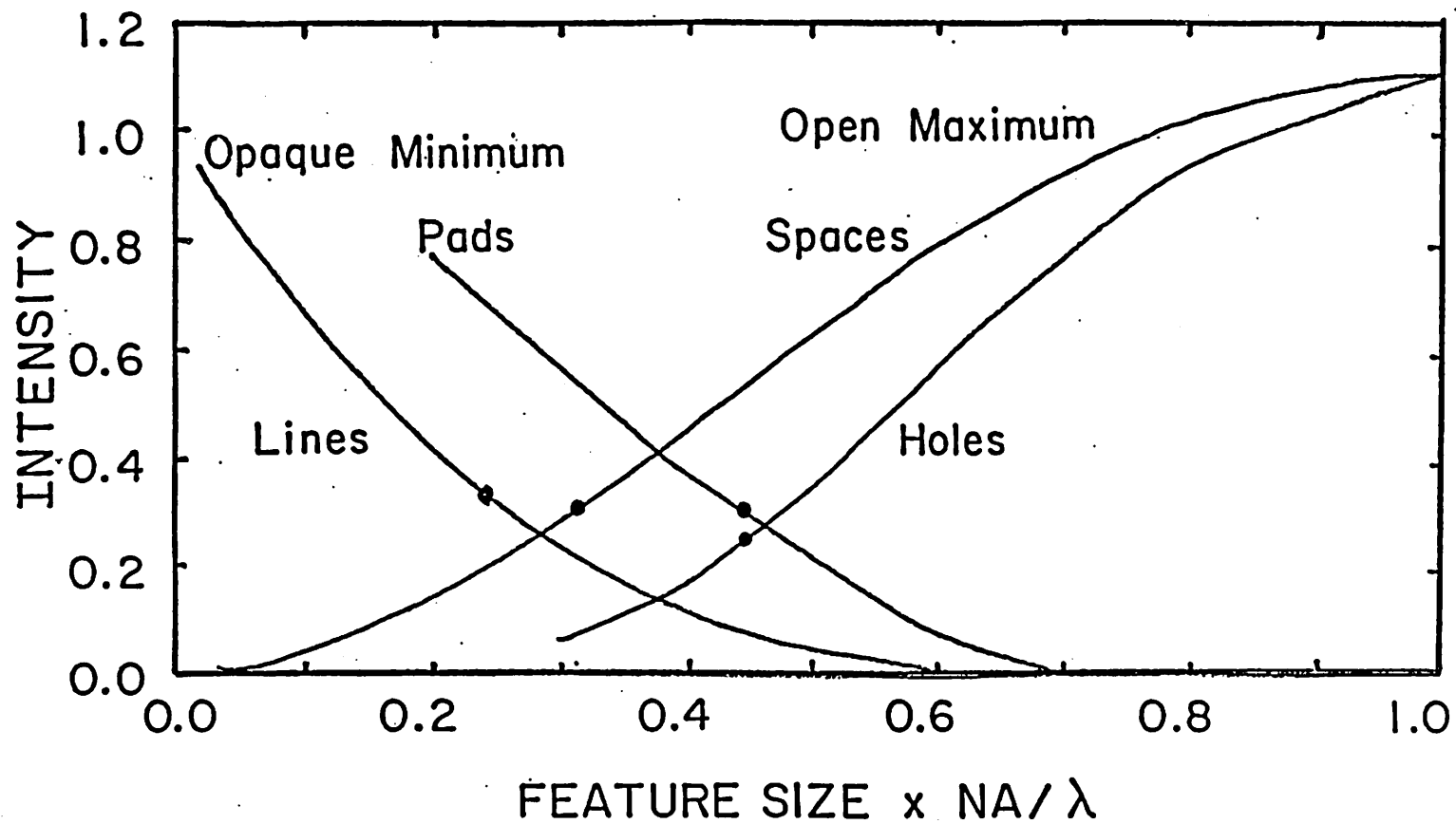
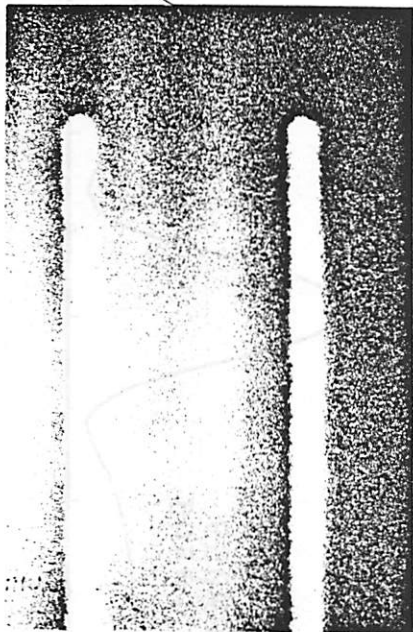
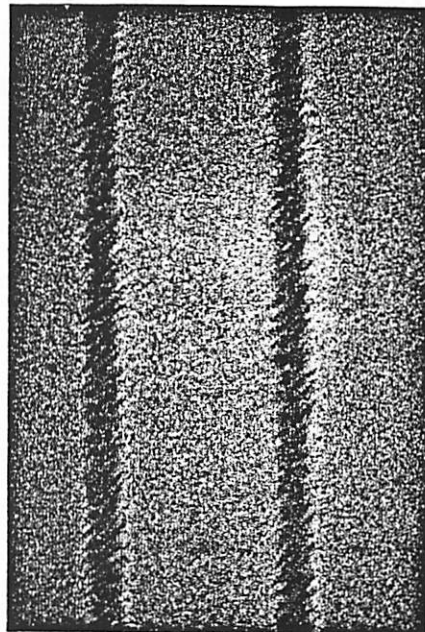


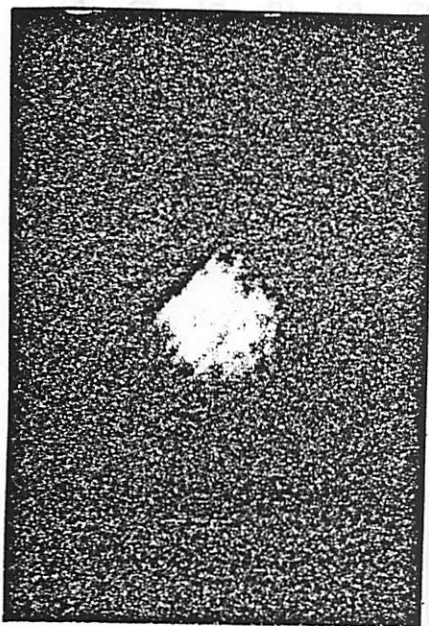
Fig. 6.11



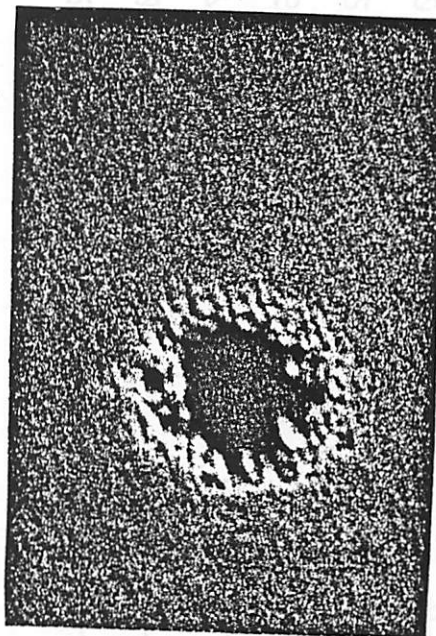
(a)



(b)



(c)



(d)

Fig. 6.12

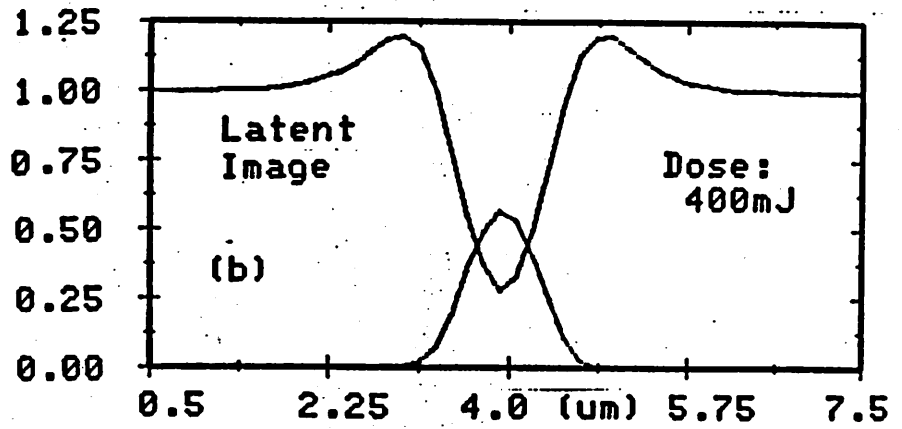
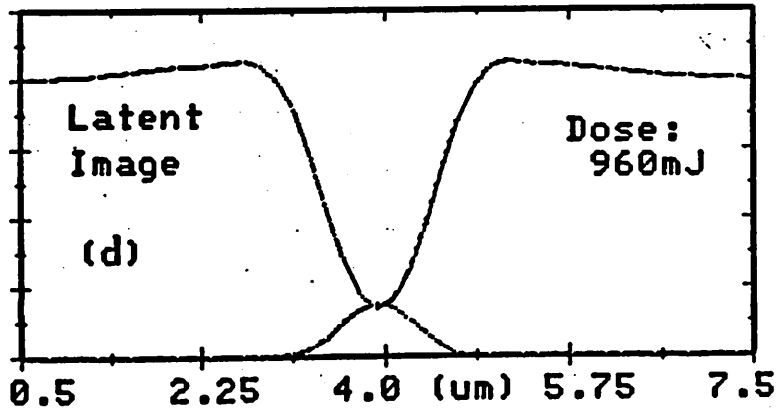
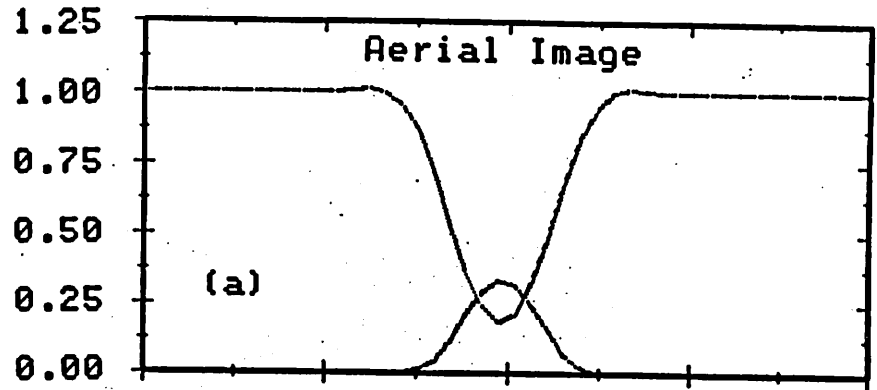
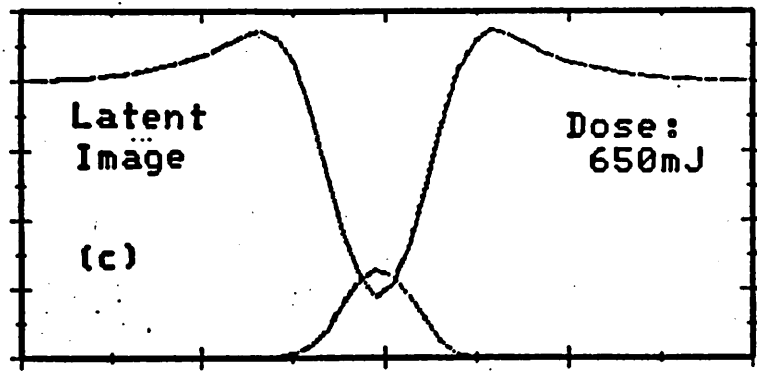


Fig. 6.13

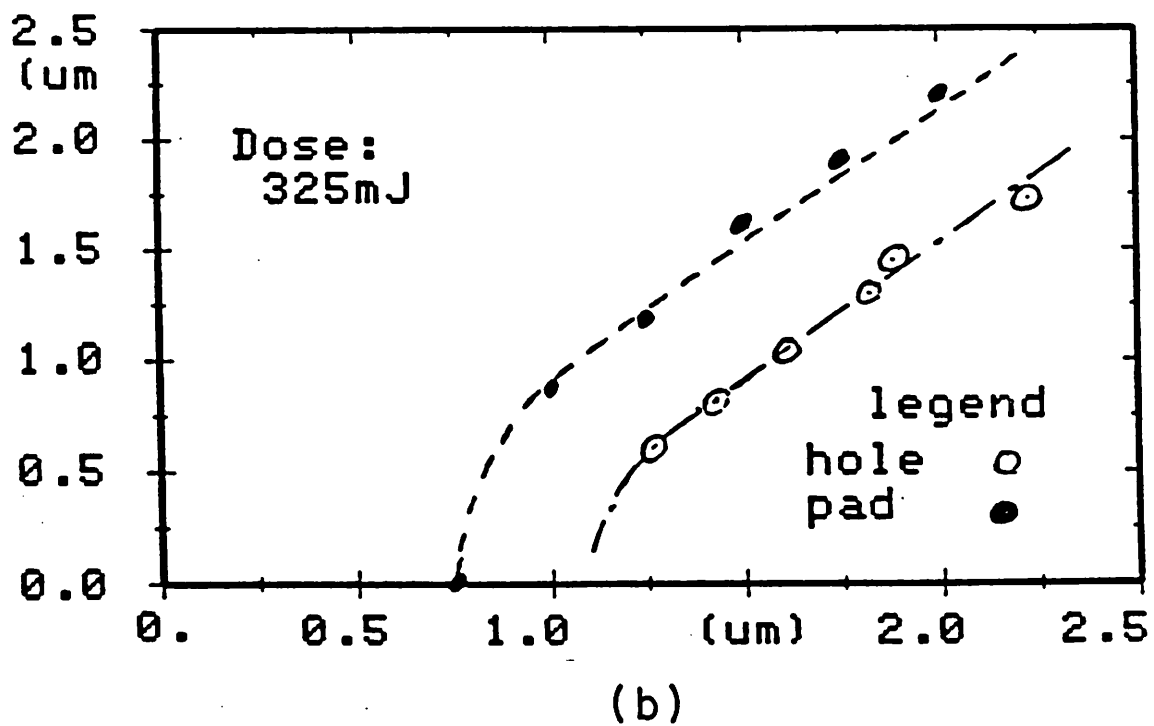
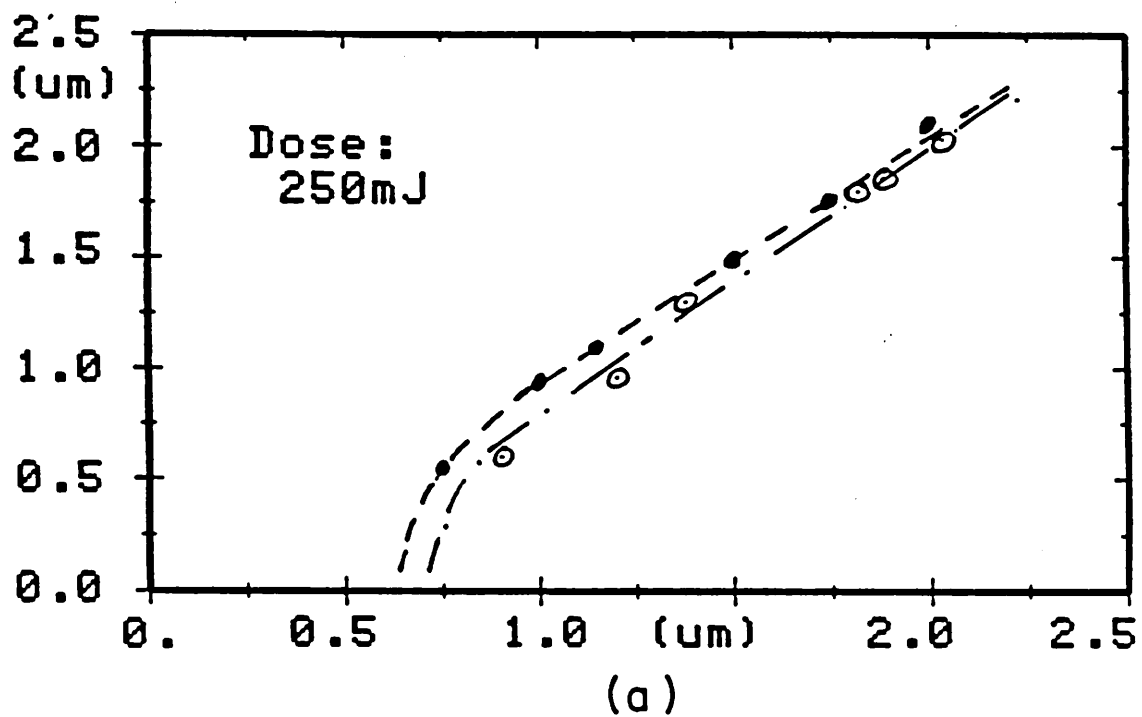


Fig. 6.14

Resist on Si substrate	Exposure time
Ge-Se/polymer (wet dev.)	0.45s
Ge-Se/polymer (dry dev.)	0.30s
Kodak 820, AZ1350J	0.25s

Table 6.1

Chapter 7: CONTAMINATION EFFECTS OF Ge-Se RESIST

§ 7.1 Introduction

The advantages of using $Ge_{0.1}Se_{0.9}$ resist in IC fabrication have been discussed in chapter 6. Despite these advantages, the resist suffers two major disadvantages in competing with polymer resists: (1) the incompatibility of the $Ge_{0.1}Se_{0.9}$ resist process with that of the existing resist process, and (2) the potential of the resist in contaminating the devices fabricated. Since a $Ge_{0.1}Se_{0.9}$ resist system contains both Ag and Se which have deep levels and therefore are potential minority carrier life-time killers [1], the devices fabricated may be contaminated by these elements and their performance thus degraded. The incompatibility issue is left to be addressed by equipment vendors. The issue of contamination is the subject of this chapter.

MOS capacitors were fabricated using $Ge_{0.1}Se_{0.9}$ and polymer resist (KTI820) with the same process procedure. Electrical characteristics of the capacitors fabricated with the two resists are measured and compared. Contamination effects of $Ge_{0.1}Se_{0.9}$ resist are characterized by the oxide trapped charges, minority carrier life-time and mobile ionic charges.

MOS transistors and junction diodes were fabricated using $Ge_{0.1}Se_{0.9}$ resist. The quality of the MOS transistors is characterized by their drain current as a function of drain to source and gate to source voltage. The quality of the junction diodes is characterized by their reverse leakage current. The reverse leakage current also gives a measure of the density of defects, recombination sites and heavy metal ions.

§ 7.2 Experimental

§ 7.2.1 MOS capacitors

The MOS capacitors were fabricated on N-type, <100>, 4-inch Si wafers with a resistivity of 4-7 ohm-cm. Two wafers were processed with the processing sequence

listed in Appendix II. A $0.6\mu m$ thick layer of field oxide was first grown. The wafers were then separated for active area definition. One wafer was defined using $Ge_{0.1}Se_{0.9}$ resist and the other was defined using KTI820 resist. To avoid cross contamination, the oxide etch for the two wafers was carried out in separate baths of buffered HF. Resist stripping was also performed in separate baths of Piranha ($5:1 H_2SO_4: H_2O_2$). Subsequently, the wafers were recombined for oxide growth, poly deposition, poly definition and back-side contact.

The capacitors fabricated had an oxide thickness of $20nm$. The top plate of the capacitors is formed by the $0.5\mu m$ phosphorous-doped polysilicon. Back-side contact was established by a $0.5\mu m$ layer of sputtered palladium. The resultant capacitors have areas of 100, 200 and $300\mu m^2$. Fig. 7.1 (a) shows the SEM micrograph of a $100\mu m^2$ capacitor fabricated with $Ge_{0.1}Se_{0.9}$ resist. The schematic of its cross section is shown in Fig. 7.1 (b).

§ 7.2.2 MOS transistors and junction diodes

The MOS transistors and junction diodes were fabricated on P-type, $\langle 100 \rangle$, 4-inch Si wafers with a resistivity of 20-50 ohm-cm. The wafers were processed with the processing sequence listed in Appendix III. The NMOS process, originally developed for VLSI circuits, consists of six masking steps: active area, depletion implant, buried contact, polysilicon gate, contact hole and metal definition. The gate definition was carried out using $Ge_{0.1}Se_{0.9}$ resist but the other masking steps were performed using polymer resist (KTI820).

The MOS transistors are n channel devices with a gate oxide of $20nm$. Both enhancement and depletion devices were fabricated, however the depletion devices have a threshold of 0.7 volt instead of the desired value of -0.7 volt. The shift in the threshold voltage is caused not by the contamination of $Ge_{0.1}Se_{0.9}$ resist but by the incorrect implantation dosage. The incorrect implant dosage is confirmed by devices fabricated using the same process but without the use of $Ge_{0.1}Se_{0.9}$ resist. Fig. 7.2 shows one of the

enhancement transistors with a gate length of $1.25\mu m$ and a gate width of $100\mu m$. The junction diodes are formed by an area of arsenic dopant on the p-type substrate. The arsenic dopant was introduced during the implantation of the source and drain regions of the MOS transistors.

§ 7.3 Results

§ 7.3.1 Overview

In this section, results on the measurement of the CV (capacitance-voltage) characteristics, transient response (Ct characteristics) and CV characteristics after temperature stress of the MOS capacitors are discussed. The electrical characteristics of the MOS transistors, in particular the transconductance and output resistance, are examined. Results on the measurement of the reverse-biased characteristics of the junction diodes is reported. The CV response gives a measure of the density of fixed oxide charges, surface states and trapped oxide charges. The transient response (Ct characteristic) of the capacitors biased to deep depletion gives an estimate on the density of recombination centers in the silicon. The CV response of the capacitors after high field and temperature stress allows the estimate on the amount of mobile ionic charges. The leakage current of a reverse-biased junction gives a measure of the defect site and heavy-metal-ion density.

§ 7.3.2 CV characteristics

High frequency CV (capacitance voltage) characteristics of the MOS capacitors were measure at 10M hertz frequency using a HP4192 impedance analyzer. The characteristics of the MOS capacitors fabricated with $Ge_{0.1}Se_{0.9}$ and KTI820 resist are shown in Figs. 7.2 (a) and (b) respectively. Comparing the CV response of the capacitors fabricated using $Ge_{0.1}Se_{0.9}$ resist (test samples) with those of the capacitors fabricated using KTI820 resist (control samples), the result show that the capacitors have identical CV characteristics. Therefore the density of fixed oxide charges and surface states in the two devices may be the same. CV measurements of five other pairs of samples on different

locations of the wafer show the same result, that is the CV characteristics of the control and test samples have no noticeable difference. The absence of hysteresis in the CV curves shows that the amount of oxide trapped charges in the capacitors is small [2]. The results in turn show that $Ge_{0.1}Se_{0.9}$ resist, when used in device fabrication, does not produce any observable effect on the density of fixed oxide charges, surface states and trapped oxide charges.

§ 7.3.3 Minority carrier life-time

Minority carrier life-time can be estimated by biasing an MOS capacitor to deep depletion with a voltage step and measuring the transient response, that is, the capacitance as a function of time. The step voltage pulses the MOS capacitor from accumulation to deep depletion and causes a large depletion region to form almost instantaneously [3]. The rate at which the depletion region relaxes depends on the bulk and surface generation and the relaxation rate is reflected in the transient response. For the case when the generation is bulk limited, the transient response has a gradual slope and the minority carrier life-time can be estimated using the Zerbst analysis [4]. It consists of plotting $d \left[\frac{C_{ox}}{C} \right]^2$ as a function of $\frac{C_f}{C} - 1$ where C_{ox} and C_f are the high frequency capacitances of the MOS capacitor in the accumulation and strong inversion region respectively. The minority carrier life-time τ can be calculated using the equation

$$\tau = 2n_i \frac{C_{ox}}{AN_B C_f} \quad (1)$$

where A is the slope of the linear portion of the transient response, n_i is the intrinsic carrier concentration of Si, and N_B is the dopant concentration of the substrate.

The transient responses of a test sample (fabricated with $Ge_{0.1}Se_{0.9}$ resist) and a control sample (fabricated with KTI820) are shown in Figs. 7.3 (a) and (b) respectively. The input bias applied to the capacitor is a step voltage which has an abrupt transition from 10 to -10 volt. The gradual slope of the transient response from 0 to 100 second shows that carrier generation in both samples is bulk limited. The close resemblance of

the curves shows that the generation rate in the samples is approximately equal. The corresponding $-\frac{d(C_{ox}/C)^2}{dt}$ versus $\frac{C_f}{C}-1$ plots are shown in Fig. 7.4. Substituting the slope of the linear portion of the graphs in equation (1), the calculated minority carrier life-time in the test and control sample are 18.5 and 17.5 μs respectively. Measurements in other locations of the wafers produce results within 20% of these values. The results show that $Ge_{0.1}Se_{0.9}$ resist, when used in device fabrication, have no observable effect on the density of surface or bulk recombination centers which affect the minority carrier life-time.

§ 7.3.4 Mobile ionic charges

The amount of mobile ionic charges trapped in the thin oxide layer was measured using the procedure suggested by Snow [5]. First, the initial high frequency CV characteristic of a MOS capacitor is measured. Next, the substrate is heated to 300°C and a bias of 5 volt is applied to the capacitor, which produces an electric field of $2.5 \times 10^6 v/cm$ in the oxide layer, for 5 minutes. Then the sample is cooled to room temperature under bias and the high frequency CV response is measured. Next, the sample is heated up to 300°C and a bias of -5 volt is applied for 5 minutes. Subsequently, the sample is cooled to room temperature under the same bias and the high frequency CV response is measured again. Then the shift in flat band voltage δV_{FB} is estimated by comparing the CV characteristic of the MOS capacitor after the positive stress to that of the capacitor after the negative bias stress. The number of effective number of mobile ions per unit square at the $S_i-S_iO_2$ N_{SS} is calculated using equation (2):

$$N_{SS} = \delta V_{FB} \frac{C_{ox}}{qA} \quad (2)$$

where q is the electron charge and A is the area of the capacitor.

Figs. 7.5 (a), (b) and (c) show the high frequency CV characteristic of a capacitor fabricated with $Ge_{0.1}Se_{0.9}$ resist before the stress, after the positive-bias stress, and after the negative-bias stress respectively. The three characteristic curves show close

resemblance. The shift in flat band voltage δV_{FB} is less than 25mV and the number of mobile ions per unit area N_{ss} in the oxide layer is less than $10^{10}/\text{cm}^2$ which is smaller than the resolution limit of this method [4].

§ 7.3.5 IDVDS characteristics

The performance of a MOS transistor is best characterized by its IDVDS response, that is the drain current (I_d) as a function of gate bias (V_{gs}) and drain to source voltage (V_{ds}). Fig. 7.7 (a) shows the IDVDS characteristics of the transistor shown in Fig. 7.2. The transistor has a threshold voltage (V_t) of 1 volt. The contact resistance of the transistor is larger than that of normal transistors. The high contact resistance is reflected by the large V_{dsat} ($>V_{gs} - V_t$), the drain voltages at which I_d saturates. The fact that the high contact resistance is not associated with $\text{Ge}_{0.1}\text{Se}_{0.9}$ resist contamination is proved by the IDVDS characteristics of another device shown in Fig. 7.7 (b). The device was fabricated with the same NMOS process described in section 7.2.2 except that the gate of the transistor was defined using KTI820 instead of $\text{Ge}_{0.1}\text{Se}_{0.9}$ resist and etched in CClF_3 plasma instead of mixture of NH_4F and water diluted HNO_3 . In fact the V_{dsat} values of the transistor is approximately equal to those of the transistor in Fig. 7.7 (b). Despite the relative high contact resistance, the transistor fabricated by $\text{Ge}_{0.1}\text{Se}_{0.9}$ resist has a large transconductance of 2.94 mmho in the saturation region at V_{gs} of 4 volt and a reasonably large output resistance G_{ds} of 25k ohm. The large transconductance makes the device very attractive for circuit applications.

§ 7.3.6 Junction leakage

Contamination can increase the density of defects, recombination centers and heavy metal ions in the wafer. The leakage current of a reverse-biased junction gives a measure of these contamination effects. Fig. 7.8 (a) shows the leakage current as a function of voltage of a reverse-biased junction fabricated using $\text{Ge}_{0.1}\text{Se}_{0.9}$ resist. The junction has an area of $270 \times 400 \mu\text{m}^2$. For a reverse bias of 10 volt or smaller, the junction leakage

current is less than $1 \times 10^{-12} A$ which corresponds to a leakage current density of $1 nA / cm^2$. The leakage current shown is below the resolution limit of the instrument $1 \times 10^{-12} A$ and the actual leakage current is smaller. The result show that $Ge_{0.1}Se_{0.9}$ resist when used in device fabrication does not have observable effect on the density of defects, heavy ions and recombination sites. The conclusion is further confirmed by the leakage characteristic of a pn junction of the same area shown in Fig. 7.8 (b). The junction was fabricated using the same process but without the use of $Ge_{0.1}Se_{0.9}$ resist. The leakage characteristic is almost identical to the one shown in Fig. 7.8 (a).

§ 7.4 Conclusion

The contamination effect of $Ge_{0.1}Se_{0.9}$ resist on integrated circuit devices was studied. MOS capacitors, transistors and junction diodes were fabricated with and without $Ge_{0.1}Se_{0.9}$ resist. High frequency CV characteristics of the MOS capacitors were measured. The absence of hysteresis in the CV curves show that the amount of oxide trapped charges in the capacitors is small. The close resemblance of the CV characteristics of the capacitors fabricated with and without $Ge_{0.1}Se_{0.9}$ resist show that the density of fixed oxide charge, surface states and trapped oxide charges in the capacitors may be equal. The transient response of the MOS capacitors to a step bias voltage was measured. The transient characteristics show that carrier generation is bulk limited. The calculated minority carrier life-time in the capacitors fabricated with and without $Ge_{0.1}Se_{0.9}$ resist is 18.5 and 17.5 second respectively. CV characteristics of the capacitors before and after high temperature and high field stress were measured. The CV curves after the negative and positive bias stress show no noticeable difference. The shift in flat band voltage measured is less than 25mV and the number of mobile ions per unit area in the capacitors is less than $10^{10} / cm^2$.

Electrical characteristics of the MOS transistors were measured. The MOS transistor with $1.25 \mu m$ gate length and $100 \mu m$ gate width has a transconductance of 2.94 milli mho and an output resistance of 25 kilo ohm. The reverse-biased characteristics of the

pn junctions was measured. The junctions had an area of $270 \times 400 \mu m^2$. For a bias voltage of 10 volt or less, the measured leakage current density was less than $1 nA / cm^2$. The low leakage current density shows that the junctions fabricated has low density of defects, heavy ions and recombination sites.

In summary, devices fabricated using $Ge_{0.1}Se_{0.9}$ resist do not show observable change in the density of fixed oxide charges, surface states, recombination sites, oxide trapped charges, defect sites, and heavy metal ions. MOS capacitors, transistors and junction diodes fabricated using $Ge_{0.1}Se_{0.9}$ resist have electrical characteristics comparable to their counter parts fabricated with conventional polymer resist.

References

- [1] A. G. Milnes, *Deep Impurities in Semiconductors*, New York, John Wiley and Sons, p.14, 1973.
- [2] F. P. Heiman and G. Warfield, "The Effects of Oxide Traps on the MOS Capacitance," *IEEE Trans. Electron Dev.*, vol. ED-12, no. 4, p. 167, 1965.
- [3] F. P. Heiman, "On the determination of Minority Carrier Life-time from the Transient Response of an MOS Capacitor," *IEEE Trans. Electron Dev.*, vol. 14, no. 11, p. 781, 1967.
- [4] M. Zerst, "Relaxation Effects at Semiconductor-Insulator Interfaces," *Z. angew. Phys.*, vol. 22, p. 30, 1966.
- [5] E. H. Snow, "Ion Transport Phenomena in Insulating Films," *J. of Appl. Phys.*, vol. 36, no. 5, p. 1664, 1965.

Figure Captions

Fig. 7.1 (a) SEM micrograph of a capacitor fabricated using $Ge_{0.1}Se_{0.9}$ resist. (b) Schematic of its cross-section.

Fig. 7.2 SEM micrograph of a MOS transistor with a gate width of $100\mu m$ and gate length of $1.25\mu m$.

Fig. 7.3 High frequency CV characteristic of a MOS capacitor fabricated (a) with $Ge_{0.1}Se_{0.9}$ resist. (b) without $Ge_{0.1}Se_{0.9}$ resist.

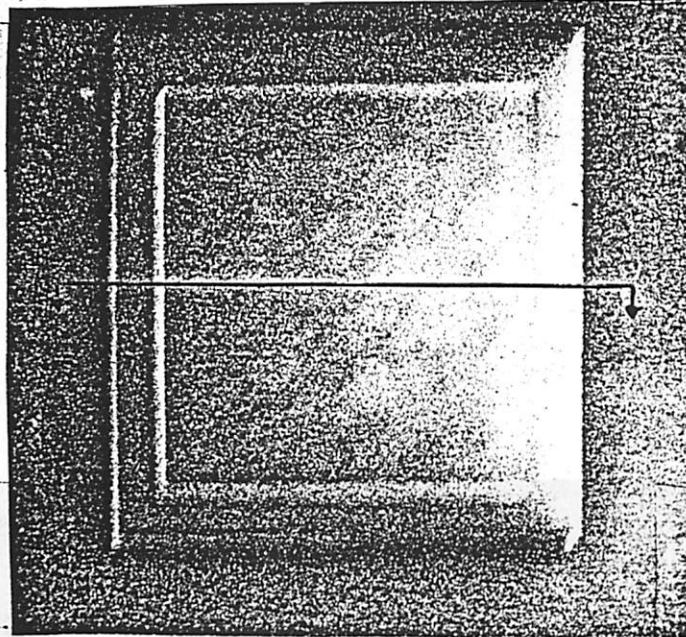
Fig. 7.4 C_t characteristic of a MOS capacitor fabricated (a) with $Ge_{0.1}Se_{0.9}$ resist. (b) without $Ge_{0.1}Se_{0.9}$ resist.

Fig. 7.5 $-d\frac{C_{ox}^2}{C}$ of a (a) test sample. (b) control sample as a function of $\frac{C_f}{C}-1$.

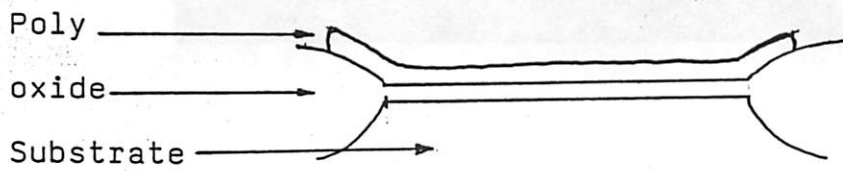
Fig. 7.6 High frequency CV characteristic of a MOS capacitor fabricated using $Ge_{0.1}Se_{0.9}$ resist (a) before temperature stress, (b) after the stress of $-5V$ at $300^\circ C$, and (c) after the stress of $5V$ at $300^\circ C$.

Fig. 7.7 IDVDS characteristics of a MOS transistor fabricated (a) with $Ge_{0.1}Se_{0.9}$ resist. and (b) without $Ge_{0.1}Se_{0.9}$ resist.

Fig. 7.8 Reverse-bias characteristic of a junction diode fabricated (a) with and (b) without $Ge_{0.1}Se_{0.9}$ resist.



(a)



(b)

Fig. 7.1

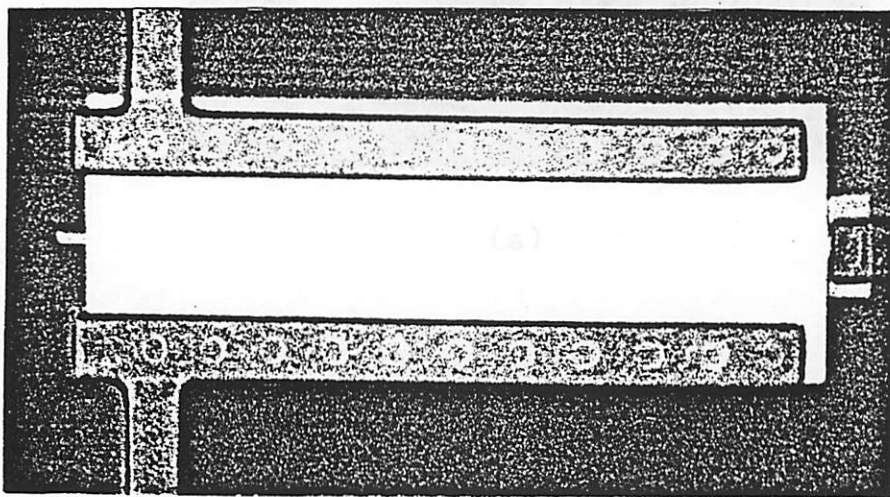


Fig. 7.2

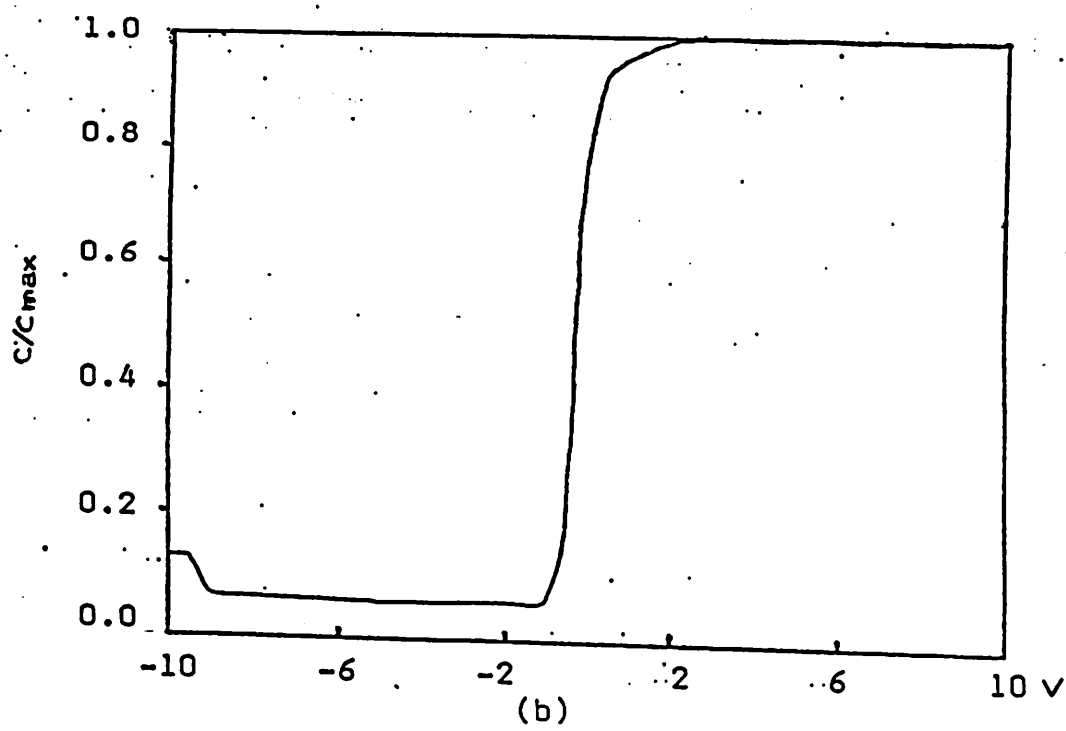
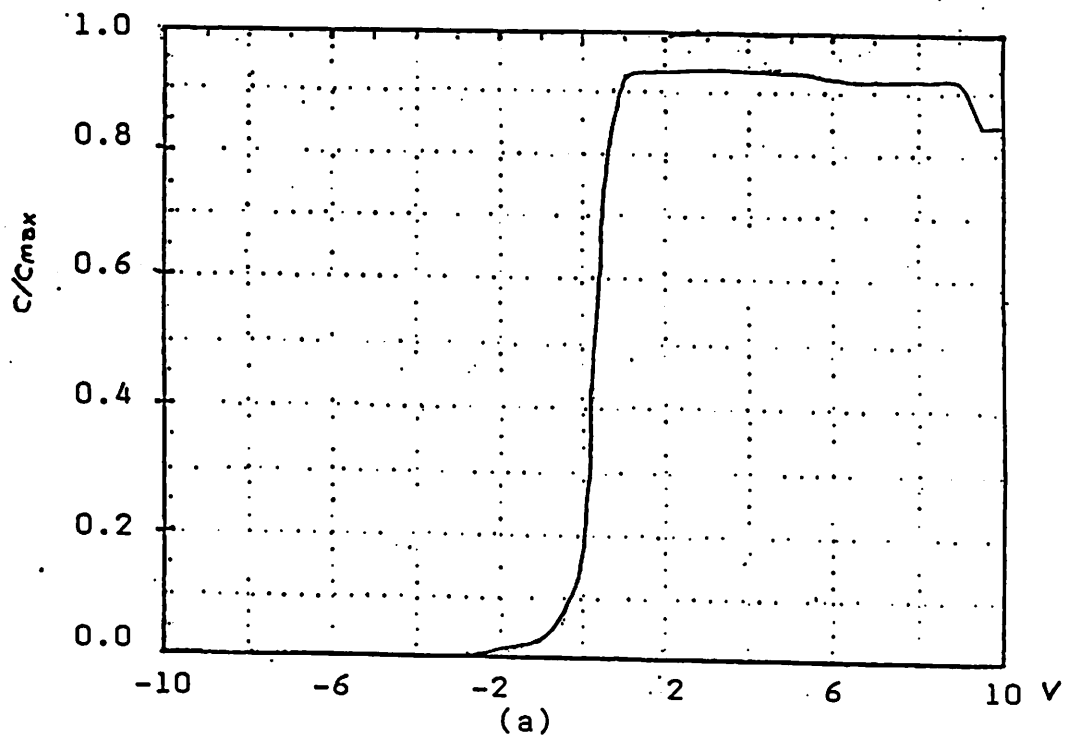
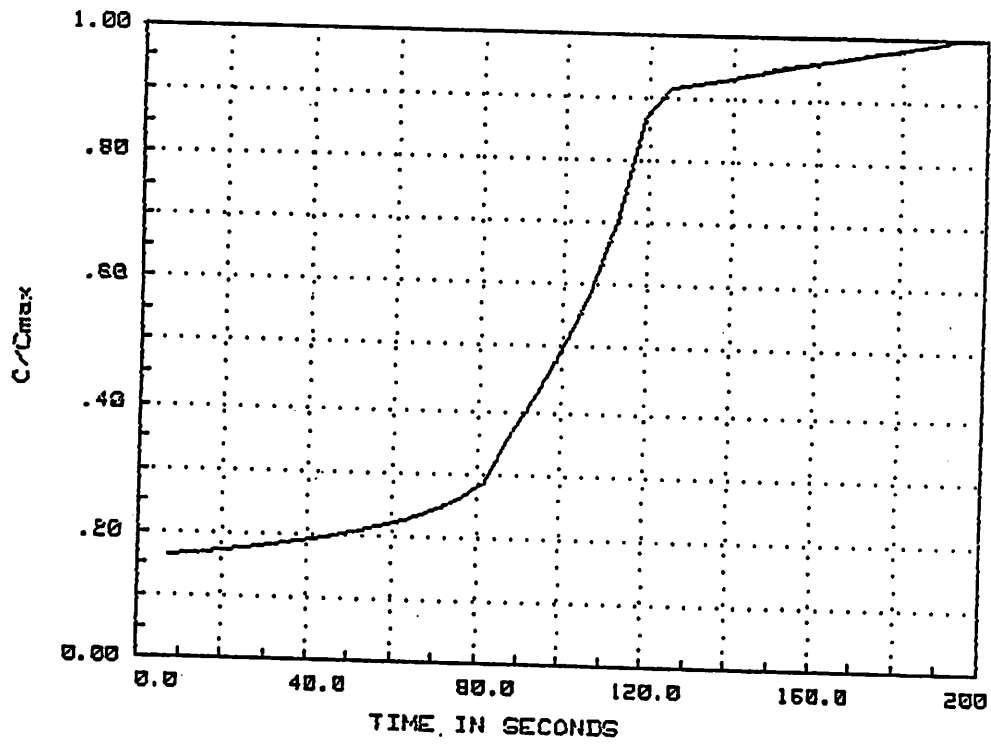
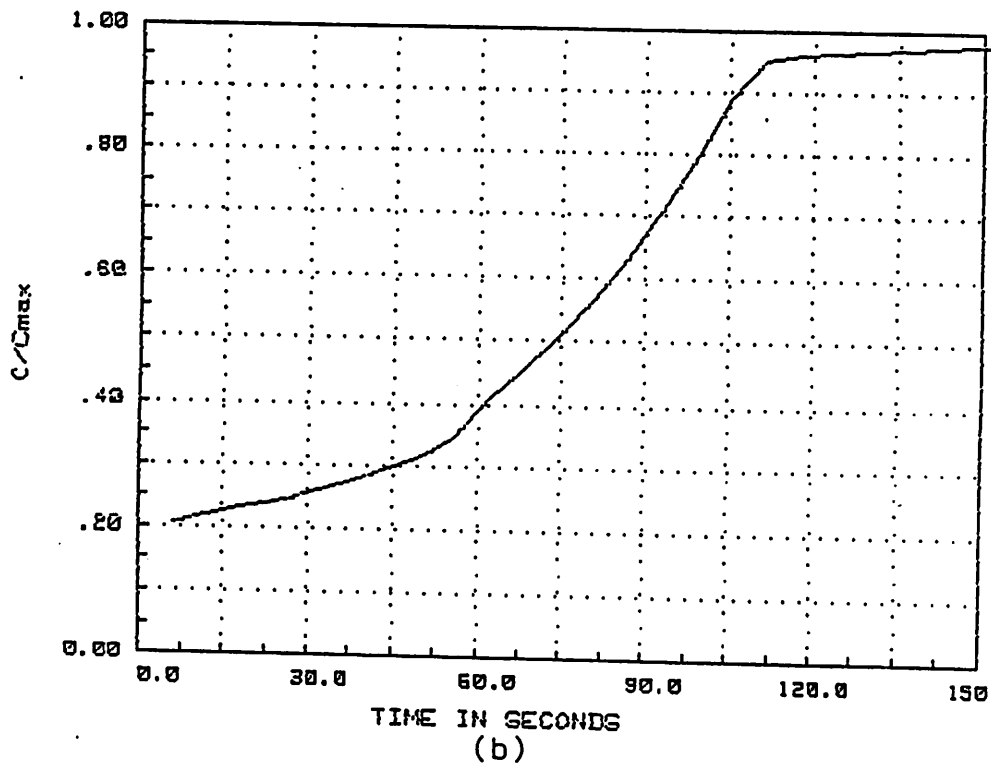


Fig. 7.3



(a)



(b)

Fig. 7.4

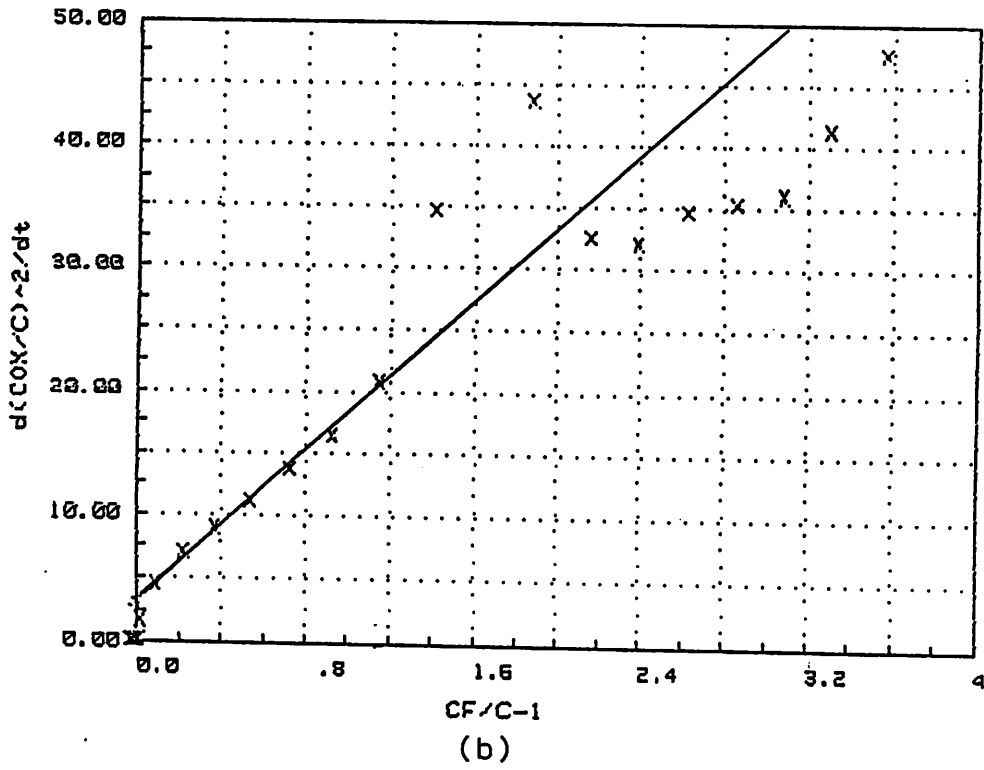
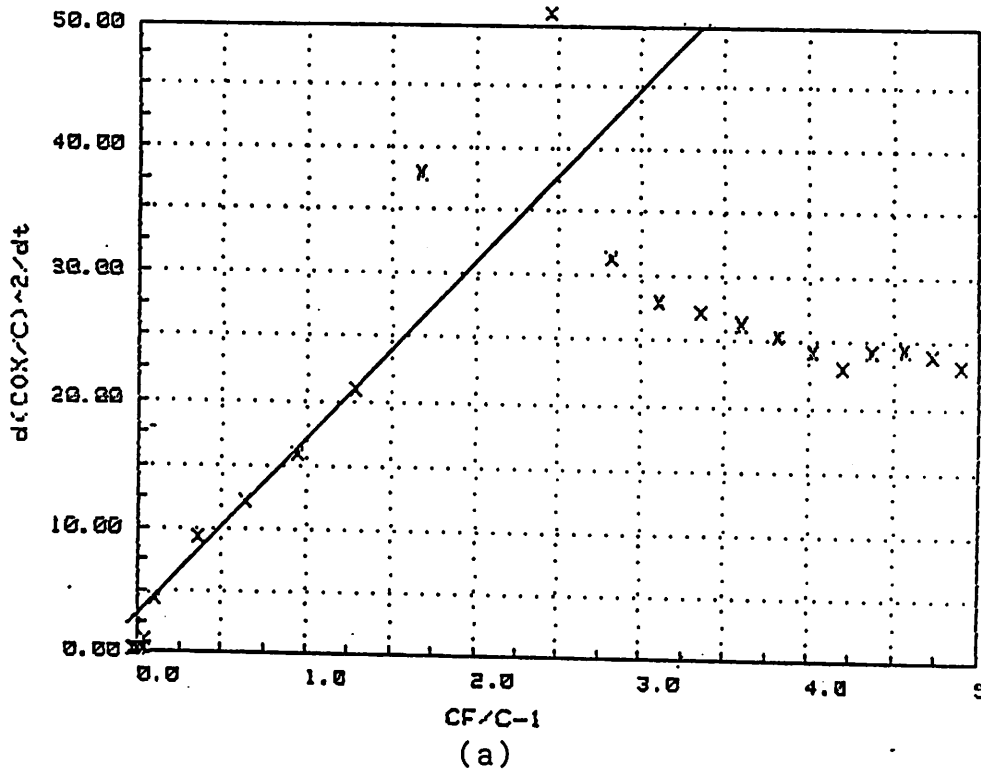


Fig. 7.5

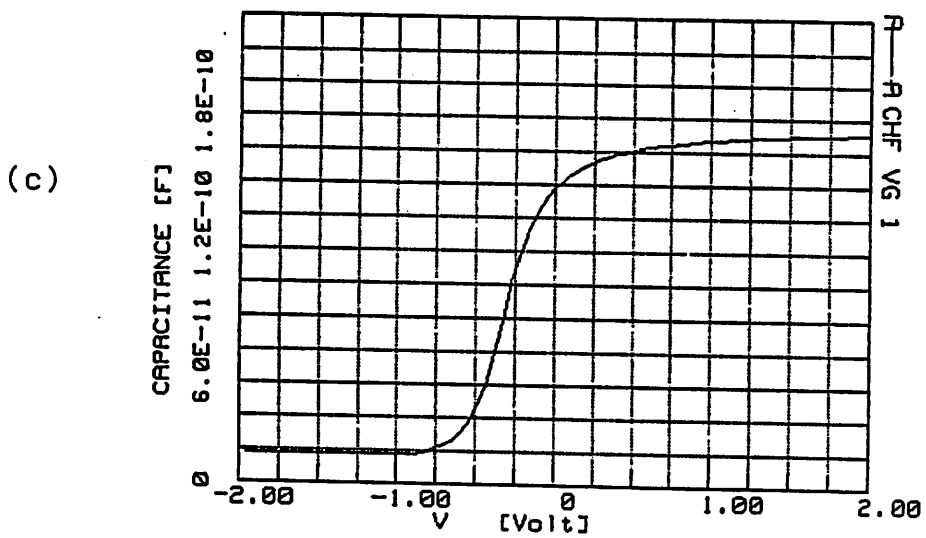
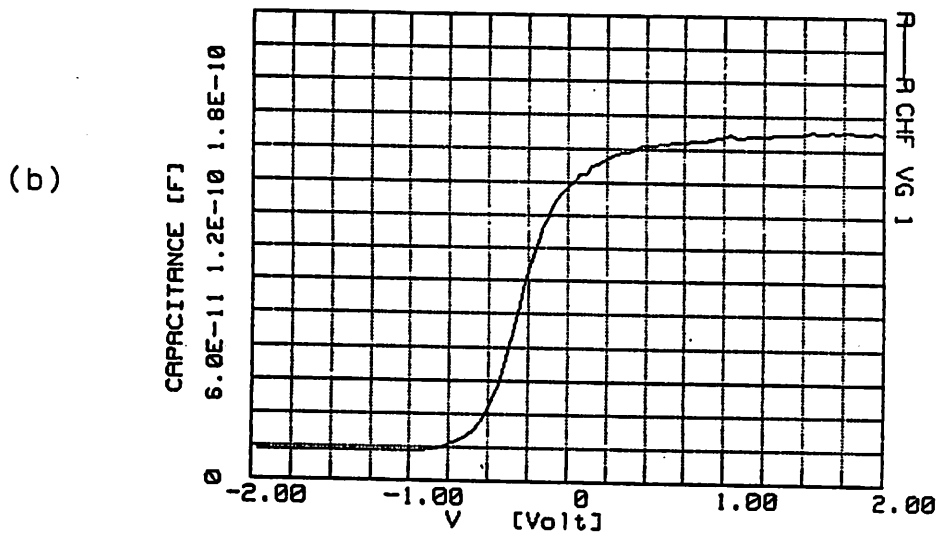
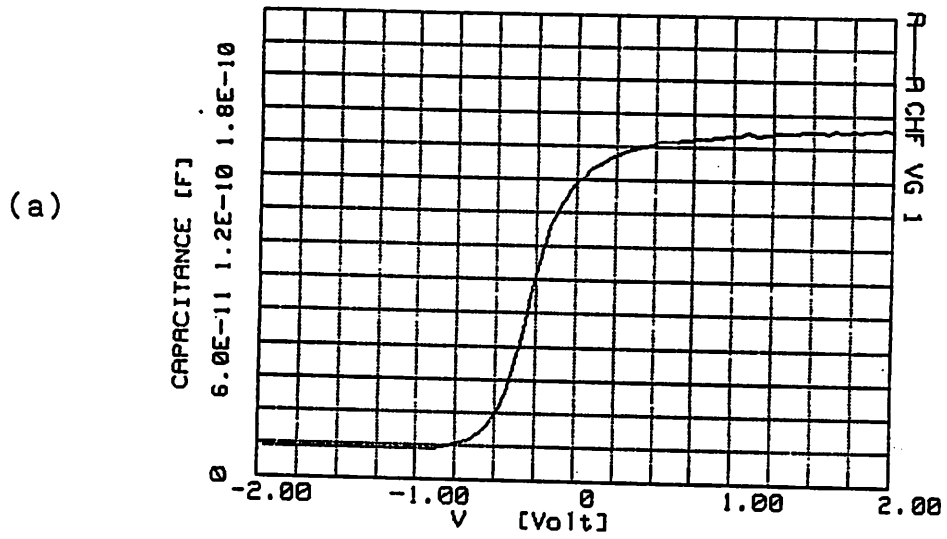
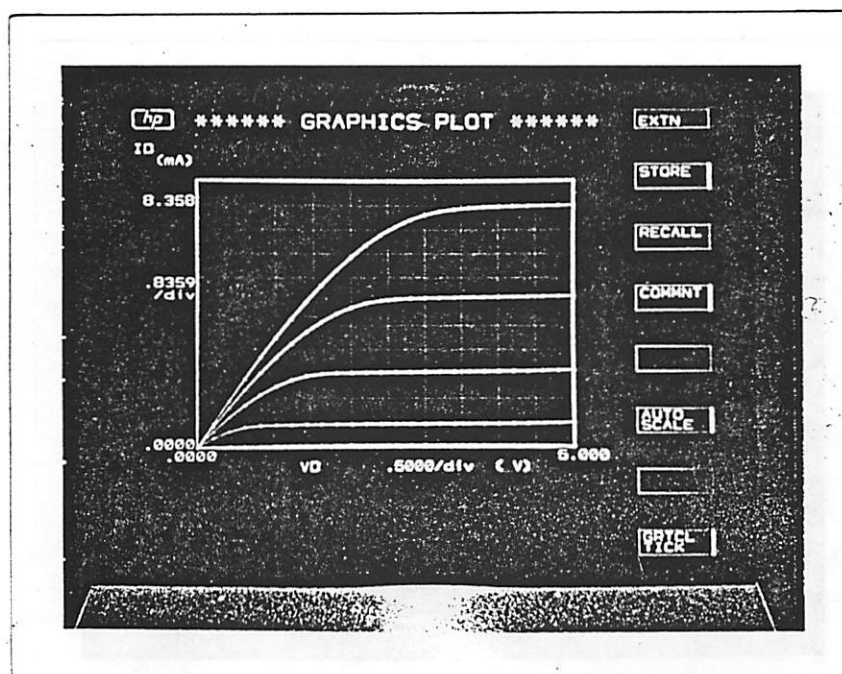
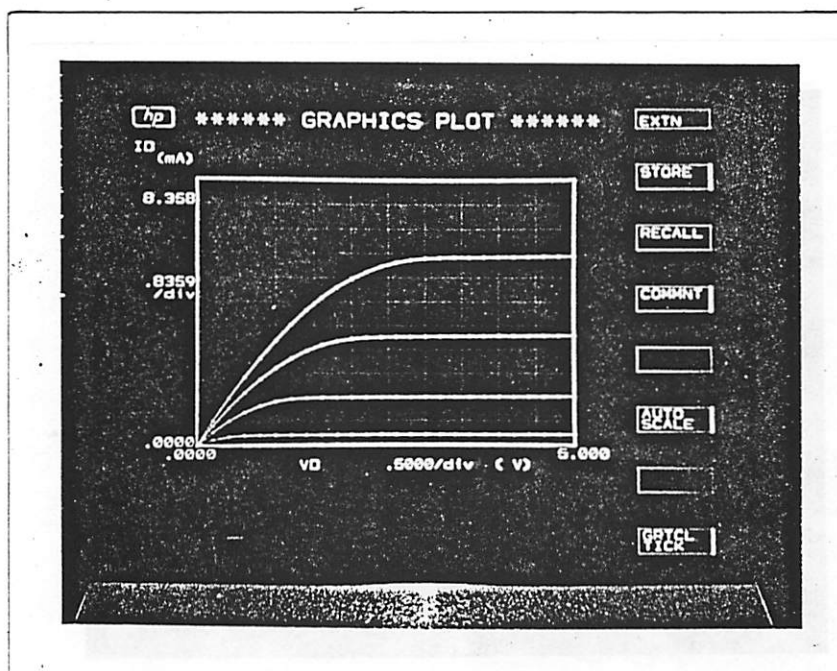


Fig. 7.6

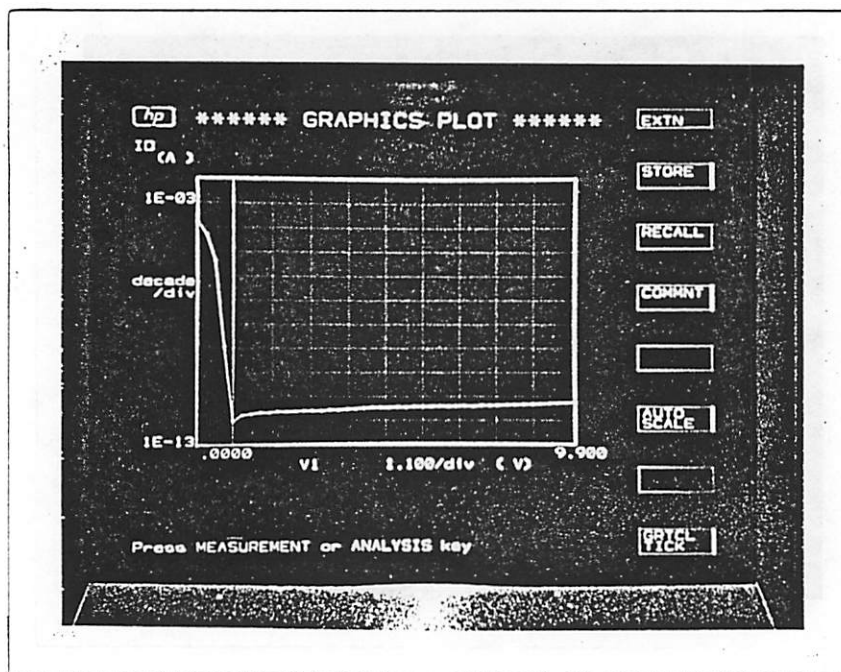


(a)

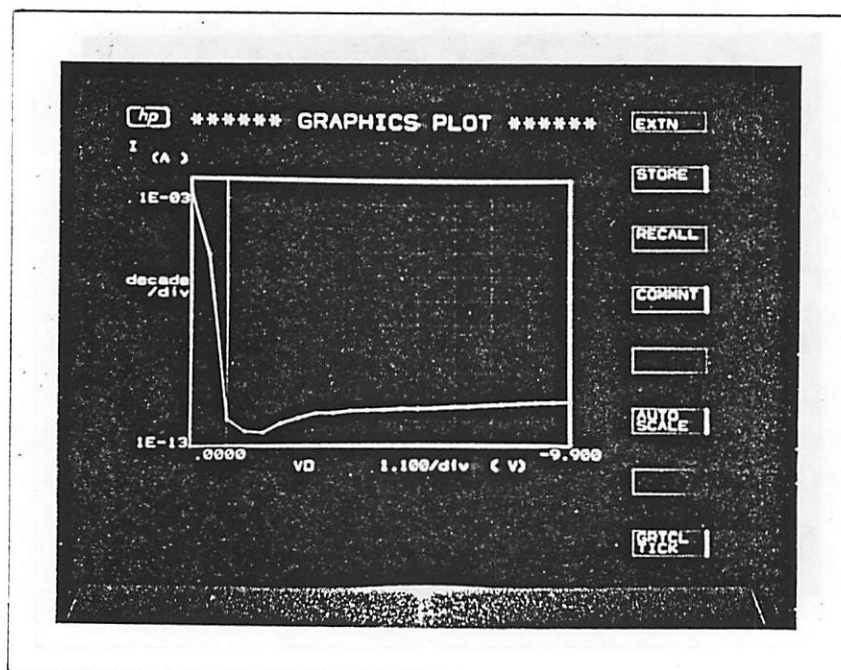


(b)

Fig. 7.7



(a)



(b)

Fig. 7.8

Chapter 8: CONCLUSIONS AND SUGGESTIONS FOR FUTURE WORK

§ 8.1 Summary

This dissertation concentrates on the study of the image formation mechanisms of the bilevel $Ge_{0.1}Se_{0.9}$ resist system and the assessment of its potential for VLSI fabrication. The unique material characteristics of the resist system, which gives the resist a resolution capability unmatched by any reported resist system, make the resist very attractive for VLSI fabrication.

A laboratory $Ge_{0.1}Se_{0.9}$ resist process has been developed similar to that developed by Tai and coworkers at Bell Labs. The resultant resist has resolution comparable to that reported by Tai et al for their resist. Both wet and dry development has been implemented and submicron features have been successfully resolved. Dry development showed a 40% improvement in sensitivity with no loss of developed image quality.

A simulation program for the exposure model of the resist has been written and incorporated to the IC process-simulation program SAMPLE. In the model, the resist is characterized by four parameters: the bleachable absorption coefficient A, the non-bleachable absorption coefficient B, the sensitivity factor C, and the lateral diffusivity of Ag in the sensitization layer D. Output of the program is the Ag concentration distribution in the Ag_2Se and $Ge_{0.1}Se_{0.9}$ layer. The simulation model has been verified with extensive experimental data.

The photodoping mechanisms of the $Ag_2Se / Ge_{0.1}Se_{0.9}$ system have been explored experimentally. Results confirmed that Ag photodoping is essentially a photo-induced diffusion process. Three diffusion mechanisms during the exposure process have been identified. They are the vertical diffusion of Ag in $Ge_{0.1}Se_{0.9}$, the lateral diffusion of Ag in $Ge_{0.1}Se_{0.9}$ and the lateral diffusion of Ag in Ag_2Se . The vertical diffusivity of Ag in $Ge_{0.1}Se_{0.9}$ at $21^\circ C$ has been found to be $2.7nm^2/sec$ using the RBS technique. Using a microlithography technique to localize Ag sensitization in certain area of a $Ge_{0.1}Se_{0.9}$ film.

lateral diffusion distance of Ag up to $9\mu m$ has been observed. Using this technique, the dependence of the lateral diffusivity of Ag in $Ge_{0.1}Se_{0.9}$ glass on temperature has been found to follow a Arrhenius-type equation. The lateral diffusivity has also been found to directly proportional to the irradiation intensity.

The exposure phenomena of $Ge_{0.1}Se_{0.9}$ resist have been explored. The conditions for the occurrence of contrast enhancement bleaching, edge sharpening diffusion, exposure saturation and pattern dependent level amplification phenomena have been identified. Contrast enhancement occurs when M is greater than 2 and the feature size is greater than the average diffusion length of Ag in the sensitized layer. Edge sharpening occurs when the exposure dose is greater than the dosage at which photodoping saturation occurs in the resist. Feature-dependent amplification occurs when the average diffusion distance of Ag in Ag_2Se is greater than the feature size. Feature-dependent photodoping suppression occurs when the absorptivity of the Ag_2Se layer is high ($A > 2$). The practical impacts of these phenomena have also been evaluated. It has been found that the exposure phenomena do not occur at normal exposure dose ($< 140 mJ / cm^2$). The possibility of using feature-dependent phenomena to compensate aerial image proximity effects and suppress the printability of open defects has been demonstrated by adjusting the Ag_2Se layer thickness and the exposure time.

The assessment of the resist for IC fabrication has been carried out. An overhanging resist structure suitable for lift-off processes has been constructed using the bi-level $Ge_{0.1}Se_{0.9}$ resist system. Palladium patterns with $0.8\mu m$ critical dimension have been defined using such a structure in the lift-off process. The contamination effect of $Ge_{0.1}Se_{0.9}$ resist on IC devices has been studied. Junction diodes, MOS transistors and capacitors of different sizes have been fabricated with and without the $Ge_{0.1}Se_{0.9}$ resist. The resultant MOS devices do not show observable threshold voltage shift in the CV curves. Minority carrier life-time in the devices fabricated with and without $Ge_{0.1}Se_{0.9}$ resist is 18.5 and 17.5 μs respectively. CV measurement after high temperature stresses

show a flat-band voltage shift of less than $25mV$. The number of mobile ions per unit area in the devices is less than $10^{10}/cm^2$. The junction diodes has a reverse leakage current density of less than $1nA/cm^2$ at a biased voltage of 10 volt. The devices fabricated with $Ge_{0.1}Se_{0.9}$ resist have IV similar to those fabricated using ordinary positive resist. Thus no difference in the density of oxide trapped charge, surface state, mobile ions, heavy metal ions and defects could be observed in the devices fabricated with and without $Ge_{0.1}Se_{0.9}$ resist. for IC fabrication. With its high resolution and dry etch resistance to oxygen plasma, $Ge_{0.1}Se_{0.9}$ resist can eliminate many lithography problems associated with VLSI fabrication and has a good potential of extending the limits of optical lithography.

§ 8.2 Suggestions for future work

The photodoping mechanism of Ag in $Ge_{0.1}Se_{0.9}$ glass is still not completely known. The force which causes Ag to diffuse when the $Ag/Ge_{0.1}Se_{0.9}$ system is exposed to light has not been identified. In chapter 3, we found that light absorption in the $Ge_{0.1}Se_{0.9}$ glass has a long range effect ($3\mu m$). Since electrons and holes diffusion over such a long distance in amorphous semiconductor is not likely. The result may rule out the possibility that Ag diffusion is triggered by the diffusion of holes and electrons which are generated in the Ge_xSe_{1-x} film by light excitation. The photo-induced diffusion may be caused by photo-contraction as suggested by J. C. Phillips at Bell Labs [1]. To completely understand the photodoping mechanism requires the identification of the force which acts on the Ag atoms and causes them to diffuse.

In chapter 3, the temperature dependence of photodoping diffusion is found to follow the Arrhenius-type behavior. That is the colder the temperature, the shorter the diffusion distance of Ag. Under normal wet or dry development conditions, the concentration distribution of Ag in the top region of the $Ge_{0.1}Se_{0.9}$ film determines the quality of the developed image [2]. By decreasing the exposure temperature, the photodoping distance is shortened and the region in which photodoped Ag congregates is made shallower.

The photodoped Ag concentration for the same exposure dose may thus be increased and the sensitivity of the resist can thereby be increased. The sensitivity of the resist is important especially in a production environment where the bottle neck of the lithography process is usually in the resist exposure.

With the advent of excimer lasers for high intensity light sources, deep UV projection printer is expected to be available in the foreseeable future [3]. The lack of resist materials sensitive to radiation in the deep UV region has fueled major research efforts in the development of deep UV resist [4]. $Ge_{0.1}Se_{0.9}$ resist is sensitive to radiation with wavelength down to $200nm$ with the sensitivity increasing with decreasing wavelength. Its high sensitivity makes it a deep UV resist with good potential of further extending the optical lithography limit. Investigations of using Ge_xSe_{1-x} resist for deep UV lithography have been carried out [5,6], however much work is still required to fully understand the image formation mechanism of the resist under deep UV exposure.

$Ge_{0.1}Se_{0.9}$ resist is also sensitive to electron beam exposure. Investigations on the electron beam exposure on Ge_xSe_{1-x} resist have been carried out [7-9], however the image formation mechanism of $Ge_{0.1}Se_{0.9}$ resist under electron beam exposure is still not known. An e-beam exposure model equivalent to the one given in chapter 4 of this dissertation would allow computer simulation and speed up the work in this area.

The contamination effects of $Ge_{0.1}Se_{0.9}$ resist on integrated circuit devices have been studied in chapter 7. However, the experimental results were obtained from two wafers, a small statistical source. In addition, all the characterizations discussed in this thesis have been carried out in a research environment where a tight control of the processing conditions can easily be achieved. The transfer of the $Ge_{0.1}Se_{0.9}$ resist to production environment requires the build-up of a large data base of process characterizations so that an operating condition which gives the widest process latitude can be chosen. More statistical data from devices fabricated with $Ge_{0.1}Se_{0.9}$ resist will give a more concrete decision on the contamination effects of $Ge_{0.1}Se_{0.9}$ resist on the performance of the dev-

References

- [1] J. C. Phillips, Private communication.
- [2] K. L. Tai, E. Ong, R. G. Vadimsky, C. T. Kemmerer and A. M. Bridenbaugh, "Model of image formation in $Ag_2Se / Ge-Se$ resist system: Implications for microlithography", Proc. of ECS, vol. 82-9, p. 49, 1982.
- [3] K. Jain, C. G. Willson, S. Rice and L. Pederson, "Ultrafast Deep UV Lithography Using Excimer Lasers," Proc. Regional Tech. Conf. on Photopolymer, Principles, Processes and Material, Midhuson Section, SPE, Ellenville, N. Y., p.173, 1982.
- [4] R. L. Hartless and E. A. Chandross, "Deep-UV photoresists: Poly(methyl methacrylate-co-indenone)," J. Vac. Sci. Technol., vol.19, no.4, p.1333, 1981.
- [5] E. Ong, K. L. Tai, and R. G. Vadimsky, "Application of GeSe as a deep UV resist for submicron lithography." Proc. of ECS, vol.82, no.9, p.71, 1982.
- [6] K. J. Polasko and R. R. W. Pease, "Excimer laser exposure of $Ag_2Se / GeSe_2$: High contrast effect." J. Vacc. Sci. Technol. B, vol.3, no.1, p.319, 1985.
- [7] A. Yoshikawa, O. Ochi, H. Nagai and Y. Mizushima, "A new inorganic electron resist of high contrast." Appl. Phys. Lett., vol.31, no.3, p.161, 1977.
- [8] K. Balasubramanyam and A. L. Ruoff, "Oblique deposition of enhanced sensitivity in electron beam exposed $g-Ge_xSe_{1-x}$ inorganic resist". J. of Vacc. Sci. Technol., vol.19, no. 4, p.1374, 1981.
- [9] K. J. Polasko, R. F. W. Pease, "Electron beam exposure of Ge_xSe_{1-x} ", Proc. of SPIE, vol.393, 1983.

Appendix I: Ge-Se RESIST SIMULATION PROGRAM

```
program main
c
c   This program calculate the silver distribution profile
c   of the inorganic resist under exposure
c
c   The program has 8 input parameters:
c
c   ai an exposure dependent absorption term
c   bi an exposure independent absorption term
c   ci an optical sensitivity term
c   d the lateral diffusion constant of silver
c   tau the value of time increament in msec;
c   the initial exposure time;
c   riniti the final exposure time;
c   finati the number of plots required within the
c   range of exposure time;
c   deltx the increment of x
c
common /io1 / itermi,ibulk,iprout,iresv1,iin,iprint,ipunch
common /horing/ deltx, mnhpts, nmhpts, horint(50)
common /inorpa/ ai, bi, ci, d, p, tau, ikey
common /time / riniti, finati, number
common /sildis/ exptim(20), x(50), si(20,50), jpctr
double precision p
c
c   Input/output handling:
c   read input parameters
c
read (5,30) ai, bi, ci, d, tau
30  format (/,4(1x,f8.5),/,1x,f8.5)
read (5,40) riniti, finati, rnum, flg
40  format (4(1x,f8.4))
number = int(rnum)
ikey = int(flg)
read (5,20) (x(i),horint(i),i=1,50)
20  format (11(1x,f6.3))
nmhpts = 50
c
c   open output data file
c
open (7, file="f77punch7")
ipunch = 7
c
call tral98
end
c
subroutine tral 98
c
c   1-dimensional inorganic reist model
c
common /horing/ deltx, mnhpts, nmhpts, horint(50)
common /sildis/ exptim(20), x(50), si(20,50), jpctr
```

```

common /inorpa/ ai, bi, ci, d, p, tau, ikey
common /time / riniti, finati, number
common /simarr/ c(50), cim(50)
double precision c, cim
double precision p

c
tau=tau*0.001

c
c limit number of silver concentration profile per run to 5
c
if (number .gt. 20) goto 29

c
write (6,50)
50 format(1x,"*****"
1 /,1x,"* 1-dimensional model of inorganic resist *"
1 /,1x,"*****")

c
c pretty-print the values of the parameters
c and execute the trial statement
c
write (6,60) ai, bi, ci, d
60 format(1x," A = ",f10.4/,1x," B = ",f10.4/,
1 1x," C = ",f10.4/,1x," D = ",f10.4)

c
deltx = (x(50)-x(1))/49
write (6,42) deltx
42 format (1x," x-inc=",f7.5)
write (6,44) tau
44 format(1x," time inc=",f7.5)

c
c Calculate constant
c
p=d*tau/(2*deltx**2)

c
c The following manages the data operations.
c It initializes variables and performs
c input-output formating.
c
c initializations
c
do 11 i=1,nmhpts
c(i)=1.
si(1,i)=0.
11 continue

c
ts=0.
te=riniti
if (number .gt. 1) goto 23
number=1
pltinc=0.
goto 22
23 continue

c
pltinc=(finati-riniti)/(number-1)

```

```

        if (pltinc .ge. 0.0) goto 22
        pltinc=0.
22  continue
c
c  keep on timing
c
        jptr=1
37  continue
        call cranic(ts.te)
        exptim(jptr)=te
        if (ikey .eq. 0 .or. ikey .eq. 2) goto 101
        call outpf1( te )
101 continue
c
        if (jptr .ge. number) goto 33
        do 35 j=1,nmhpts
        si(jptr+1,j)=si(jptr,j)
35  continue
c
        jptr=jptr+1
        ts=te
        te=te+pltinc
        goto 37
33  continue
c
c  check total amount of silver in the system
c  after exposure.
c
        sum=0.
        do 55 j=1,nmhpts
55  sum=sum+c(j)+si(jptr,j)
c
        total = nmhpts
c
        write (6,12) total
12  format(1x,"total amount of silver before
+ process =" .f8.2)
        write (6,77) sum
77  format(1x,"total amount of silver after
+ process=" .f10.5)
c
        call outprf(number)
        write (6,78) (exptim(i),i=1,number)
78  format(1x,"exposure time=" .5(1x,f10.7))
        write (6,70)
70  format(1x,"data is stored in the output file 7")
        return
c
29  write (6,39)
39  format(1x,"the maximum number (20) of silver-distribution",
1 /,4x,"profile is exceeded. Check input parameter 7")
        stop
        end
c

```

```

c   Number crunching routine
c
c   subroutine cranic (ts,te)
c   common /sildis/ exptim(20), x(50), si(20,50), jptr
c   common /horimg/ deltx, mnhpts, nmhpts, horint(50)
c   common /simarr/ c(50), cim(50)
c   common /inorpa/ ai, bi, ci, d, p, tau, ikey
c   double precision p
c   double precision c, cim
c   double precision alpha(50),cons(50),rim(50),con(50)
c
c   The model used here is a 1-dimensional diffusion
c   model with source and sink terms
c   The interface layer is assumed to have a thickness of 10A
c   Crank-Nicolson implicit method is used to discretize
c   the continuous partial differential equation. The
c   resultant finite-difference equations are solved
c   directly by using Gauss's elimination method.
c
c   In the following, the finite-difference equations
c    $-p*c(i-1)+a*c(i)-p*c(i+1)=cons(i)$ 
c   is first transformed into
c    $alpha(i)*c(i)-p*c(i+1)=cons(i)$ 
c   These equations are then solved by backward substitution.
c
c   nnn = 1
c   time=ts
10  time=time+tau
c   nnn = nnn +1
c
c   do 91 i=1,nmhpts
91  cim(i) = c(i)
c
c   do 20 i=1,nmhpts
20  rim(i) = tau*horint(i)*ci*exp(-ai*c(i)-bi)
c
c   con(1) = (c(2)-c(1))*2*p+c(1)*(1-rim(1)/2)
c   do 21 j=2,nmhpts-1
21  con(j) = p*(c(j+1)+c(j-1)-2*c(j))+c(j)
c   + *(1-rim(j)/2)
c
c   con(nmhpts) = (c(nmhpts-1)-c(nmhpts))*2*p+
1  c(nmhpts)*(1-rim(nmhpts)/2)
c
c   alpha's
c
c   alpha(1) = 1+2*p+rim(1)/2
c   alpha(2) = 1+2*p+rim(2)/2-2*p**2/alpha(1)
c   do 22 j=3,nmhpts-1
22  .alpha(j) = 1+2*p+rim(j)/2-p**2/alpha(j-1)
c   .alpha(nmhpts) = 1+2*p+rim(nmhpts)/2-2*p**2
c   + /alpha(nmhpts-1)
c
c   cons's

```

```

c
  cons(1) = con(1)
  do 30 j=2,nmhpts-1
30  cons(j) = con(j) + p*cons(j-1)/alpha(j-1)
c
  cons(nmhpts) = con(nmhpts) + 2*p*cons(nmhpts-1)
  + /alpha(nmhpts-1)
c  Calculate the silver distribution
c
c  backward substitution
c
  c(nmhpts)=cons(nmhpts)/alpha(nmhpts)
  do 32 j=nmhpts-1,2,-1
  c(j)=(cons(j)+p*c(j+1))/alpha(j)
  if (c(j) .lt. 0.) goto 15
32  continue
  c(1)=(cons(1)+2*p*c(2))/alpha(1)
c
  do 60 j=1,nmhpts
60  si(jptr,j)=si(jptr,j)+(c(j)+cim(j))*rim(j)/2
  if (time .lt. te) goto 10
  te = time
c
  write (6.11) time
  write (6.31) nnn
31  format(1x,i7)
11  format(1x,"time=",f10.5)
c
  write (6.40)
40  format(1x,"silver distribution in the
  + sensitized layer")
  write (6.12) (c(i),i=1,nmhpts)
12  format(11(1x,f6.3))
c
  return
15  write(6.25)
25  format(1x,"negative silver concentration
  + detected".
  1 /,1x,"check input parameters")
  write (6.36)
36  format(1x,"array of alpha")
  write (6.35) (alpha(j),j=1,nmhpts)
  write (6.37)
37  format(1x,"array of cons")
  write (6.35) (cons(j),j=1,nmhpts)
  write (6.38)
38  format(1x,"silver concentration at the
  + interface")
  write (6.35) (c(j),j=1,nmhpts)
35  format(11(1x,f6.3))
  stop
  end
c
c  The following routine writes data in the

```

```

c   f77punch7 file with format similar to that
c   of f77punch7 file generated by SAMPLE.
c
c   subroutine outprf(number)
c   This program writes the output-profile data points to
c   the file 7
c
c   common /horimg/ deltx, mnhpts, nmhpts, horint(50)
c   common /io1 / itermi,ibulk,iprout,iresv1,iin,iprint,ipunch
c   common /sildis/ exptim(20), x(50), si(20,50), jptr
c   common /inorpa/ ai, bi, ci, d, p, tau, ikey
c   common /objms2/ rlw, rsw, rlw2, rsw2
c   double precision p
c
c   xlth=deltx*float(nmhpts-1)
c   rnout=float(number)
c   rnpts=float(nmhpts)
c   simin=0.
c
c   To find ymax
c
c   simax=si(1,1)
c   do 5 i=1,jptr
c   do 5 j=2,nmhpts
c   if (si(i,j) .le. simax) goto 6
c   simax=si(i,j)
6   continue
5   continue
c
c   write (ipunch,10) x(1), x(50), simin, simax, rnout
10  format (/,4(1x,f8.5),/,1x,f8.5)
c
c   do 9 i=1,number
c   write (ipunch,20) rnpts
20  format (1x,f9.5)
c   write (ipunch,30) (x(j),si(i,j),j=1,nmhpts)
30  format (11(1x,f6.3))
9   continue
c
c   output message
c
c   jline = 7
c   write (ipunch,11) jline
11  format (1x,i1)
c   if (ikey .eq. 2 .or. ikey .eq. 3) goto 17
c   write (ipunch,18)
18  format
1  (1x,"silver distribution profile
1  (rectangular coordinate)" )
c   goto 19
17  write (ipunch,13)
13  format(1x,"silver distribution profile
1  (circular coordinate)" )
19  write (ipunch,41)

```

```

41  format(1x,"1-dimensional inorganic resist model")
    write (ipunch,14) rlw, rsw
14  format (16x,"lw=" ,f6.2," sw=" ,f6.2)
    write (ipunch,15) ai, bi, ci, d
15  format(6x,"A =" ,f8.4,3x,"B =" ,f8.4,3x,
1  "C =" ,f8.4,3x,"D =" ,f8.4)
    write (ipunch,16) (exptim(i),i=1,number)
16  format(1x,"profile time:" ,5(1x,f6.2))
    return
    end
c
c
c  subroutine outpf1(exti)
c  This program writes the output-profile data points to
c  the file 7
c
c  common /horimg/ deltx, mnhpts, nmhpts, horint(50)
c  common /io1 / itermi,ibulk,iprout,iresv1,iin,iprint,ipunch
c  common /simarr/ c(50), cim(50)
c  common /sildis/ exptim(20), x(50), si(20,50), jptr
c  common /inorpa/ ai, bi, ci, d, p, tau, ikey
c  common /objms2/ rlw, rsw, rlw2, rsw2
c  double precision c, cim
c  double precision p
c
c  xlth=deltx*float(nmhpts-1)
c  rnout=1.0
c  rnpts=float(nmhpts)
c  cmin=0.
c
c  To find ymax
c
c  cmax=c(1)
c  do 5 j=2,nmhpts
c  if (c(j) .le. cmax) goto 6
c  cmax=c(j)
6  continue
5  continue
c
c  write (ipunch,10) x(1), x(50), cmin, cmax, rnout
10  format (/ ,4(1x,f8.5) ,/ ,1x,f8.5)
c  write (ipunch,20) rnpts
20  format (1x,f9.5)
c  write (ipunch,30) (x(i),c(i),i=1,nmhpts)
30  format (11(1x,f6.3))
c
c  output message
c
c  write (ipunch,12)
12  format(1x,"remnant-silver distribution profile")
c  write (ipunch,14) rlw, rsw
14  format (16x,"lw=" ,f6.2," sw=" ,f6.2)
c  write (ipunch,15) ai, bi, ci, d
15  format(6x,"A =" ,f8.4,3x,"B =" ,f8.4,3x,

```

```
1 "C=" ,f8.4,3x,"D=" ,f8.4)
write (ipunch,16) exti
16 format(1x,"profile time:" ,2x,f10.7)
return
end
```

Appendix II: MOS Capacitor Process

1. INITIAL WAFER PREPARATION

1.1. Wafer Selection

N-type, 4-inch, $\langle 100 \rangle$, 4-7 ohm-cm, Si wafers.

1.2. Piranha Clean

5:1 Sulfuric acid:hydrogen peroxide; clean for 10 mins.

1.3. Oxide Dip and Water Break Test

Dip the wafer in 10:1 solution of HF until the wafer becomes hydrophobic. HF solution will completely clear off the surface if the wafer has been properly cleaned.

2. Field Oxide

2.1. Oxidation

Wet-oxidation Furnace. Target : 7000 Å

Temp = 950 °C			
Push	O ₂	1.0	10 min
	N ₂	2.2	
Oxidation	Wet O ₂	2.2	400 min
	dry O ₂	2.2	20 min
Anneal	N ₂	2.2	20 min
Pull	O ₂	1.0	10 min
	N ₂	2.2	

3. Active Area Definition

3.1. Ge-Se Resist Process

3.1.1. Bottom resist layer

Kodak-820 4300 rpm 30 sec
Hard bake 180 °C 60 min

3.1.2. Ge-Se resist layers

Ge-Se evaporation; Ag sensitization 60 sec;

3.1.3. Exposure

Equipment: GCA DSW6200; Dose: 238 mJ/cm²;

3.1.4. Development

Ag stripping; Ge-Se development;

3.1.5. Pattern transfer

RIE in oxygen plasma.

3.2. Oxide Etch

Buffer HF etch

3.3. Photoresist Removal Immerse in Piranha bath for 10 min

3.4. Piranha Clean

Remove remaining Ag and Se.

Immerse wafers in a clean piranha bath for 10 min.

4. Gate Oxidation

4.1. Oxidation

Gate Oxidation Furnace : TCA Clean prior to use

Target : 200 Å

Temp = 1000 °			
Push	O ₂	1.0	10 min
	N ₂	2.2	
Oxidation	O ₂	2.2	36 min
	N ₂	2.2	20 min
Pull	O ₂	1.0	10 min
	N ₂	2.2	

5. Polysilicon Gate Deposition

5.1. Polysilicon Deposition

The in-situ phosphorous doped polysilicon is deposited right after the oxidation to prevent contamination.

Target : 0.5 μm

6. Gate definition

6.1. Standard Lithography

Kodak-820	4300 rpm	30 sec
Hard bake	90 °C	20 min
Exposure	GCA DSW6200	0.23 sec
Development	Kodak 809	1 min
Hard bake	120 °C	20 min

6.2. Polysilicon Etch

315:16:1 Nitric acid : Ammonium Floride : DI water

6.3. Photoresist Removal

Immerse in piranha for 10 min.

7. Backside Metalization

7.1. Protective Photoresist Spin-on

dehydration Bake	150 °C	30 min
Kodak-820	4300 rpm	30 sec

Hard Bake 120 °C 20 min

7.2. Backside Polysilicon Etch

Trilogy etch

7.3. Backside Oxide Etch

Etch in BHF until the wafer becomes hydrophobic.

7.4. Palladium Sputtering

Target : 0.5 μm

7.5. Photoresist Removal

Acetone 3 min - Methanol Rinse - DI Rinse

Appendix III: Modified NMOS Process

1. INITIAL WAFER PREPARATION

1.1. Wafer Selection

P-type, 4-inch, <100>, 20-50 ohm-cm, Si wafers.

1.2. Piranha Clean

5:1 Sulfuric acid:hydrogen peroxide; clean for 10 mins.

1.3. Oxide Dip and Water Break Test

Dip the wafer in 10:1 solution of HF until the wafer becomes hydrophobic. HF solution will completely clear off the surface if the wafer has been properly cleaned.

2. Buffer Oxide Growth

Target: 200 Å of oxide. TCA clean furnace prior to oxidation.

TEMP=950 °C

Push	O ₂	2.2	30 min
	N ₂	1.0	
Ox	O ₂	2.2	36 min
Anneal	N ₂	2.2	20 min
Pull	O ₂	2.2	10 min
	N ₂	1.0	

3. Nitride Deposition

To prevent contamination, nitride is deposited immediately after the oxidation.

Target : 1000 Å

4. Active Area Definition

4.1. Standard Photolithography**4.2. Nitride Etch**

Etch Lam etcher SF_6 O_2 60°C 100 W

4.3. Field Implantation

Boron 100 keV 4° 1.5×10^{13}

5. Backside Implantation**5.1. Standard Photoresist Removal****5.2. Spin on Protective Photoresist**

dehydration bake

KTI-820	4300 rpm	30 sec
Hard bake	120 °C	10 min

5.3. Backside Oxide Etch

Etch in BHF until wafer becomes hydrophobic.

5.4. Implantation

BF_2 200keV 4° 2×10^{15}

6. LOCOS**6.1. Standard Photoresist Removal****6.2. Oxidation**

Wet-oxidation Furnace. Target : 7000 Å

Temp = 950 °C

Push	O_2	1.0	10 min
	N_2	2.2	
Oxidation	Wet O_2	2.2	400 min
	dry O_2	2.2	20 min

Anneal	N ₂	2.2	20 min
Pull	O ₂	1.0	10 min
	N ₂	2.2	

7. Nitride Removal

Oxide Dip: HF : DI 1 : 10 40 sec

Phosphoric Acid 155 °C 30 min

8. Gate Oxidation

8.1. Buffer Oxide Removal

HF : DI Water 1 : 10

8.2. Oxidation

Gate Oxidation Furnace : TCA Clean prior to use

Target : 200 Å

Temp = 1000 °

Push	O ₂	1.0	10 min
	N ₂	2.2	
Oxidation	O ₂	2.2	36 min
Anneal	N ₂	2.2	20 min
Pull	O ₂	1.0	10 min
	N ₂	2.2	

9. First Polysilicon Deposition

9.1. Polysilicon Deposition

The in-situ phosphorous doped polysilicon is deposited right after the oxidation to prevent contamination.

Target : 500 Å

10. Threshold Implantation

Boron 50 keV 4 ° 7×10^{11}

11. depletion implant

11.1. Standard Photolithography

11.2. Depletion implant

As 150KeV 0° 1×10^{12}

11.3. Photoresist Removal

Remove in oxygen plasma

12. Buried Contact

12.1. Standard Photolithography

12.2. Polysilicon Etch

Equipment: Lam etcher; Gas: CClF_3

12.3. Oxide Etch

Buffer HF etch for about 20 sec.

12.4. Photoresist Removal

12.5. Oxide Etch

Short dip (about 5 sec) in 1:10 HF to remove the oxide

13. Second Polysilicon Deposition

Piranha clean and 5 sec 1/5 HF dip before deposition

Target : 3000Å

14. Gate Definition

14.1. Ge-Se Resist Process

14.1.1. Planarization

Dehydration Bake 150 °C 20 min

KTI-820 4300 rpm 30 sec

Hard Bake 180 °C 60 min

14.1.2. Ge-Se Resist Deposition

Ge-Se evaporation; Ag sensitization 60 sec

14.1.3. Exposure

Equipment GCA DSW6200; dose 238 mJ/cm²

14.1.4. Development

Ag stripping; Ge-Se development

14.1.5. Pattern Transfer

Equipment: Technics; RIE in oxygen plasma.

14.2. Polysilicon Etch

315:1:16 Nitric acid : Amonium Floride : DI water

14.3. Photoresist Removal

Remove both Ge-Se and KTI820 resist in Piranha

14.4. Piranha Clean Clean for 10 minutes

15. S/D Implantation

15.1. Standard Lithography**15.2. Implantation**

As 180 keV 4° 3 × 10¹⁵

15.3. Photoresist Removal

Plasma Asher O₂ 1 Torr 120 W 40 min

Piranha Clean 5 min

15.4. Polysilicon Re-oxidation

Oxidation Furnace

Temp = 900 °C

Push	O ₂	1.0	10 min
	N ₂	2.2	
Wet Oxidation	O ₂	2.2 cm	30 min
Anneal	N ₂	2.2	20 min
Pull	O ₂	1.0	10 min
	N ₂	2.2	

16. Contact Definition**16.1. Standard Photolithography****16.2. Contact Hole Etch**

Etch in BHF

16.3. Standard Photoresist Removal**17. Metalization**

17.1. Oxide Dip HF : DI 1 : 10 5 sec

17.2. Dehydration Bake

Dry wafers in 110 °C oven.

17.3. Aluminum Evaporation

Target : 0.5 μm

18. Metal Definition**18.1. Standard Photolithography****18.2. Aluminum Etch**

Aluminum Etchant Type A 40 °C

19. Backside Metalization**19.1. Protective Photoresist Spin-on**

Dehydration Bake 150 °C 20 min

KTI-820 4300 rpm 30 sec

Hard Bake 90 °C 20 min

19.2. Backside Polysilicon Etch

Trilogy etch

19.3. Backside Oxide Etch

Etch in BHF until the wafer becomes hydrophobic.

19.4. Palladium Sputtering

Target : 0.5 μm

19.5. Photoresist Removal

Acetone 3 min - Methanol Rinse - DI Rinse

20. Sintering

Sintering Furnace

Temp = 200 °C

